Localised States in Organic Semiconductors and their Detection

Dissertation

zur Erlangung des akademischen Grades
Doktor der Naturwissenschaften
(Dr. rer. nat.)
in der Wissenschaftsdisziplin Festköperphysik

Eingereicht an der
Mathematisch – Naturwissenschaftlichen Fakultät
der Universität Potsdam

von
Paolo Imperia
geboren in Anagni (Italien)

Potsdam, im Februar 2002

Contents

1. Introduction

In recent years tremendous progress has been made in the field of organic light emitting devices and organic electronics. The commercialisation of displays based on organic compounds is a reality and the progress in organic technology is setting a revolution in the every day electronic devices.

Despite of the technological progress open questions about the underlying physics remain. In particular a deeper knowledge of charge transport properties of polymers and low molecular compounds is a necessity in order to make further developments.

The study of localised levels in technologically relevant materials like oxadiazoles and quinoxalines in this context is of fundamental importance. Several scientific tools enable to study localised levels in solids and among others the thermally stimulated techniques give the most direct evidence of their presence.

Though the subject is rather general, the present work is focused on theoretical and experimental study of localised levels in organic materials suitable for light-emitting devices and organic electronics by means of thermal techniques.

1.1. Importance

The high potential of the new field of plastic electronics in the future consumer market makes the study of fundamental characteristic of conjugated materials to better understand their properties and to optimise the design of future electronic and optoelectronic components a highly urgent task. Recently, pilot plants for studying the production issue related to the fabrication of such devices were developed. But despite of the technological progresses there are still open fundamental questions. One is the problem related to the presence of localised levels and their role both in charge transport and optical properties.

It is widely known for inorganic[1] and organic[2] semiconductors that localised states strongly influence transport properties. The low temperature mobility is governed by shallow traps and impurity scattering. Optical properties and in particular luminescence, are affected by localised levels that can act both as non-radiative centres, reducing the light emission efficiency[3] or even as emission sites[4].

It was demonstrated, for organic photoconductors, that the low mobility has to be ascribed to the presence of traps and that hopping transport between trap centres, localised on pendent photoconductive groups, is dominant[5].

More recently, applying the band theory model to organic crystals, the presence of traps has been recognised and studied to better understand the behaviour of interface energetic alignment and the occurrence of band bending[6-8].

In that frame the combined spectroscopy and electrical investigations, like ultraviolet photoelectron spectroscopy (UPS) combined with thermally stimulated techniques (TSTs), dielectric spectroscopy (DES) and current voltage (I/V) measurements, gives a more complete sketch of the band-band and intra-band features[9,10] opening the way for further development of the devices technology and enlightening the complex electronics properties of organic materials.

1.2. Localised states

The transport mechanism in organic molecular crystals and polymers is not fully understood until now. Many studies on transport properties of heterocyclic polymers and low molecular compounds have been carried out, but without a clear knowledge about trapping states and of the deep impact that localised states have on the conduction properties it is difficult to clarify which are the complex mechanisms governing their transport properties and, consequently, which theoretical frame could better describe them. It was proven[11] by current-voltage measurements on monopolar devices, that electron transport in poly(p-phenylene vinylene) (PPV) is limited by the presence of an exponential distribution of traps with a density about 10^{18} cm^{-3}. Moreover, on the same material it was proposed that the transport mechanism is dominated by presence of a Gaussian distribution of states[4]. Albeit the presence of bands, the band transport mechanism and also the presence of traps was strongly under question[12]. However, recent results make us confident that under certain conditions the band theory is a good approach in understanding the electronic properties of organic materials for opto-electronic applications[13].

The discussion about the presence of localised states and their density naturally leads to the question about the kind of traps we are dealing with. In a first approach we should distinguish between intrinsic and extrinsic defects. In the first type we should inscribe polymer end groups, grain boundaries, structural defects, conformational disorder up to molecular groups with large permanent dipole moment that could increase the level of energetic disorder[4]. For the second type we should mention the chemical impurities, somehow unavoidable in the synthesis of organic molecules. We can further distinguish the kind of traps in function of their location, interfacial or bulk, or in term of energy, deep traps or shallow traps. Also polarons could be seen, in a simplistic way, like defects caused by an electron plus an induced lattice polarisation[14] followed by a lattice distortion.

Traps are into the samples in a great variety and in different proportion, often despite the “same” preparation procedure. For that reason sometimes their nature is difficult to investigate and the data must be handled with care.

In the studies of trapped states because of the above underlined variety of defects in solids the most successful approach is to start introducing a single type of defect in a well known system in a controlled way. Although that should be the most effective method, very few studies were devoted to introduce localised states deliberately in an organic crystal or in a well ordered thin film[15].

Clearly the knowledge of occurrence of distributed traps and their type and density is the only way to solve the puzzling nature of conduction in organic materials and a current limit in progress results from the lack of direct measurement of trapped states in organic semiconductor devices.

The above described scenario justifies the experimental efforts in studying traps in materials for organic optoelectronic devices by using the instruments and the methodologies already successful developed during the past years for studying the localised states in inorganic semiconductors like silicon, germanium, GaAs and many other technological important inorganic materials[16] so successfully employed in the development of electronic devices of every day life.

1.3. OLEDs

A well-known phenomenon shown by several inorganic as well as organic materials is electroluminescence. The effect occurs when a film of a suitable material is subjected to a voltage across two electrodes adjacent the film that drives a current trough the solid. The electrical excitation produced by means of the current is subsequently followed by a de-excitation under light emission.

The earlier reports about electroluminescence in organic crystals appear in the 60s of the last century. In a paper of 1963 Pope[17] states the observation of electroluminescence in an anthracene single crystal. This earlier report did not give effect on further practical applications because of the small amount of emitted light and the quite high voltage necessary to apply in order to obtain it. In effect the luminescence was observed for applied voltages above 400 V and with current densities of about 1 μA.

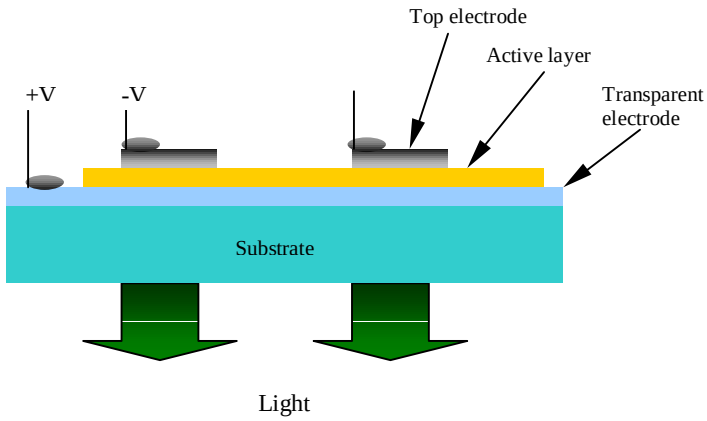

Fig. 1.1 Single layer OLED arrangement.

Only in the late 1980s the interest for organic electroluminescence grew suddenly with the astonishing report of C. W. Tang and S. A. VanSlyke[18,19] about high brightness at low driving voltage of an organic light emitting device (OLED) having a thin layer, about 60 nm, of 8-hydroxyquinoline (Alq_3) like active material.

The successful idea behind the breakthrough was to build-up not a single layer OLED, but to couple the emitting material with a second layer of about 75 nm of an aromatic diamine, capable of only monopolar (hole, in such case) transport. The resulting device emits light at about 2.5 V and it clearly demonstrates that organic compounds are a real alternative for optoelectronic applications.

A further step, few years after, was the J. H. Burroughes and co-workers report[20] about the first OLED prepared with the conjugated polymer poly(p-phenylene vinylene) PPV, manufactured in a very easy way from a solution processable precursor. The novelty of a such PPV OLED with respect to an Alq_3 one consists in the different preparation process. While the Alq_3 device must be produced with vacuum deposition techniques, the PPV device can be easily manufactured by spin-coating and subsequent thermal conversion in vacuum.

The reports of Tang and of Burroughes initiated two different philosophies in devices preparation. The vacuum sublimation procedure requires expensive facilities, but enables to realise exceptionally

performing devices. Solution processed devices are easy to produce on small and medium sized surfaces by means of several different techniques like spin coating, doctor blading and casting. Furthermore, it is possible to use ink jet printing and other techniques developed for paper printing in order to pattern large surfaces with real economical advantages.

Table 1.1

Metal	Work function (eV)
Ca	2.6÷2.9
Ag	4.3÷4.7
Al	4.1÷4.4
Mg/Ag (10:1)	3.5÷3.7

Figure 1.1 shows the typical arrangement of a single layered OLED. The basic structure consists of a thin (10÷100 nm) organic film sandwiched between two electrodes. The active material is typically deposited on glass or a transparent flexible plastic substrate carrying a transparent anode. The anode consists usually of a layer of indium tin oxide (ITO) that is both highly transparent, in the visible, and a fairly good conductor. It also possesses optimal substrate adhesion characteristic.

The heterojunction formed between ITO and the organic layer is determined by the relative work functions of the two adjacent materials that usually tend to create a barrier at the interface. The ITO possesses a relatively high work function ranging from 4.1 up to 5.5 eV, depending on the preparation conditions and on the surface pre-treatment. Plasma[21,22] or a simple acid treatment[23] could, in principle, fine tune the work function of the ITO causing better conditions for hole injection into the overlying organic layer.

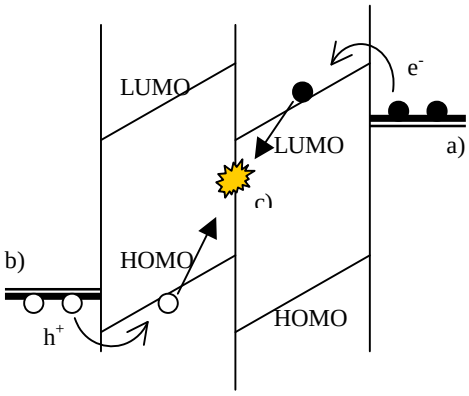

Fig. 1.2 A simple energy diagram of an OLED.
a) cathode, b) anode, c) recombination

An alternative to the ITO anode is to use a fluorine tin oxide (FTO) layer[24]. FTO has a work function of 4.4 eV, it is less sensible to the surface cleaning treatment and does not contain indium that has the tendency to diffuse into the emissive layer[25]. Furthermore FTO is more stable to oxidation. Different tuning techniques involve the usage of a thin layer of AlF_3 or a different suitable wide band gap materials in order to modify the injection conditions at the ITO interface.

The cathode consists generally of an evaporated metal layer with a low work function, like calcium or an alloy, that makes the injection of electrons easy. Two important points to take into account in the device preparation are the reactivity of the metal with oxygen and moisture and the metal diffusion into the near surface region of the organic layer[26].

Table 1.1 shows few commonly used cathode materials with their work function taken from literature[27,28]. Calcium, that is widely used because of its low work function, is highly reactive making necessary to encapsulate it with a less reactive metal layer.

A good matching of the work function at the interface metal/organic is a major requirement in order to assure a low barrier and definitely better OLED performances[26,29]. Also at the cathode side injection conditions can be improved by inserting a thin interlayer of a wide gap material like LiF or MgF_2. The mechanism of improvement is still under discussion. It is possible that a dissociation of a small fraction of LiF coupled with subsequent doping of the organic interlayer is the mechanism responsible.

The active layer constitutes the core of the electroluminescent device. The fundamental processes in an OLED, summarised in a schematic way, are shown in figure 1.2. This includes:

1) injection, of electrons and holes from the cathode and anode, respectively,
2) transport of the two types of carriers,
3) formation of the exciton at the interface between the two organic layers,
4) subsequent recombination, i.e. the relaxation process to the ground state accompanied by the emission of light.

The wavelength of the emitted light depends on the electronic structure of the emitting organic

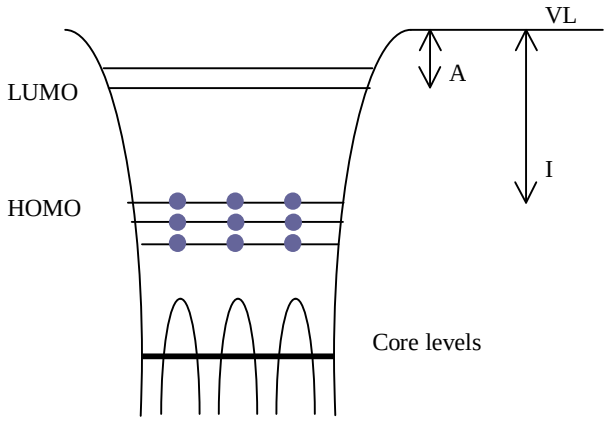

Fig. 1.3 Electronic structure of a polyatomic molecule; VL is the vacuum level, A is the electron affinity and I the Ionisation potential.

material and can be changed by chemical modification.

The performance of an OLED depends on the injection conditions for holes and electrons. Usually, in a single layer structure, electrons and holes are unbalanced, unless the situation occurs where the anode and cathode are very well matched to the molecular levels of the organic compound. In the unbalanced case a dominant carrier can cross the whole structure without finding a carrier of opposite sign to recombine, raising an energy waste and leading to low efficiency in the conversion of electrical into optical power.

To achieve a better balance two (or more) organic layers must be added. One matching the anode, optimised for transport of holes, and a second one, matching the cathode, optimised for electron transport. In that way the charge injection can be balanced. Since a barrier occur at the organic/organic interface, carriers tend to accumulate there, improving the probability in finding an available partner for recombination. In such way the recombination process is moved away[30] from the metal/organic interface where exciton quenching usually occurs.

1.3.1. Molecular orbitals

In order to elucidate the design of a real OLED, it is necessary before to briefly describe the electronic structure of an organic solid. Of course several excellent books[2,31] and many papers (see for example Seki[32] and references therein) discuss the matter and here we would like to give only the basic concepts in order to have a key to understand the theoretical background.

We can start considering a polyatomic molecule. The ions are arranged in a way that exhibits a spatial periodicity and the solution of the hamiltonian gives rise to allowed energy bands separated by regions that are forbidden[33]. The atomic orbitals are deeply localised in the potential well. However, the shared upper part constitutes the delocalised molecular orbitals. Figure 1.3 gives a pictorial representation

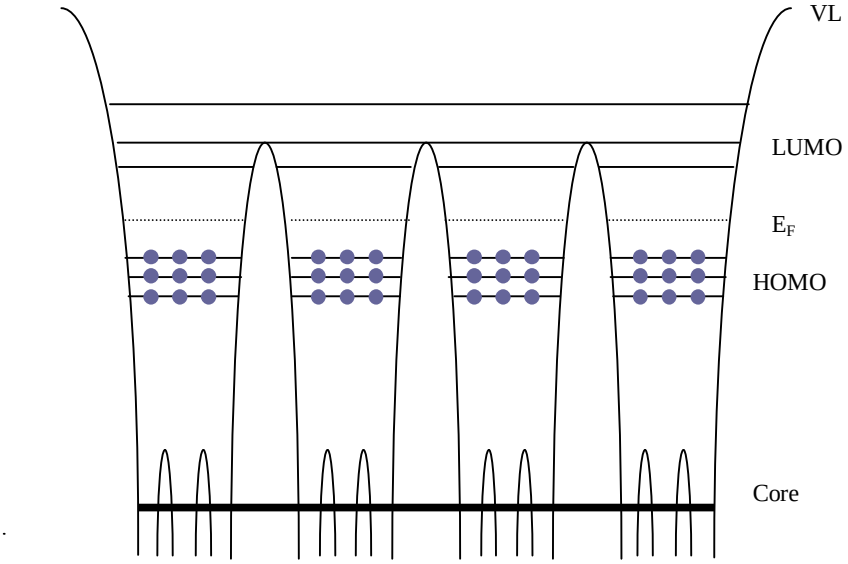

Fig. 1.4 Electronic structure of an organic solid. VL is the vacuum level and E_F is the Fermi level.

of molecular orbitals. There I is the ionization potential defined by the energetic difference between the highest occupied molecular orbital (HOMO) and the vacuum level (VL). The quantity A is the electron affinity, i.e. the energetic separation from the lowest unoccupied molecular orbital (LUMO) and the VL.

If we further consider weak interactions between the molecules, like in a van der Waals solid, the picture that describe the solid is the one shown in figure 1.4. The most peculiar feature of that description is the localisation of the valence band and of the conduction band in each molecule with narrow band width, estimated[34] to be in the order of 0.05÷0.2 eV, depending on the organic crystal type. This is a point of great importance: the main transport properties of organic solids arise from the localisation of the HOMO and LUMO and from the energetic width of the intermolecular band. With this approach the validity of the band theory still holds, but with the major limitation of the width of the band. Of course the situation varies between materials, depending on the strength of the interaction between the molecules of the solid and their arrangement in the crystal. However, in well ordered films the presence of bands can not be neglected, as can be concluded from ultraviolet photoelectron spectroscopy experiments which allow to explore the complete momentum (k)-resolved band structure[35].

An energy level scheme for a heterolayer OLED is given in figure 1.5. The active layer and hole transporting material in this example is PPV. In order to obtain a better matching between the cathode and the active material a further layer of an electron transporting[36,37] material, namely trisphenylquinoxaline (1,3,5-tris[(3-phenyl-6-trifluoromethyl)quinoxaline-2-yl]benzene) (TPQ), is inserted. In this figure the

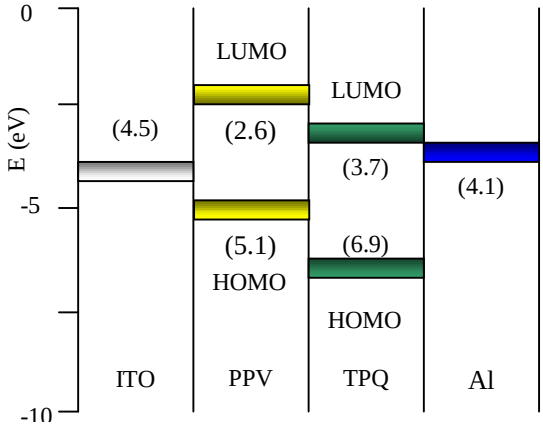

Fig. 1.5 A simplified energy diagram of a PPV/TPQ OLED. In brackets the HOMO LUMO level values and the work function of the metals.

HOMO and LUMO energy levels of PPV and TPQ are given. The hole blocking properties of TPQ results from the high barrier between the two HOMO levels of the organic layers.

The proposed schema of figure 1.5 is an oversimplified picture of a real device. In a real case it should be take into account the interface effects, like the vacuum level shift[32,35] and the possible formation of an interface dipole as well as the band bending effect for films thicker than few monolayers[32].

Using the basic structure governing interfaces, transport and optical properties above described, it is possible to design and then to produce OLEDs with extraordinary features, combining favourable optical

and electrical characteristics with outstanding mechanical advantages. The state of the art of OLED technology enables full colour, full motion, light and flexible flat panel displays simply not possible with other technologies. This kind of display starts to be available on the market[38] now. Furthermore, new kind of products can be designed starting from organic molecular compounds and π-conjugated polymers. They range from revolutionary application for illumination, new organic field effect transistors[39] up to unbelievable challenging mono molecular electronic devices that will be the next future exciting top research field[40].

Very recent experimental and theoretical works[41], show that the commonly believed theoretical upper limit for the internal quantum yield of 25% can be overcome. This estimation of the 25% limit arises from spin statistic arguments that neglect the intersystem crossing from the triplet to singlet states. Excitons generated at the organic/organic interface may be either in a long lived triplet state, that decays with a very low quantum yield for light generation, or in a singlet state that spontaneously generates fluorescence. The ground state into which the excitons has to decay in order to generate a photon is a singlet state. It seems that the intersystem crossing singlet-triplet states cannot be neglected in π-conjugated polymers and oligomers. In such case revolutionary devices for illumination competing with the traditional light sources, having a very high internal quantum yield, can be designed.

The plastic electronic applications really have the strength to change the current concepts of storing data and the low cost every day life electronics[42]. Thanks to organic materials, memory tags and new interactive packaging for any kind of commercial product can be designed and developed in the next future. The study and development of organic field effect transistors represents the new frontier in the organic research technology.

1.4. Materials

One key issue to improve the OLED characteristic is to achieve an efficient exciton formation[43]. This is possible, like underlined above, by balanced injection and transport of electrons and holes and by keeping the recombination process away from the anode and cathode where quenching effects can occur. There are several possibilities to achieve balanced injection. One way could make use of tuning the electronic structure of the organic material by chemical means, obtaining a better match to the work function of the electrodes. An opposite way consists in choosing accurately electrode materials matching the organic layer

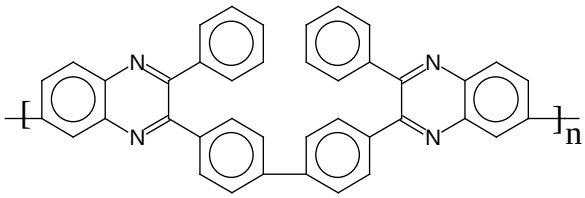

Fig. 1.6 Poly-[2,2'-(1,4-phenylene)-6,6'-bis(3-phenylquinoxaline)] (PPQ IA)

electron affinity. A different and preferable way to achieve this objective is to use layers optimised for injection of electrons and holes, respectively. The obtained structure has then an enhanced efficiency and also shows a reduced threshold field[43].

In that frame it is possible to optimise each single layer studying their ionisation potential, for example by ultraviolet photoelectron spectroscopy and their transport characteristic.

In our work we focused on low molecular compounds as well as on polymers, especially of two classes of materials: oxadiazoles and quinoxalines. Both organic compounds are well know as electron transport materials in OLEDs.

1.4.1. Quinoxalines

Quinoxalines are characterised by heterocyclic rings enhancing their ionisation potential and their electron affinity and making them very interesting as electron transport or hole blocking materials. In organic chemistry they are well-known as temperature stable and chemically resistant organic materials.

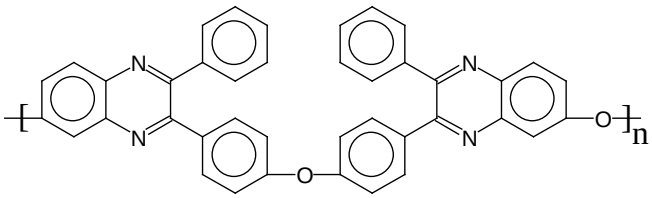

Fig. 1.7 Poly[2,2'-(4,4-oxybiphenylene)-6,6'-oxybis(3-phenylquinoxaline)] (PPQ IIB)

The polyphenyl-quinoxalines (PPQs) were first developed[44] in the late 60s early 70s for aerospace applications especially because of their excellent mechanical[45], thermal and film forming properties. In that frame many studies were devoted to their thermo-mechanical characteristics, but their electrical properties were not exploited. We studied two kinds of PPQs as well as several low molecular phenylquinoxalines (PQs), and a very promising star shaped trisphenylquinoxaline (TPQ).

Poly[2,2'-(1,4-phenylene)-6,6'-bis(3-phenyl quinoxaline)] shortly called PPQ IA (figure 1.6) and poly[2,2'-(4,4-oxy biphenylene)-6,6'-oxybis(3-phenylquinoxaline)] shortly called PPQ IIB, shown in figure 1.7 belong to the first class. PPQs in general show very high solubility[46] in a variety of common organic solvents, and according to literature they exhibit a glass transition at quite high temperature (250-350 °C). Furthermore they have the polymer decomposition temperatures between 515-540 °C, depending on their chemical structure[46]. These features make them a good candidate for spin coating, casting and other solution based preparation techniques.

Low molecular model compounds with a chemical structure related to PPQ IA and PPQ IIB were studied by means of UPS in order to get information about their electronic structure[47]. Figure 1.8 shows the structure of a) 1,4-bis[2-(3-phenyl-quinoxalyl)]benzene (BPQ), b) 1,4-bis[2-(3-phenyl-benzo[g]quinoxalyl)]benzene (BPBQ) and c) 2,2',3,3'-tetraphenyl-6,6'-diquinoxaline (TPDQ). Their ionisation potential measured by means of UPS is quite high[48] (> 6 eV).

Figure 1.9 shows the starburst CF_3-TPQ. Synthesised[36] in the group of P. Strohriegl, at the University of Bayreuth, this molecule was especially designed for electron transport purposes[49]. CF_3-TPQ shows excellent stable glass formation properties and a high electron mobility in the range of $10^{-5} \div 10^{-4}$ cm^2/V, depending on sample preparation conditions. Thin films prepared by vacuum depositions and

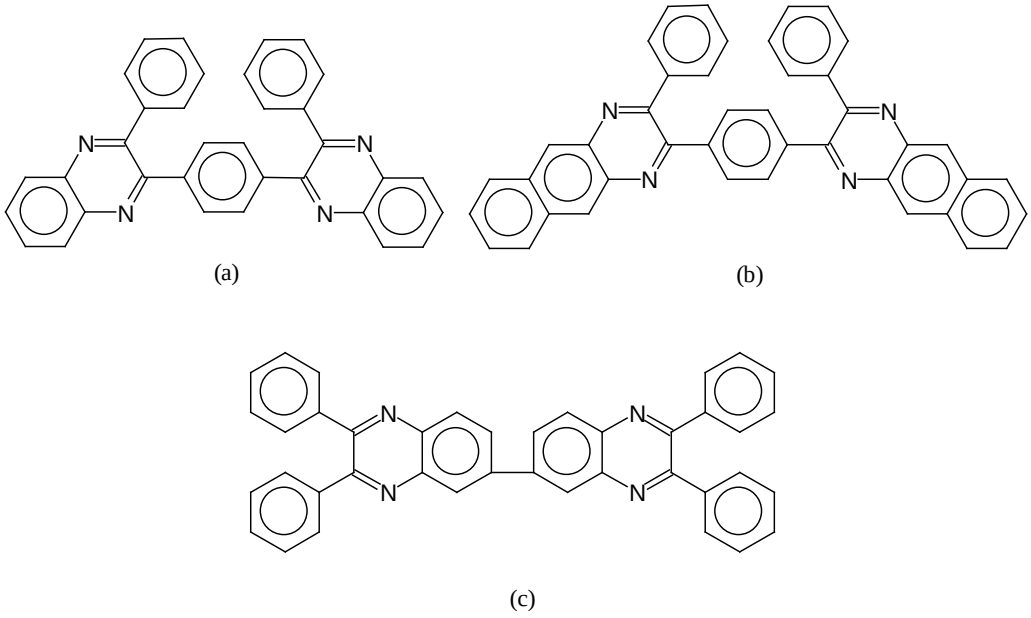

Fig. 1.8 a) 1,4-bis[2-(3-phenyl-quinoxalyl)]benzene (BPQ)
b) 1,4-bis[2-(3-phenyl-benzo[g]quinoxalyl)]benzene (BPBQ)
c) 2,2',3,3'-tetraphenyl-6,6'-diquinoxaline (TPDQ)

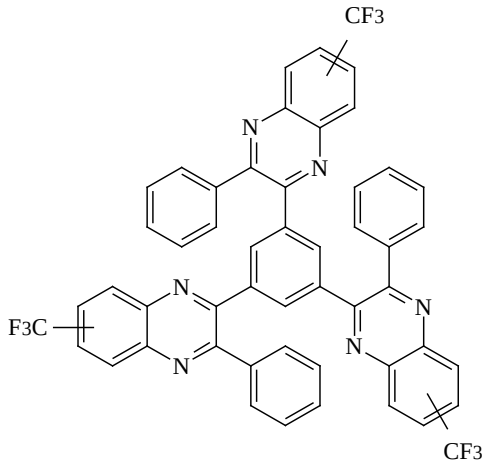

Fig. 1.9 1,3,5-Tris[(3-phenyl-6-trifluoromethyl)-quinoxaline-2-yl]benzene (CF_3-TPQ)

studied by means of photoelectron spectroscopy show an ionisation potentials of 6.0 eV and a work function, measured with the sample negatively biased, of 4.2 eV[10,37,50]. Moreover, OLEDs with the configuration ITO/PPV(150nm)/TPQ(30nm)/Ag show good devices performance[51]. The devices so configured have an onset voltage of about 5.7 V, brightness of 236 Cd/m^2 at 25 V and show an external quantum efficiency of 0.11%.

1.4.2. Oxadizoles

A second class of very promising materials for optoelectronic applications are oxadiazoles. Oxadiazoles are well known for their excellent mechanical properties and high thermal stability. Applications range from fibres to membranes and coatings[52]. Substituted oxadiazoles have excellent solubility in common solvents. In particular it was successfully possible to prepare well ordered and stable Langmuir–Blodgett (LB) multilayers with a very smooth and uniform surface structure[53] of the amphiphilic substituted 2-(p-

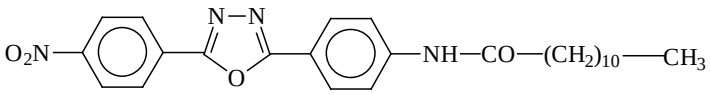

Fig. 1.10 2-(p-nitrophenyl)-5-(p-undecylamidophenyl)-1,3,4-oxadiazole (NADPO)

nitrophenyl)-5-(p-undecylamidophenyl)-1,3,4-oxadiazole (NADPO) shown in figure 1.10. The vacuum deposition of NADPO is also possible, resulting in well ordered films[54] depending on the deposition conditions, evaporation rate and substrate temperature.

Many differently substituted 2,5-diphenyl-1,3,4-oxadiazoles have been synthesised. Because of their electron acceptor properties several of them are especially suitable for the needs of electron transport / hole blocking layers as well as for the emissive layer[55] in OLEDs. Some oxadiazoles show a brilliant green, yellow and even blue light emission[56].

The ionisation potential of several amorphous films of aromatic oxadiazoles were measured[50, 57] and because of their ordered nature it was also possible to determine the complete k-resolved band structure of a well ordered LB film of NADPO samples by means of UPS measurements[35]. This oxadiazole, particularly interesting because of its film forming properties, shows an ionisation potential of 7.9 eV and a value for the electron affinity of 4.8 eV.

1.5. Experimental Techniques

The determination of the parameters describing a set of localised states in an organic and inorganic semiconductor can be done using different experimental techniques. We can, in a coarse way, roughly divide the techniques into isothermal and non isothermal ones. To the first group belong techniques like deep level transient spectroscopy, time of flight (TOF) and current voltage characteristics (I/V), especially measurements of the space charge limited current (SCLC). Non isothermal techniques include thermally

stimulated depolarisation currents (TSDC), thermally stimulated currents (TSC) and thermally stimulated luminescence (TSL).

The study of the I/V characteristics provides important information about the electronic bulk properties of a material and, reaching the space charge limited current region, it is possible to study the trap density, the activation energy as well as to get information about the type of trap distribution[4,58]. The main request in order to successfully apply the technique is the ability to prepare ohmic contacts on the surface of the samples.

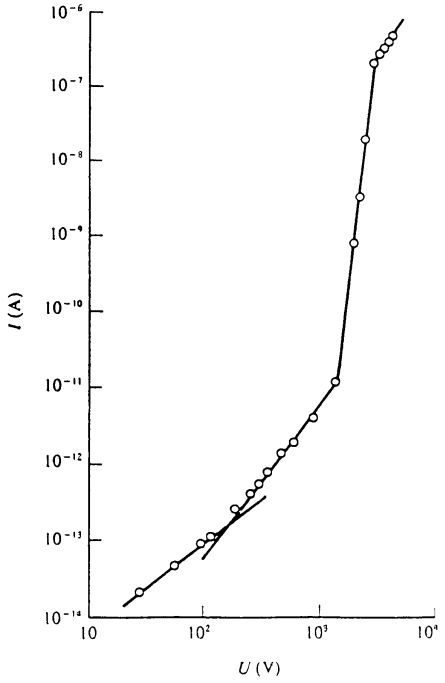

Fig. 1.11 current voltage characteristic of a naphthalene single crystal. (After [59]).

According to Sze[1] we define an ohmic contact as a metal/semiconductor contact that has a negligible resistance relative to the bulk resistance of the semiconductor. A satisfactory ohmic contact should not affect the device performance and it should supply the required current with a voltage drop negligible with respect to the one across the device. In that case, and only if an actual ohmic contact that injects only monopolar charges into the bulk is realised, it is possible to apply the SCLC theory to describe the I/V characteristics and to discuss the presence of localised states.

The theory was developed in the late 60s and is widely applied in device studies. The interaction of the injected current with localised states determines the shape of the I/V characteristics and its magnitude that results reduced in function of the presence[58] of traps.

Figure 1.11 shows the strong influences of the presence of traps on the I/V characteristic of a naphthalene single crystal[59]. In the figure it is possible to distinguish four well defined regions. At low applied voltage there is the typical ohmic region where the current has a direct proportionality to the applied voltage, $I \propto V$. Then, increasing the applied voltage the shallow trap region follows. Here, the current is proportional to the square of the voltage $I \propto V^2$. The injection of charges provokes the displacement of the quasi-Fermi level trough the band gap as the traps get filled. The step like region in the figure indicates exactly the cross of the quasi-Fermi level of a single level of traps. Such crossing means that all the traps, that are still below the quasi-Fermi level, are filled. This occurrence is marked by a dramatic increases of the current over the sample. The injected charge carriers can not get any more trapped and are free to move through the conduction band increasing the total amount of current. The above region, at high voltage, is now the trap free insulator region where the characteristic can be described in the frame of SCLC theory by the famous Child's law[58], equation (1.1).

$$J = \frac{9}{8}\varepsilon\mu\frac{V^2}{L^3} \tag{1.1}$$

Here J is the current density, ε is the static permittivity, μ the free electron mobility and L is the sample thickness. Only reaching that trap free region it is possible to easily obtain data about the free carrier mobility.

The displacement between the two square law regions indicates the energetic location of the traps in the band gap, while the voltage at which the current rises nearly vertically yields directly the concentration of the trapped states[58]. A characteristic feature of the SCLC region, according to equation (1.1), is the cubic dependence on thickness. This is a useful test for an experiment, whether the SCLC region has really been reached. Only in the trap free region it is possible to extract the fundamental information about the intrinsic mobility of the charge carriers in the material, and cubic dependence on thickness should always be carefully checked in order to test the reliability of the results. Often the current is just limited by the contact quality. In such case of contact limited currents the SCLC theory cannot be applied. "If space-charge conduction is balanced partly by double injection, or if the current is injection-limited by contact barriers, extraction of reliable mobility data is a rather hopeless enterprise"[60].

Polymers and organic crystals often possess wide trap distributions having a Gaussian character and very rarely single levels of traps are encountered. Furthermore, large distributed concentrations of defects inhibit the current injection at practical voltages. In such a case the SCLC region cannot be reached and the simple Child's law cannot be applied. The I/V characteristic in case of a Gaussian trap distribution was studied by E. A. Silinsh and S. Nešpůrek and several approximate equations have been proposed to fit the trap filling region in order to get information about the distribution parameters[34,61,62].

A second experimental technique widely used in order to study the transport properties of a material is time of flight technique. TOF allows to observe the time resolved current generated in an illuminated thin layer of the material, drifting across the film under the influence of an external applied bias voltage. The "flight" of the charge carriers is likely influenced by the impurities that form electron and hole traps. From the measurement of the photocurrent produced, mathematical models allow to evaluate the possible presence of a trap distribution[63] and to extract the related parameters.

In a trap free perfect crystal a TOF experiment shows a rectangular pulse indicating the transit time of the carriers from the illuminated electrode to the collecting one. In the real case the shape of the pulse is distorted by the finite flight pulse duration, the finite light penetration depth and, especially, by the presence of charge carrier traps. In case of shallow traps the sequential trapping and thermal release of the charge carriers causes a current decrease, and an increase of the transit time, resulting in a distortion of the ideal TOF pulse. Moreover, deep localised levels induce a rapid decay of the current pulses before carriers can reach the exit electrode.

It is widely known that only in case of small density of traps it is possible to observe the transport of free charges over macroscopic distances without very large losses. In such case it is possible to measure the transit time t_f and, hence, the charge carriers drift mobility. The TOF method, illustrated by means of equation (1.2), connects the effective drift mobility μ with the square of the sample thickness L and the applied voltage V.

$$\mu = \frac{L^2}{V \cdot t_f} \tag{1.2}$$

The trap parameters, in a more generalised case, can be measured using the temperature dependence of the effective drift mobility[64] applying equation (1.3).

$$\mu = \mu_0(T)\left[1 + \frac{N_t}{N_e} e^{\frac{E_t}{kT}}\right]^{-1} \tag{1.3}$$

Here μ_0 is the mobility of the pure ideal crystal, N_e is the density of the electronic states at the conductivity level, k is the Boltzman constant and T the absolute temperature. The plot of $\log[(\mu^0 / \mu)\text{-}1]$ versus the inverse of the absolute temperature $1/T$ allows to determine the values of the density of traps N_t and their energetic depth E_t.

Non isothermal techniques, applied to the study of localised levels in organic and inorganic semiconductors, are essentially thermally stimulated current (TSC) and thermally stimulated luminescence (TSL). A further technique is the thermally stimulated depolarisation technique (TSDC) which especially allows to study relaxation processes in polymers. The thermal techniques are particularly designed in order to give direct evidence of existence of localised levels in a sample.

In typical thermally stimulated process experiments a sample is heated in a controlled way and the current, in case of TSC and TSDC, or the light emission, in case of TSL, or both simultaneously are monitored. The effect appears only when an optical or electrical excitation takes place prior to the heating. TSC, in contrast to TSL, requires the presence of good ohmic contacts. These are not always easy to prepare, especially in organic samples. Furthermore, the manufacture of the metallic contacts by itself determines the presence of shallow traps and defect states at the interfaces.

A further non-isothermal technique is the TSDC. The technique is both sensitive to release of trapped carriers and to dipole relaxation processes. In a typical TSDC experiment a voltage is applied across the sample at high temperature and then the sample is cooled down. At low temperature the electrical field is removed and then the sample is short circuited. While the temperature is raised in a controlled way a current, driven by the internal field is recorded. The method was successfully applied for the first time to study crystals containing dipolar ionic defects[65,66]. It provides a very sensitive tool for determining the dipolar kinetics especially combined with dielectric spectroscopy (DES) measurements. Since the current can arise both from the re-orientation of dipoles, and from electronic charges present in the samples, the interpretation of the peaks is much less straightforward compared to TSL and TSC techniques.

In this work we especially focus on the study of localised states by means of the thermally stimulated techniques.

2. Thermally stimulated techniques

The thermally stimulated techniques TSL, TSC and TSDC are powerful instruments in order to study de-trapping and relaxation processes in organic materials. TSL is a contactless technique that allows to distinguish between deep and shallow trapping states. The proposed mathematical model for the TSL enables to study trap levels and recombination centres inside the band gap. The analytical solution of the rate equations allows two different de-trapping regimes, including or excluding subsequent re-trapping effects. The first order solution kinetic indicates that no re-trapping phenomena are permitted. The electron released from a localised level recombines with a hole in a recombination centre and its re-trapping probability, before to recombine, is negligible. The second order equation deals with the opposite extreme case. The phonon assisted release of an electron is followed by multiple re-trapping. In this second order kinetic regime the probability of a released electron to get re-trapped is very high.

The main factors governing both solutions are the energy depth of the traps calculated with respect to the conduction band edge and the frequency factor. This second important factor in general indicates the attempt-to-escape frequency of electrons from the localised levels.

The mathematical model takes also into account the occurrence of distributions of localised levels. In case of a Gaussian distribution of localised states a meaningful parameter is the width of the distribution. Numerical simulations, calculated with the proposed model, show that while a first order peak is characterised by an asymmetric peak shape with a steep decreasing side, the second order kinetic peaks are characterised by a more symmetric shape. The signal is smeared along the whole peak temperature range due to the re-trapping effect.

The same theoretical description holds for both techniques, TSL and TSC. However, TSC theory requires the presence of an extended conduction band. During a TSC experiment a driving voltage is applied to the sample and the de-trapped charges are extracted at the device contacts. However, the equations describing a TSC peak are similar to equations describing TSL. Additionally, it is possible to determine the density of the trapping states evaluating the area under a TSC peak.

Simultaneous TSL and TSC measurements give useful information about the localised states combining the best possibilities of both thermal techniques. Unambiguous information about trap depth, density of states, kinetics order and frequency factor can be extract making use of the full possibilities of the combined measurements.

On the other hand the further thermal technique, TSDC, investigates the depolarisation effects on a polymeric material. TSDC peaks are related both to charge release and (if present) to dipole reorientation, where the latter one is caused by motion of polar groups (end groups, side groups, impurities) as well as, at higher temperature, of the polymer backbone of the material under investigation. The depolarisation phenomena are described by a Debye model that leads to equations similar to the first order TSL-TSC de-trapping equation.

In the case of Arrhenius relaxation type a correspondence between the TSDC depolarisation peak and a dielectric spectroscopy peak is established. While dielectric spectroscopy can be carried out both as an isothermal and as a non isothermal technique, TSDC is non-isothermal only. For that reason the two

methods combined can be regarded as complementary. Both study the same phenomena in two distinct domains, the frequency domain the DES and the temperature domain the TSDC.

A DES experiment is conducted applying a sinusoidal signal to a sample kept at constant temperature. The phase shift between the incoming voltage signal and the resulting displacement current signal is then recorded.

The combination of the three temperature domain techniques together with the dielectric spectroscopy investigations in frequency domain gives a more complete description of the depolarisation and de-trapping phenomena in organic materials.

2.1. TSL

Probably the best way to introduce the thermally stimulated luminescence is to give a simple phenomenological definition: TSL is the type of light emission that occurs when an insulator or a semiconductor, previously irradiated by a radiation of appropriated wavelength, is heated.

From the definition it follows that the thermoluminescence is different from fluorescence and can be understood as a sort of long lived phosphorescence. The intensity of the emitted light, generally, is very low and in order to explain it, how we will see in detail in the following, it is necessary to introduce the concept of forbidden gap and to postulate the presence of localised levels inside the gap.

Roughly, we can distinguish between fluorescence and phosphorescence looking at the characteristic time, τ_c of the emission after irradiation. In case of fluorescence such time is very short $\tau_c < 10^{-8}$ s, while a longer characteristic time, $\tau_c > 10^{-8}$ s, characterises the phosphorescence phenomena. In thermoluminescence the characteristic time can be quite large, in the order of minutes, hours and more. The charges, stored at low temperature, stay on their traps and are released only by thermalization due to phonon assisted jumps.

The difference between the two processes can be easily explained in the frame of the band theory.

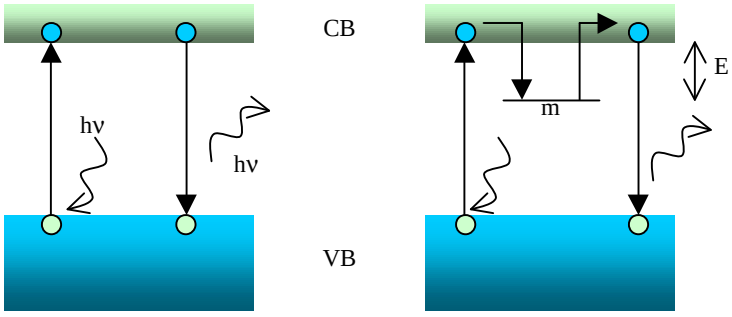

Fig. 2.1 Energy transitions involved in fluorescence a) and thermoluminescence b). Letter m indicates a metastable level, E trap depth, CB conduction band, VB valence band.

While fluorescence involves an energy transition between a singlet excited state and the ground state, the phosporescence involves a further step; a transition to a triplet state, involving a localised level which has a forbidden transition to the ground state. In the localised states the charge carrier can be stored and it delays its backward jump to the ground level.

Figure 2.1 illustrates schematically fluorescence and phosphorescence processes. In fluorescence energy is transferred from an incident radiation to the electron, that is excited from the ground state to an upper one trough the gap. Then the electron returns to the ground state emitting a photon in a time shorter than 10^{-8} s. Like a signature, the process do not show any temperature dependence. Instead phosphorescence involves a metastable level in the band gap. The incident radiation $h\upsilon$ raises an electron to the excited level and subsequently the charge relaxes into a metastable level within the band gap with a forbidden transition to the ground state transition. Here it will stay until it acquires enough energy in order to raise again to the excited level and then to recombine.

Though the trapping and de-trapping mechanism above illustrated is basically the same, the traps can appear in an organic crystal in many different shapes. Shallow traps, that have mostly a structural origin, are characterised by depth $E < 0.03$ eV and by a mean capture time about 10^{12} s. The capture time in this case is larger than the average lattice relaxation time, making a lattice polarisation effect possible followed by a lattice deformation that corresponds to the formation of a molecular polaron.

The formation mechanism of a molecular polaron can be illustrated as follows. A free electron (or symmetrically a hole) can be created ionising a neutral molecule by means of incident radiation of appropriate wavelength. The so created charge polarises the electronic subsystem of the surrounding molecules of the solid. In such a way the energy of the electronic polaron corresponds definitively to the energy of the effective electronic polarisation. The main contribution to the effective polarisation is given by the charge induced dipole and the charge-permanent quadrupole interactions[34]. Then the localised charge carriers produce a vibronic polarisation in the molecule skeleton where the charge is located that propagates also to the nearest neighbours. The result is the formation of relaxed electronic polaronic states that are the so called molecular polarons.

Besides the shallow traps, structural defects can produce also charge carriers localised levels having higher energetic depth. Furthermore, local electronic polarisation variations give rise to local charge carrier trapping states[34] in both cases of shallow or deeper traps that can have quasi continuous energy spectra. The charge carrier trapping states are located in regions of structural irregularities of the organic crystal. Irregularities can have very different origin: unoccupied sites, i.e. vacancies, misalignment of molecules, interstitial molecules, dislocation lines and grain boundaries are all causes of localised states.

The energetic spectra of localised states in organic crystals follow, for statistical reasons, a Gaussian distribution[34]. The quasi-continuous local trapping states can be approximated by a density of states $N(E)$ centred around the distribution maximum at an energetic depth E_m. A Gaussian distribution of states is characterised by the distribution width σ that we will further define in the following of the chapter. For values of $\sigma \to 0$ the distribution reduces to a single level of traps having an energetic depth E_m which can be expressed as a δ distribution function. Also impurity molecules, inserted into the molecular crystal, give rise to localised states. Usually this kind of traps is called chemical traps, while the traps arising from lattice distortions are usually called physical traps.

In a very rough way the presence of an electronic localised state derives from the difference in the electron affinity between the hosting molecular crystal and the introduced chemical impurities. Symmetrically, a hole localised state is determinate by the ionisation energy differences between the host crystal and the impurity. Dopants, that are electron acceptors, typically create trapping states for electrons, while donors can create localised levels only for holes. Furthermore, the presence of a chemical impurity creates a displacement in the original crystal structure, giving rise to further localised states having, indeed, a structural origin. This means that the presence of chemical traps can create also physical traps.

The situation can be complicated because of the simultaneous presence of several kinds of traps having different origin and with different energy distribution spectra. The real trapping and de-trapping dynamics in such case is quite complex. Electrons released from a level of traps have high probability to get re-trapped by a following level before to recombine. The presence of multiple localised levels of different origin definitely increases the probability of multiple re-trapping of a single electron or hole, resulting in rich TSL spectra, sometimes impossible to analyse completely. In this extreme complex case the resulting sum of several levels forms a single very broad peak of TSL, where the underlying single components cannot be distinguished.

Furthermore, an organic solid can contain both electron traps and hole traps. It is not possible with a single experiment to discriminate between the two kinds of traps as well as to discriminate between chemical and physical traps. Almost in all cases it is necessary to compare different samples doped in a controlled way. The TSL thermograms are, in such controlled way, modified and it is possible to connect the developing of a certain peak with the new introduced local level. The comparison and the observation of the induced modifications in the thermograms is a fruitful approach in order to study the origin of a certain level of traps.

Moreover TSL cannot distinguish between hole and electron traps. For that reason in the further discussion we will refer only to one kind of traps, the electron traps, silently assuming that the discussion can be made symmetrically also for localised hole states.

The general description of phosphorescence phenomena was established in the 1935 by Jablonski[67] and the mathematical formalism was subsequently developed by Randall and Wilkins[68] and successfully applied to explain thermoluminescence of many materials.

The mean time τ spent by a charge carrier in a trap at temperature T is given by equation (2.1) where p is defined as the probability per unit time of the release of an electron from the trap.

$$p = \tau^{-1} = s \cdot e^{\frac{-E}{kT}} \qquad (2.1)$$

Here s is a constant that represents the attempt-to-escape frequency of an electron in a trap, E is the difference in energy between the trap level and the band states, called trap depth (see figure 2.1) or activation energy and k is Boltzmann's constant. First consequence of that picture is the exponential temperature dependence of the time spent by an electron in a localised level.

The description of the thermoluminescence processes assumes that there are localised states inside the band gap. The proposed model was primarily developed for crystalline semiconductors and insulators of inorganic materials. In the case of organic compounds it is necessary to distinguish between organic

crystals and amorphous polymers. In case of organic crystals the general description cannot be very different with regard to the inorganic cases. According to theoretical calculations[34] and experimental results[35] the presence of the gap between the valence and conduction band is determined by the crystal periodicity and by the nature of the forces between the interacting organic molecules. In case of polycrystalline samples, the dimensions of the crystallites does not alter the theoretical treatment. The polycrystalline structure just introduces further localised states at the grain boundaries. TSL does not require an applied field to be performed. The recombination process is strongly restricted to a few molecules depending on the density of available recombination centres. In case of a trap density of the order of about $1x10^{16}$ cm^{-3}, typical for several technologically interesting materials[69], it means the presence of one defect per about a single molecule.

In case of well oriented polymer chains and in particular for π conjugated materials, the situation, with respect to a molecular crystal, is not really different. The periodicity of the film structure and the van der Waals forces acting between the chains theoretically and experimentally assures again the presence of bands.

A TSL experiment does not require any applied voltage and, in general, there is no carrier drift over macroscopic distances before the recombination process takes place. In case of amorphous polymers there is a lack in long range order. It is not possible to speak about extended valence and conduction bands. However, the recombination process, in case of geminate couples, can be well localised over a few repeat units. The existence of HOMO and LUMO levels that extend over several repetitive units can provide a solid base in order to interpret the thermoluminescence phenomena in the same theoretical background than for crystalline materials.

Very recently[70] a new model was proposed to interpret TSL glow curves for organic polymers in the frame of the hopping theory developed in the 80s and 90s of the last century by Bässler and coworkers[71]. In the proposed model the optical excitation, generated during the illumination of the sample, can dissociate into both on-chain and off-chain geminate pairs. The on-chain geminate pairs are quite unstable and recombine in a short time. They do not play any active role in thermoluminescence, where the photoexcited sample usually is kept for a certain time, in the order of few minutes, at low temperature before the heating cycle starts.

The of-chain pairs, more stable, are responsible for the delayed photoluminescence. The carriers get trapped in deep localised states during the low temperature energy relaxation time. Then, the carrier random walk is accelerated within the random network of trapping sites insides the coulomb potential well of the geminate pairs when temperature increases. In order to fit the glow curves the authors use a double peaked Gaussian density of states (DOS). The shallow group of hopping sites serves as an effective transport band, while direct jumps between deeper states are essentially considered impossible. In this hopping model the intra-chain carrier motion can be explained only by introducing that narrow band of hopping sites whose density is sufficient to provide a quasi band transport mechanism. According to the model it is possible to measure the width of the Gaussian distribution analysing the shape of the glow curves.

Despite the elegance of the model, the proposed recombination mechanism is not completely clear, e. g. it is not explained how geminate pairs can still be bound after several jumps, and in addition it is

necessary to introduce a second density of localised states, behaving like a quasi de-localised band structure, in order to get a reasonable fit to the experimental curves.

A different approach to the problem of distributed localised states involves the introduction of disorder in a crystalline lattice. With this approach it is possible to describe the rather complex experimental features and to cope also with the broad peaks that are sometimes obtained from TSL measurements.

2.1.1. TSL model

In the following a TSL experiment is described in more detail and the rate equations derived. The sample, in an equilibrium state at room temperature where all the shallow traps are empty, is cooled down to a low temperature. Then, it is illuminated with electromagnetic radiation of a certain energy. The incident radiation excites the electrons from the valence band to the conduction band trough the gap.

In the case of prompt fluorescence the generated electrons recombine promptly. Otherwise they can form an electron hole pair followed by geminate recombination or by dissociation with subsequent trapping. Charge carriers can get trapped in localised levels that, considering the random fluctuation of the potential in disordered materials, are distributed in energy. From statistical consideration, the distribution type should be generally Gaussian. However, different kinds of distributions, in principle, cannot be excluded. The thermal emission from traps at low temperature is negligibly small. Therefore, the perturbed equilibrium created by the incident radiation resists for a long time and the electrons are just stored in the localised levels.

Temperature is then raised in a controlled way, electrons acquire energy and finally escape from the traps by means of a phonon assisted jump and recombine with holes trough a recombination centre where

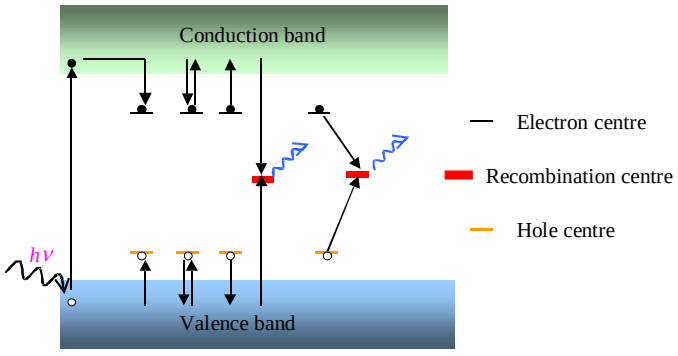

Fig. 2.2 Energy diagram describing the elementary process of the simple model for TSL

recombination occurs with subsequent photon emission. By means of spectrally resolved TSL experiments it is possible to get information about recombination centres studying the wavelength of the emitted light as function of temperature and intensity.

The above described processes are illustrated in figure 2.2. Recombination processes can be both radiative or non-radiative and of course only in the first case we can detect a signal with a photomultiplier.

Non-radiative recombination processes are difficult to identify according to the fact that in such case the energy is dissipated by phonons.

The illustrated scheme for thermoluminescence is simple, but despite of its simplicity it can describe all fundamental features of a thermoluminescence process. Nevertheless, the mathematical treatment can be difficult and the related differential equations stiff. Only with some simplifications it is possible to get analytical equations suitable to provide an approximate solution which serves to fit successfully the experimental glow curves.

Following Chen[16], the electron exchange between the HOMO and LUMO levels, during the trap emptying, can be described by the following three differential equations:

$$\frac{dn_h}{dt} = -n_c \cdot n_h \cdot A_r \tag{2.2}$$

$$\frac{dn}{dt} = n_c (N - n) \cdot A - n \cdot p \tag{2.3}$$

$$\frac{dn_c}{dt} = n \cdot p - n_c (N - n) \cdot A - n_c \cdot n_h \cdot A_r \tag{2.4}$$

Here n_h is the concentration of holes in the recombination centres, n_c is the concentration of electrons in the conduction band, A_r is the recombination coefficient for electrons in the conduction band with holes in the recombination centres, n is the concentration of electrons in traps, N is the function describing the concentration of electron traps at depth E below the edge of the conduction band, A is the transition coefficient for electrons in the conduction band becoming trapped and p is the same probability of thermal release of electrons from traps defined in equation (2.1), which represents in fact their release rate.

Equation (2.2) describes the change of hole density n_h in recombination centres versus time. The recombination rate depends both from the concentration of free electrons (n_c) and from the concentration of holes already present in the recombination centres trough a probability coefficient (A_r) that depends on the cross section and the thermal velocity[72] of electrons. An increase in these parameters results in an increase of the recombination probability.

Equation (2.3) describes the exchange of electrons between conduction band and traps. The first term in the right hand side includes the probability A for an electron to be trapped. That probability A, like A_r, also depend on the thermal velocity of electrons and on the cross section of traps. The second term on the right hand side is the de-trapping term. It is proportional to the concentration of trapped electrons and to the Boltzmann's function, i.e. equation (2.1). The proportionality factor s, often called frequency factor or pre-exponential factor, should be, when interpreted in terms of attempt to escape of an electron from the potential well, in the order of magnitude of $10^{10} \div 10^{14}$ s^{-1}. Actually, in literature, values of several orders of magnitude lower can be found. Such low frequency factors values are generally interpreted in a speculative way taking into account competitive effects simultaneously acting. A saturation effect for carrier release from traps, caused by a limited number of available states in the conduction band, is neglected in this

model. In each moment the number of available states in conduction band is much higher than the released amount of electrons from the localised states.

Equation (2.4) describes the variation of electron density in the conduction band and essentially it takes into account the charge neutrality of the whole system. The variation rate of electrons in the conduction band depends on electrons being released (first term on the right hand side), electrons being trapped (second term), and electrons that recombine (third term). Electrons and holes in that model are generated at the same time (geminate couples), but they are not necessarily still bound. Saturation effects due to filled deeper traps or recombination centres that have already an hole on them are not considered.

Of course, the proposed model is simplified, but this relatively simple picture has the great advantage to allow an analytical solution having a minimum number of parameters. More sophisticated models, probably also not describing in a complete way the complex phenomena happening during the thermal cycle, exist and can be found in literature. Nevertheless, complex models have the disadvantage to introduce an increased number of parameters. Actually, several combinations of too many parameters can generate the same shape of a real glow curve, making impossible to find a most probable fit. For that reason it is preferable to deal with a reasonable simple model that involves few reliable parameters. Actually, the proposed simple model can successfully describe the experimental glow curves, but it is necessary to take also the energetic distribution of localised states into account in order to describe the complex behaviour of disordered systems, like amorphous polymers or organic polycrystalline thin films. In such case the total number of traps is represented by the following equation (2.5). The traps do not have a single activation energy, but they are continuously energetically distributed.

$$N = \int_{E_1}^{E_2} N(E)dE \qquad (2.5)$$

N(E) can be in principle any kind of distribution, but considering the statistical disorder in organic materials it should have a Gaussian shape. In principle also the frequency factor should have the same energetic distribution. In such case there are not further mathematical complications. However, the introduction of a frequency factor distribution increases again the number of parameters; different combination of distribution parameters for *N(E)* and *s(E)* can lead to the same shape for the same experimental glow curve. That approach, in general, is not fruitful and considering that *s(E)* varies slowly[73] respect *N(E)* it is preferable to consider only an energetic distribution of traps having a single average frequency factor *s*.

In order to solve the system of differential equations (2.2)-(2.4), equation (2.6), regarding the time dependence of temperature, should be add.

$$T = T_0 + \beta \cdot t \qquad (2.6)$$

In equation (2.6) β is the experimental constant heating rate. It should be note that as long as *T* is a well know function of the time the only real variable is the time. For that reason it is very important, experimentally, to have a perfect control of the temperature linearity.

The system of differential equations (2.2)-(2.4) can be also easily solved numerically. In this case the number of parameters is still too large. Different combinations[74] of the 7 factors E, s, A_r, A, N, β, n_h, and initial conditions $n_0 = n$ ($t = 0$) and n_c ($t = 0$) = 0 involved, allow several possible fits for the same experimental glow curve shape, but with different shift behaviour concerning e. g. the heating rate.

2.1.2. First order equation

An analytical solution of the equations system is then preferable. However, in order to obtain the solutions it is necessary to introduce two new hypothesis. The first assumption, illustrated in equation (2.7), states that the net rate of density variation for electrons in conduction band is much smaller than the variation rate of concentration of trapped electrons. This is the quasi adiabatic approximation, the free carrier life time is very short due to fast recombination, this means that de-trapping connected phenomena are fast events in the time scale of the conduction band.

$$\left|\frac{dn_c}{dt}\right| << \left|\frac{dn}{dt}\right| \tag{2.7}$$

The second assumption, equation (2.8), states that in each moment during the heating process the concentration of electrons in the conduction band is much smaller than the concentration of trapped electrons, i.e. electrons do not accumulate in the conduction band, but recombine rapidly.

$$n_c << n \tag{2.8}$$

The two statements, in general, enunciate that we are considering fast recombination events and the substantial impossibility of cumulating charges in conduction band. The two assumptions will be further discussed later.

Using the conditions (2.7) and (2.8) it is possible to reduce the system of differential equations (2.2), (2.3) and (2.4) to the single equation (2.9).

$$-\frac{dn_h}{dt} = \frac{n \cdot p \cdot A_r \cdot n_h}{A_r \cdot n_h + A(N - n)} \tag{2.9}$$

The luminescence intensity is directly proportional to the hole density variation in the recombination centre. As temperature rises, electrons are released and the recombination process takes up reducing the concentrations of trapped holes and increasing the thermoluminescence intensity. The electron traps are progressively emptied, the rate of recombination decreases and thus the thermoluminescence intensity, accordingly, decreases producing the TSL peak. According to the above described scenario it is possible to write the following equation (2.10) that states the connection between the intensity of the emitted light and the density of holes in recombination centres.

$$I(t) \propto -\frac{dn_h}{dt} \tag{2.10}$$

Equations (2.9) and (2.10) describe a characteristic TSL peak.

If we assume, after the release of electrons, a negligible re-trapping and a quick recombination process we can write:

$$A_r \cdot n_h >> A \cdot (N - n) \tag{2.11}$$

Inequality (2.11) states that the number of available "free places" in the recombination centres for an electron is much larger than the number of "available traps". The probability for an electron to get again re-trapped is, in such way, negligible.

Using statements (2.7) and (2.11) to simplify equation (2.9) and substituting equation (2.1) we obtain the first order differential equation (2.12).

$$I(T) = -\frac{dn_h}{dt} = n \cdot s \cdot e^{-E/kT} \tag{2.12}$$

Equation (2.12) can be solved with the ordinary integration mathematical methods. Starting from $t = t_0$ and assuming the linear heating rate expressed in equation (2.6), we finally obtain the so called first order kinetic equation for a TSL peak:

$$I(T) = n_0 \cdot e^{-E/kT} \cdot e^{-\frac{s}{\beta}\int_{T_0}^{T} e^{-E/kT} dT} \tag{2.13}$$

At time t_0 all traps are filled and the electrons n are distributed in energy following the same distribution of the traps N between the two energy levels E_1 and E_2 of equation (2.5). Substituting the distribution of localised states (2.5) in the kinetic equation for a TSL peak, we can write the following equation (2.14).

$$I(T) = \int_{E_1}^{E_2} n(E) \cdot e^{-E/kT} \cdot e^{-\frac{s}{\beta}\int_{T_0}^{T} e^{-E/kT} dT} dE \tag{2.14}$$

While Equation (2.13) describes a TSL peak with a single energetic level of traps, equation (2.14) takes into account that the traps are energetically distributed. At low temperature the integral included in the second exponential is very small. The first exponential prevails, the TSL peak increases and reach its maximum. Increasing the temperature T the importance of the integral in the exponential part increases. Then, this competitive negative exponential prevails against the first increasing exponential and it gives a net decrease to zero. The peak dies away.

$$n(E) = \frac{n_m}{\sigma\sqrt{2\pi}} \cdot e^{-\frac{(E-E_m)^2}{2\sigma^2}} \tag{2.15}$$

Equation (2.15) describes the normalised Gaussian distribution of traps used in the numerical simulations of equation (2.14). In this equation n_m represents the maximum concentration of electrons at

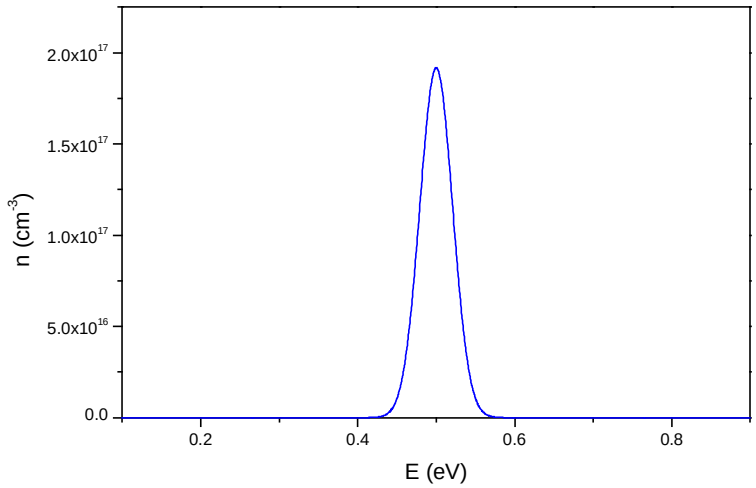

Fig. 2.3 Gaussian distribution with parameters: n_0 = 1x10^{16} cm^{-3}, E_m = 0.5 eV, σ = 0.02 eV.

energy E_m and σ is the constant describing the width of the distribution. Bigger σ wider the distribution, σ can be see like a measure of the broadening of the localised state distribution.

Of course *n(E)* can be, in principle, any kind of distribution. Because of the previously discussed stochastic nature of trap levels in organics, we turned our attention especially on Gaussian distributions.

Figure 2.3 shows the Gaussian distribution of states, relative to equation (2.15), employed for the simulations. The simulation parameters, n_0 = 1x10^{16} cm^{-3}, E_m = 0.5 eV and a small σ = 0.02 eV, produce a Gaussian curve characterised by a very narrow peak. However, the same parameters producing such a narrow peak are adequate in order to produce important changes in the shape of the first and, how we well see, in the second order glow curves.

The following figure 2.4 compares a simulated glow curve, having a single energy level of traps described by equation (2.13), with a simulated curve that includes the Gaussian distribution of localised states of equation (2.14). Clearly, the presence of the distribution broads[75] the peak and slightly changes its shape. Even though both simulations shown in figure 2.4 have the same parameters, we observe a slightly shift of the maximum. While the peak temperature maximum T_m in case of a first order equation with a single level is at T_m = 183 K, the maximum, in case of a first order having Gaussian distributed states, is at T_m = 181 K.

Like expected, also for a quite small distribution having σ = 0.02 eV, the Gaussian distributed simulated peak results broader respect to the peak having only a single level of traps, but it should be note that such peak keeps the characteristic asymmetric shape. The complete list of parameters used for generate the two curves is the following: n_0 = 1x10^{16} cm^{-3}, E = 0.5 eV, T_0 = 140 K, T = 210, β = 0.1 K/s, s = 1 x 10^{12} s^{-1} and for the Gaussian distribution: σ = 0.02 eV, n_m = 1x10^6, E_m = 0.5 eV with integration limits E_1 = 0.4 eV and E_2 = 0.6 eV.

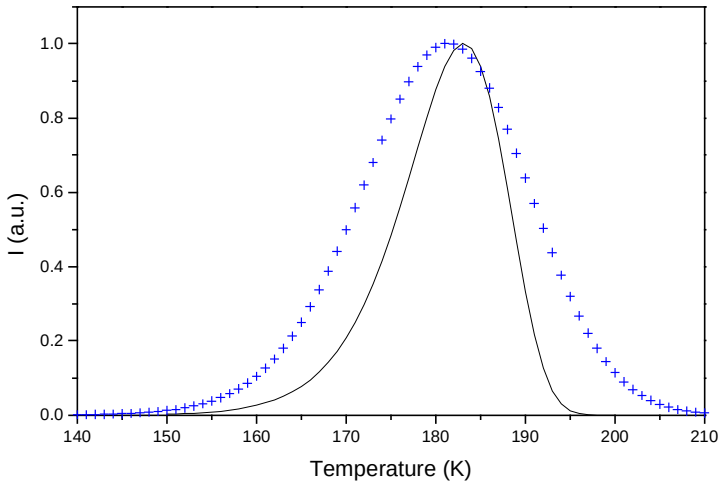

Fig. 2.4 Comparison between the first order equation (2.13) (black line) and the Gaussian distributed first order equation (2.14) (scatter blue line). Simulation parameters: n_0 = 1x10^{16} cm^{-3}, E = 0.5 eV, T_0 = 140 K, T = 210 K, β = 0.1 K/s, σ = 0.02 eV, s = 10^{12} s^{-1}, n_m = 1x10^{16} cm^{-3}, E_1 = 0.4 eV, E_2 = 0.6 eV and E_m = 0.5 eV.

2.1.3. Second order equation

A different and, somehow, opposite way that we can go trough in order to obtain an analytical solution of equation (2.9) is to assume a strong re-trapping effect. The condition, stated with inequality (2.16), means that electrons before to recombine can be re-trapped several times.

$$A_r \cdot n_h << A \cdot (N - n) \tag{2.16}$$

$$n << N \tag{2.17}$$

Using together inequalities (2.16) and (2.17), that establishes the concentration of trapped electrons is much less than the concentration of traps, i.e. free traps are always available, we can write down the second order differential equation (2.18).

$$-\frac{dn_h}{dt} = \frac{n^2 \cdot p \cdot A_r}{AN} \tag{2.18}$$

Using equation (2.1) and stating the condition (2.19) that defines the pseudo frequency factor *s'*

$$\frac{A_r}{A \cdot N(E)} s = s' \tag{2.19}$$

we can write the so called second order kinetic differential equation (2.20).

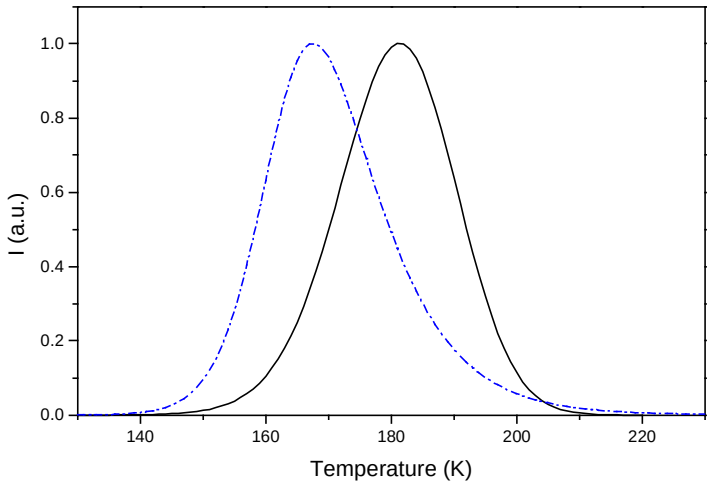

Fig. 2.5 Comparison between the peaks calculated by the Gaussian distributed first order equation (2.14) (black line) and the Gaussian distributed second order equation (2.22) (dashed blue line). Simulation parameters like in figures 2.4 and 2.6.

$$I(T) = -\frac{dn_h}{dt} = n^2 \cdot s' \cdot e^{-E/kT} \tag{2.20}$$

The solution of equation (2.20) is the second order kinetic expression (2.21) describing a TSL peak with a single level of traps subject to strong re-trapping effect.

$$I(T) = \frac{n_0^2 s' \cdot e^{-E/kT}}{\left(1 + \frac{n_0 \cdot s'}{\beta}\int_{T_0}^{T} e^{-E/kT} dT\right)^2} \tag{2.21}$$

Like in the case of the first order equation, it is necessary to introduce the statistical distribution of traps. The localised levels follow a certain energy distribution *n(E)* that replaces the initial concentration of trapped electrons. We obtain the total number of trapped states integrating the distribution over the two levels of energy E_1 and E_2. The second order equation for disordered materials is, then, the following equation (2.22).

$$I(T) = \int_{E_1}^{E_2} \frac{n(E)^2 \cdot s' \cdot e^{-E/kT}}{\left(1 + \frac{n(E) \cdot s'}{\beta}\int_{T_0}^{T} e^{-E/kT} dT\right)^2} dE \tag{2.22}$$

With respect to the first order kinetic, the photon emission during the TSL peak in this case is somehow delayed; a longer tail on the high temperature side of the peak is expected to appear.

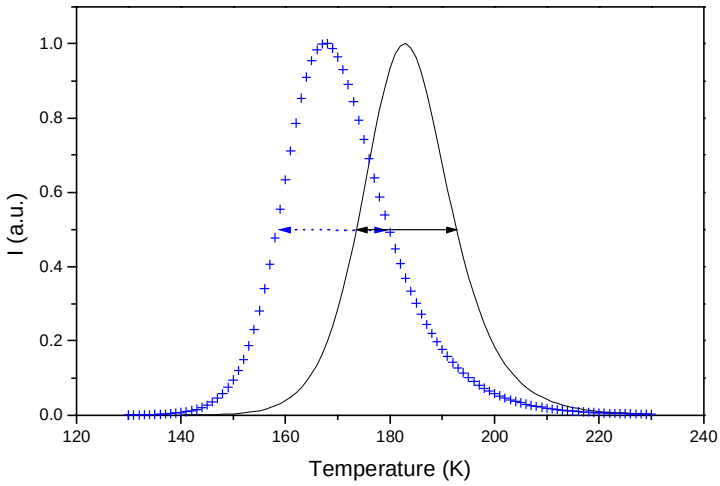

Fig. 2.6 Comparison between the peaks calculated with the second order equation (2.21) (black line) and the Gaussian distributed second order equation (2.22) (scatter blue line).
Simulation parameters: n_0 = 1x10^{16} cm^{-3}, E = 0.5 eV, T_0 = 130 K, T = 230 K, β = 0.1 K/s, σ = 0.02 eV, s' = 1x10^{-4} cm^3 s^{-1}, n_m = 1x10^{16} cm^{-3}, E_1 = 0.4 eV, E_2 = 0.6 eV and E_m = 0.5 eV. The arrows indicate the width at half maximum height.

Figure 2.5 shows a comparison between the TSL peaks produced by equation (2.14) and (2.22) with the same Gaussian distribution of traps given in equation (2.15). A large temperature shift appears between the two peaks. While the first order peak has the maximum at T_m = 181 K, the second order has its maximum at T_m = 168 K. This situation is quite different with respect to the first and second order simulated curves without a distribution (equations (2.13) and (2.21)). Both peaks, simulated with this equations, have the peak maximum at T_m = 183 K. This fact indicates that the presence of a distribution of traps strongly influences the dimensions as well as the position of a second order peak. Furthermore, the second order peak is more symmetric with respect to the first order one and, always with respect to the first order, its shape results even larger.

The TSL emission in the second order equation is distributed all long the temperature range of the peak, otherwise the first order, where more light is concentrated in the increasing part, followed by a suddenly intensity decrease. The second order curve shows on the high temperature side a longer tail. The light intensity is better distributed along the peak because of the effect of the electron re-trapping.

Figure 2.6 shows a comparison between the peaks calculated with the second order equations (2.21), that has a single level of energetic traps, and (2.22) that includes a Gaussian distribution of localised levels. The presence of the trap distribution changes the shape and the position of the peak considerably, giving to it a typical signature[76]. The shift in the maximum of the glove curve is much more pronounced with respect to the first order case. The second order equation (2.20) has the peak maximum at T_m = 183 K, while the second order having Gaussian distributed states has its maximum at T_m = 168 K, a much lower temperature with a difference of 15 K.

The arrows in figure 2.6 indicate the width of the two curves at half maximum height. The second order Gaussian peak has a width at half maximum height of 21.6 K, while the second order with a single level of traps has a smaller width of 19.5 K, with 2.1 K of difference. Again, like in the first order case, the distribution affects the width of the glow curve, expanding it of about 2 K, under the same parameters conditions.

Using only equations (2.21) and (2.22) it is not possible to determine directly the frequency factor *s*. According to equation (2.19) it is possible only to infer an approximated quantity depending on the ratio A_r/A, generally unknown. Anyhow, it is possible to deduce the order of magnitude of *s* supposing that the recombination coefficient-trapping coefficient ratio is equal to 1. In that case the pre-exponential factor can be estimated knowing the total density of traps *N*. In the simulations of figures 2.5 and 2.6 we set the ratio $A_r/A = 1$ and the total density of traps equal to the initial density of electrons in the traps, i.e. we suppose a completely filled initial state. This last condition usually keeps under real experimental conditions, when we take care to fill completely the traps, shining the sample for an adequate time.

The derivation of equations (2.14) and (2.22) is possible only with the help of two important approximations. In their general form the rate differential equations, how we already underlined, are not integrable. The first approximation, related to equations (2.7) and (2.8), can be see like a quasi-equilibrium approximation. It ignores electrons in conduction band relatively to the number of trapped electrons. This approximation involves, of course, a lack in universal validity[77].

The second approximation is the so called kinetic order approximation and it is related to equations (2.11), (2.16) and (2.17). Both approximations are questionable, leading to an error on the analysis of a real TSL glow curve. However, like already mentioned without such approximations it is not possible to obtain any analytical solution of the rate differential equation system. Furthermore, the number of parameters that must to be take into account during the direct numerical analysis of the differential equations is to high in order to give an unambiguous solution. It is proof[77] that the quasi-equilibrium assumption makes the analytical solutions valid only in case of values of $N > 10^{12}$ cm^{-3}.

In principle it is possible also to overtake the kinetic order and the quasi equilibrium approximation introducing at their place two new functions[78]. This approach leads to a parameterised new general first order equation that could be used for computer based fitting procedures. This more general equation contain six parameters, too many for any unambiguous fit. In order to reduce the number of parameters it is necessary anyway to introduce new approximations and we are back again at the starting point! However, the study on parameterised equations demonstrates, in case of first order, that the quasi equilibrium approach is very good and it leads always to excellent results[78] with negligible errors on the energy depth estimation.

Moreover, we should remark here that it is anywise necessary to make some assumptions on the system under examination before to perform any kind of analysis about the physical phenomena that we are considering. Each approximation introduces an error that affects the exact knowledge of the physical quantities we are looking for. In such a way we have only an estimation and not the true value of a physical quantity, intending for “true” a value not affected by errors. Such “true” value of a physical quantity, sometimes, does not exist at all. Without any hypothesis on the system under investigation it is simply not possible to reach any univocal conclusion.

The ability to extract information regarding the trapping parameters when all the observable properties depend on several variables is really challenging. However, there is a remarkable exception, the traps depth E can be obtained, under certain strict experimental condition, that we will see in the next chapters, by means of the "initial rise" method independently of the other parameters.

Part of the chapter 3 will be devoted to further analysis of equations (2.14) and (2.22), with different kinds of distributions. There the differences with respect to the Gaussian distribution will be further discussed by means of numerical simulations performed with the help of a personal computer.

2.2. TSC and simultaneous measurements

A thermally stimulated current peak can be explained by means of the same mechanism governing TSL. We define TSC the increase of conduction dues to charges thermally released from localised levels when the sample is heated under an appropriate applied voltage. Like for TSL, the effect can be observed only when the sample is properly excited at low temperature by means of a light of appropriated wavelength or by an electric field.

The electron release mechanism from the traps is like the one illustrated in figure 2.2. Instead of the light, generated by the recombination with the holes in the recombination centre, we collect the de-trapped free electrons running in the conduction band and driven by an applied external electric field. The conductivity is expressed by the following equation (2.23).

$$\sigma = e \cdot \mu \cdot n_c \qquad (2.23)$$

Here e is the elementary charge, μ is the electron mobility and n_c is again the concentration of free electrons in conduction band. In order to write equation (2.23) it is necessary to make three major assumptions:

a) Homogeneity, we postulate that the sample is perfectly homogeneous.

b) Absence of space charges.

c) Absence of minority carriers; the devices under investigation is monopolar.

The discussion can be symmetrically made for both holes or electrons. Assuming the electron mobility has a small dependency with respect to the temperature T, i.e. μ does not change significantly during the glow peak development, the TSC peak is described by the temperature dependence of the density of free electrons in conduction band n_c (T). Using equation (2.2), (2.3) and (2.4), making the same approximations and taking into account that the life time of the carriers in the conduction band is constant, i. e. the concentration of holes in the recombination centre is constant, it is possible to obtain a first order equation equivalent to the one obtained for a TSL peak.

However, with respect to a TSL experiment, because of the presence of the contacts, we are not measuring only the sample, but the whole system conductance, which includes the contact effects. Furthermore, the preparation of a metallic contact on the top of an organic film introduces at the interface metal/organic new localised states.

TSC measurements are widely used in order to determine the density and energy distribution of traps. While by means of TSL experiments is not possible to measure the density of traps, a TSC peak provides this information, integrating the current density *J* over time. In that way it is possible to estimate the density of released charge and knowing the volume of the sample it is possible to estimate the average trap density related to each peak.

$$\int_{total} J dt \leq e \cdot N \tag{2.24}$$

Equation (2.24) gives the lower limit of the trap density. If a TSL experiment is simultaneously performed with the TSC, it is possible to proof the condition of validity of the quasi equilibrium approximation related to equations (2.7) and (2.8).

In a TSC experiment the detected current strongly depends on the transport properties of the material under investigation. The conventional TSC model was developed in the frame of the band theory. It exist an alternative model[16] that assumes a hopping model for charge carriers. The electron (hole) moves by thermally assisted tunnelling from one localised state to another one. The model allows to derive information on the thermally activated mobility of the electrons. The peak position depends on the applied field and sample thickness. However, measurements on samples of PPV show an unexpected independence of the TSC peak position from the sample thickness. For that reason these measurements were interpreted in the frame of the band theory[79].

Simultaneous TSC and TSL measurements give more reliable information on the de-trapping and recombination kinetics of carriers. Lewandowski and co-workers[78] found an analytical solution of the differential equation system (2.2), (2.3), (2.4) improving the understanding of the quasi equilibrium approximation by the introduction of a quasi equilibrium function. The analytical solution in case of simultaneous TSL and TSC experiments contains one term whose effect explicitly depends on these approximation validity. Moreover an expression that enable to extract the energy trap depth in the case of first order kinetics without making usage of the quasi equilibrium approximation is obtained.

The following equation (2.25) implicitly defines a quantity *E'* that depends on the position of the TSC peak.

$$\frac{E'}{k}\left[\frac{1}{T^2}-\frac{1}{T_{\max}^2}-e^{\frac{E'}{k}\left(\frac{1}{T_{\max}}-\frac{1}{T}\right)}\right]=\frac{d\ln I_{TSC}(T)}{dT} \tag{2.25}$$

The TSC peak maximum temperature is T_{max}, while I_{TSC} is the maximum peak intensity. The equation can be numerically solved with the help of a personal computer. The trap depth *E* is equivalent to the value of *E'* of the TSC peak maximum $E = E'(T_{max})$.

The system, developed by Lewandowski, uses only few experimental points and considers the frequency factor dependence from temperature. This dependency normally is not contemplated with other analysis methods.

$$E = kT_{\max} \ln\left(\frac{s(T_{\max}) k T_{\max}^2}{\beta E'(T_{\max})} \right) \qquad (2.26)$$

Tests made on theoretical TSC and TSL curves[78] show that such analysis method is very reliable, providing excellent results with errors on the estimated energy values of about 1%. The major limitation is its validity only in case of a first order kinetic curve. Moreover, to perform simultaneous TSL and TSC measurements is required. However, the simultaneous measurements approach provides an useful test in order to obtain full information about not only the traps depth, the trap energetic profile, but also about the density of states with a degree of reliability not possible using the two thermal techniques, TSL and TSC, separately.

2.3. TSDC and DES

Besides the de-trapping phenomena that can be studied by means of experiments, TSL and TSC, polymers have also various types of molecular relaxation. At low temperature local movements of molecular groups, for example rotations, are possible, while at higher temperatures whole segments become mobile. Then, increasing the temperature, the main chain becomes flexible and the polymer becomes rubbery reaching its glass temperature. TSDC can check the activation energy of dipolar rotations (molecular mobilising), of main chain mobilisation and the glass transition temperature.

In a typical TSDC experiment a sample is polarised at high temperature by means of an electrical field in the order of 10^5 V/cm. Then, it is cooled down at liquid nitrogen temperature. During the cooling, by effect of the applied field, the dipoles of the polymer are oriented. At low temperature the field is switched off, the sample is short circuited over a sensitive picoammeter and after a certain time of storage at low temperature, in the order of several minutes, when all the electrical transients are gone, the sample is heated in a controlled way and the short circuit current recorded in function of temperature.

The aim of a TSDC experiment is to deduce from the obtained thermograms those kinetic parameters which determinate a specific charge release. The theoretical treatment of the discharge current arising from a polarised sample assumes that there is not current coming from the release of trapped electrons or holes. The dipolar polarisation in such case is considered space independent. Unfortunately, space charge and dipolar polarisation coexist in real samples and with a single experiment of TSDC it is impossible to distinguish between peaks rising from de-trapping of charge carriers and peaks having a depolarisation origin. However, it can append that the energetic distribution of localised charges is broad and almost homogeneous along the sample. In such case the dipolar peaks are well recognisable when an experiment is performed, standing out over the steady current increase due to the de-trapping effect.

After removing of the external field two competitive effects are responsible for the appearance of a TSDC peaks. On one side the dipoles are oriented because of the internal dielectric field due to the fixed space charges, on the other hand the thermal motion acts randomising the dipoles. Following the work of J. Vanderschueren and J. Gasiot[73] and the excellent work of J. van Turnhout[80] it is possible to describe the polarisation and the depolarisation phenomena as follow.

Assuming a Debye model the polarisation building *P* can be described by the exponential function of time (2.27).

$$P(t) = C \cdot \left(1 - e^{\frac{-t}{\tau}} \right) \tag{2.27}$$

In equation (2.27) an ideal rotational friction model is assumed, *C* is the equilibrium polarisation constant and τ is the dipolar relaxation time. During a TSDC experiment the dipoles are disoriented with a rate that can be described again by means of the Debye model. Then, considering an identical polarisation and depolarisation relaxation time, equation (2.28) describes the depolarisation decay.

$$P(t) = C \cdot e^{\frac{-t}{\tau}} \tag{2.28}$$

The density of the current generated during the decay is described by equation (2.29).

$$j(t) = -\frac{dP(t)}{dt} = \frac{P(t)}{\tau} \tag{2.29}$$

The current density *J(t)* in equation (2.29) is function of time. However, when a TSDC experiment is performed there is a well known dependency between time and temperature. Assuming the linear heating rate, like for a TSL experiment, of equation (2.6), with the heating constant parameter β, it is possible to write the Debye rate equation (2.30).

$$P(t) = C \cdot e^{-\int_0^t \frac{dt}{\tau}} \tag{2.30}$$

Finally, integrating equation (2.30) we obtain expression (2.31) describing a TSDC current peak.

$$j(T) = \frac{C(T_p)}{\tau_0} \cdot e^{-E/kT} \cdot e^{\frac{-1}{\tau_0 \beta} \int_{T_0}^{T} e^{-E/kT} dT} \tag{2.31}$$

In equation (2.31) the variation of τ as a function of temperature is given by the Arrhenius type law (2.32) equivalent to equation (2.1) describing the probability of an electron to be released from a trap.

$$\tau(T) = \tau_0 \cdot e^{\frac{E}{kT}} \tag{2.32}$$

In equations (2.31) and (2.32) τ_0 is the relaxation time at infinite temperature, it corresponds to the inverse of the natural relaxation frequency α. The activation energy for the dipolar disorientation is given by *E*.

Equation (2.31), describing a simple relaxation current peak, is totally similar to equation (2.14) for a first order kinetic thermoluminescence peak. Like the similar TSL equation (2.14), it gives a typical asymmetric curve. The first integral dominates the initial part of the peak. At higher temperature the exponential part dominates and the signal drops.

The experimental data can be fitted assuming a minimum number of Arrhenius like peaks, having each a single activation energy and a single natural frequency, or introducing a distribution function of relaxation times and activation energy. The existence of relaxation time distributions can be explained, in polymers, by means of several mechanism like dipole-dipole interactions or internal anisotropy. Furthermore, polymers have several possibilities of twisting, bending and entangling of the side chains as well as, at higher temperature, of the main chain. Nevertheless, the simpler approach, i.e. the combination of single peaks, gives excellent results fitting a real TSDC thermogram.

The simple equation (2.31) describes a TSDC peak far from the glass region. In this special case different phenomena, related to changes in the free volume, take place. An approach to the problem is described by Schrader[81]. In his analysis a non exponential decay in the time dependent kinetic is proposed. The time dependence is a result of the combination of cooling down in the glass region, as the polarisation is frozen-in and the subsequent heating when the variation of the current density is recorded. Schrader's approach allows a qualitative description of the evolution of the TSDC spectra also in the high temperature region of the thermograms.

Compared with dielectric spectroscopy it is well known that TSDC has a higher resolution and sensitivity. In a conventional DES experiment the dielectric constant ε^* is measured as a function of the frequency at various temperatures. The frequency varies for several orders of magnitude between $1x10^1$ Hz to $1x10^6$ Hz. The equivalent frequency of a TSDC experiment is lower, ranging typically between $1x10^{-3}$ Hz and $1x10^{-2}$ Hz. As a result of the lower TSDC working frequency the relaxation peaks are located at lower temperature, while the equivalent DES peaks often are located in inaccessible temperature ranges.

A suitable way in order to facilitate the interpretation of the results coming from the thermal technique is to establish a theoretical correlation between DES and TSDC measurements. The two techniques are different in a fundamental point, while TSDC is a non-isothermal technique in which time and temperature vary according to a well known law, DES is an isothermal technique. The measurements are done at constant temperature and the frequency is the varying parameter. For that reason the two techniques can be regarded as complementary.

In a DES experiment a sinusoidal signal is applied to the sample. The dipoles attempt to follow the frequency, but because they cannot respond to the voltage changes instantaneously a phase shift between the applied voltage and the system response is recorded. The signal coming from a dielectric material can be described by the complex dielectric constant ε shown in equation (2.33).

$$\varepsilon = \varepsilon' - i\varepsilon'' \tag{2.33}$$

The real part and the imaginary part of the above expression depend upon temperature and applied frequencies trough the Debye equations (2.34) and (2.35)

$$\varepsilon' = \varepsilon_\infty + \frac{\Delta\varepsilon}{1+\omega^2\tau^2} \tag{2.34}$$

$$\varepsilon'' = \Delta\varepsilon \frac{\omega\tau}{1+\omega^2\tau^2} \tag{2.35}$$

The quantity $\Delta\varepsilon$ describes the relaxation strengths trough the following equation (2.36).

$$\Delta\varepsilon = \varepsilon_0 - \varepsilon_\infty \tag{2.36}$$

In the above equations ε_0 indicates the dielectric constant at low frequencies (static limit), while ε_∞ is the dielectric constant at high frequencies, the so called optical limit, and ω is the applied angular frequency.

We can impose the equivalence (2.37) between the relaxation peak maximum and the TSDC current peak maximum.

$$\varepsilon''_{\max} \cong j_{\max} \tag{2.37}$$

The maximum condition for the imaginary part of the dielectric complex constant can be found differentiating equation (2.35) with respect to the applied frequency.

$$\frac{\partial\varepsilon''}{\partial\omega} = \Delta\varepsilon\left[\frac{\tau\cdot(1+\omega^2\tau^2)-\omega\tau(2\omega\tau^2)}{(1+\omega^2\tau^2)^2}\right] = 0 \tag{2.38}$$

$$\tau + \omega^2\tau^3 - 2\omega^2\tau^3 = 0 \tag{2.39}$$

The condition for the equivalent maximum is then equation (2.40).

$$\omega_{\max} = \frac{1}{\tau} \tag{2.40}$$

Based on equation (2.40) it is possible to write the maximum for the dipolar relaxation time τ_{max} by means of equation (2.41)

$$\tau_{\max} = \tau_0 \cdot e^{\frac{E}{kT_m}} = \frac{1}{\omega} \tag{2.41}$$

Solving equation (2.41) we find the temperature maximum in case of a dielectric peak (2.45)

$$\ln\tau_0 \cdot e^{\frac{E}{kT_m}} = \ln\frac{1}{\omega} \tag{2.42}$$

$$\frac{E}{kT_m} = \ln\frac{1}{\omega} - \ln\tau_0 = \ln\frac{1}{\omega\tau_0} \tag{2.43}$$

Using condition (2.40) and (2.41) we can write

$$\frac{E}{kT_m} = \ln\frac{\omega_0}{\omega} \tag{2.44}$$

Then, the expected temperature maximum in case of a dielectric peak is expressed by means of the following equation (2.45)

$$T_m = \frac{E}{k \ln \frac{\omega_0}{\omega}} \tag{2.45}$$

In equation (2.45) ω indicates the applied angular frequency while ω_0 is the frequency factor of the dielectric peak under investigation.

Equation (2.45) allows to determine the temperature range around the T_m value to be analysed in order to verify whether the n-peak in TSDC spectra has a dipolar nature. The value ω indicates the expected frequency maximum for the DES peak and can be fixed at $1x10^4$ Hz, in the middle of the instrumental range. The quantity ω_0 indicates the natural frequency factor of both the TSDC and the ε'' peak. This value can be easily calculated from the numerical analysis of the TSDC curve.

The thermally stimulated technique has a higher resolution with respect to the dielectric spectroscopy. For such reason the absence of a DES peak in the calculated equivalent temperature does not mean that the TSDC peak does not have a dipolar origin. Further analyses are necessary in order to verify such hypothesis. A further problem arises from the fact that DES peaks are expected at higher temperature. Well resolved TSDC peaks often have their DES equivalent at too high temperature which is beyond a temperature where the sample could be destroyed. For such reason they are inaccessible with DES measurements and then it is impossible in that way to verify the hypothesis of a dipolar peak.

On the other hand the maximum condition for a TSDC peak can be derived as follow. Considering equation (2.29) and its derivative (2.46) we can write

$$\frac{dj}{dt} = 0 = \frac{d^2P}{dt^2} = -\frac{d}{dt}\left(\frac{P}{\tau}\right) \tag{2.46}$$

From equation (2.46) according to van Turnhout[82] it is possible to verify that the current maximum occurs at

$$\frac{d\tau}{dt} = -1 \tag{2.47}$$

or equivalently:

$$\frac{d\tau}{dT} = -\frac{1}{\beta} \tag{2.48}$$

Based on equations (2.47) and (2.48) it is possible to demonstrate that the maximum condition for a TSDC Debye peak can be expressed by means of the following equation (2.48)[83].

$$T_m = \frac{E}{k\left(\ln \frac{E}{\beta \tau_0 k} - 2C\right)} \tag{2.49}$$

Here C is an approximately constant value in the range of interest for temperature and energy of the TSDC peaks. Its value is $C \approx 3.5$

Comparing equations (2.48) and (2.45) we can find the dependence of the frequency maximum ω, in case of a dielectric peak, with respect to the activation energy, and the heating rate, equation (2.49).

$$\omega \cong 10^3 \frac{k}{E} \beta \qquad (2.50)$$

This equation assigns an “equivalence frequency” to the TSDC experiment which depends on the heating rate and also on the material parameters like the mean activation energy of the relaxation process.

3. Glow curve analysis

Studying real thermograms the main problem is to obtain the highest number of reliable and useful information from the shape of an experimental peak. In the past, many experimentalists coped with such problem and several methods have been developed in order to analyse the experimental TSL, TSC and TSDC glow curves. All the developed methods can be roughly divided in two major families; the methods based on the curve shape and the methods based on some special points of the thermograms.

One of the most reliable and popular method, the initial rise method, belongs to the second category. Using the experimental points of a TSL, TSC or TSDC peak in the initial rise region, it provides fundamental information about the energy depth of a localised level of traps, independent of the other parameters, like the kinetic order or the frequency factor, governing the thermal curves.

On the other hand curve fitting belongs to the category of methods based on the whole curve shape. The numerical solution of TSL equations of first and second order permits to fit the experimental glow curves. In this case all the experimental points of a peak are equally important and all parameters are simultaneously involved in the fitting procedure, including the parameters governing the distribution of localised states, like the distribution width or the distribution type.

Because of the fact that multiple parameters are varying simultaneously, it is advisable to analyse the experimental peaks by means of different methods in order to compare the results and in such way to obtain more reliable numbers.

The dependence of the peak shape from the sensitive parameters of the rate equations is studied in more detail in the following, through numerical simulations of first and second-order kinetic equations derived in the previous chapter. Different kinds of trap distributions are take into account and their differences are also discussed.

A Gaussian distribution can be regarded as an universal distribution. Adjusting its parameters σ, that represent the distribution width, E_m, the distribution central value and the integration limits E_1 and E_2, it is possible to obtain glow curves having an exponential like distribution or even a quasi continuos distribution shape.

Simulations show how it is possible to get fundamental information about energy depth, frequency factor and the trap distribution parameters from different experimental shapes of the peaks.

3.1. Techniques for glow curve analysis

The main goal in the analysis of thermally stimulated curves is to extract the parameters concerning the localised states. The trap depth *E*, the frequency factor *s*, the kinetic order and, in case of presence of a trap distribution, the distribution shape and the related parameters are very important factors in order to understand the nature of localised states.

One of the most popular and reliable technique used to extract information about the trap depth only is the initial rise method, proposed first time by Garlick and Gibson in 1948[84]. Looking to equations (2.14) and (2.21), immediately it is possible to recognise that the value of the integral part of the equations

depending on temperature *T*, is a very small number when the sample starts to be heated. If we suppose that the density of trapped carriers *n* is approximately constant, it is possible to write the following approximate equation (3.1).

$$I(T) = c \cdot e^{-E/kT} \qquad (3.1)$$

Here *c* is a constant comprehensive of all other parameters slowly changing with temperature. Equation (3.1) is always valid it is not important whether the traps are energetically distributed, and it is also independent of the recombination kinetic order.

According to equation (3.1) the plot of the logarithm of the intensity versus the inverse of the temperature gives a straight line with slope *–E/K*. From that slope the activation energy *E* is immediately calculated. The important assumption is that the trapped carriers concentration *n* is still approximately constant up to a certain critical temperature T_c, i. e. few carriers have been de-trapped. Beyond T_c the approximation is not anymore valid and the error on the calculated *E* increases. The major drawback of the technique is that all useful points, where the assumption *n* = constant is valid, lie on the worst part of the glow curve; at the beginning of the peak. Often it coincides with the starting point of the thermogram. There, small oscillations of the heating rate that can affect the peak shape are often observed.

In other cases the complex structure of a glow curve is composed of several peaks not well resolved. In such cases it is not possible to apply directly the method because of the different trap level energies influencing the initial rise. A useful approach generally used to overcome the problem is to “clean” the peaks. The so called partial cleaning procedure consists of several cycles of sample heating and cooling. The sample is heated up until the previous neighbouring peak is completely erased. In such way its trap levels are emptied while temperature reaches a certain level beyond the peak maximum. The sample is then rapidly cooled and a new heating cycle starts. The secondary peak, that was partially hidden from the previous one, appears entirely.

After the partial cleaning procedure it is possible to apply the initial rising method to each resulting cleaned peak. Nevertheless, the procedure, also if it seems to be straightforward, requires attention in the practical application. It is quite difficult to determine the end of a peak and the beginning of the next one. The arbitrary choice of the inversion point strongly affects the calculated initial rise energy value. In effect, because of the overlapping of two peaks, a certain amount of electrons coming from the first peak, when it is not completely cleaned, can effect the second peak on the sensitive region of the initial rise, charging the calculated energy with an error difficult to estimate.

An improved version of the partial cleaning procedure is the maximum temperature recording technique. The sample is excited, like in the usual procedure, at low temperature. Then a small thermoluminescence cycle starts up to an intermediate temperature called T_{stop}. The sample is rapidly cooled and reheated, and at this time the whole glow curve is developed. The position of the first maximum T_m is then recorded. The heating rate is for each cycle exactly the same.

The procedure is repeated several times slightly increasing the stop temperature, obtaining a set of values T_m versus T_{stop}. By means of such procedure the trap population changes, the number of trapped electrons diminishes during each cycle. As a matter of fact the position of the peak maximum, in case of a

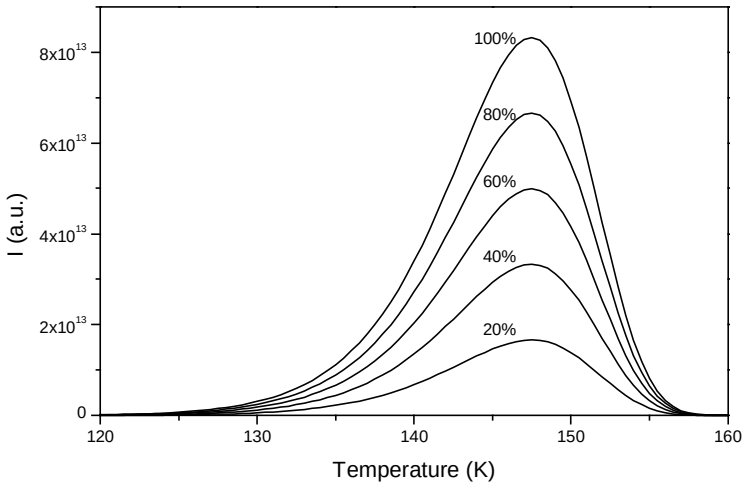

Fig. 3.1 TSL calculated first order glow curves for different initial filling densities. Simulation parameters: n_0 = 1x10^{16} cm^{-3}, E = 0.4 eV, β = 0.1 K/s and s = 1x 10^{12} s^{-1}.

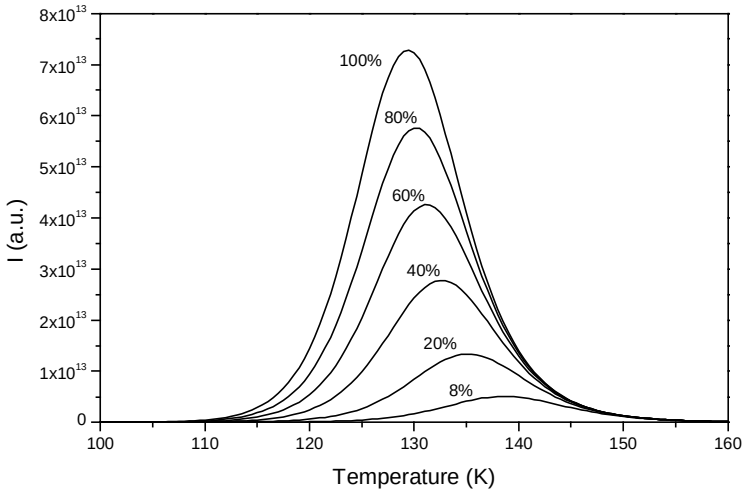

Fig. 3.2 TSL calculated second order glow curves for different initial filling densities. Simulation parameters: n_0 = 1x10^{16} cm^{-3}, E = 0.4 eV, β = 0.1 K/s, N = 1x10^{16} cm^{-3}, s = 1x 10^{14} s^{-1} and A_r/A = 1.

single trap level, does not change or changes very slowly for the first order kinetic and the second order kinetic, respectively, as shown in figures 3.1 and 3.2.

Figure 3.1 shows a first order kinetic glow curve with a single level of localised states in function of different trap filling that simulates the gradual trap emptying obtained by mean of the above explained thermal cycles. The position of the peak maximum does not change, though, the relative intensity of the peaks changes dramatically.

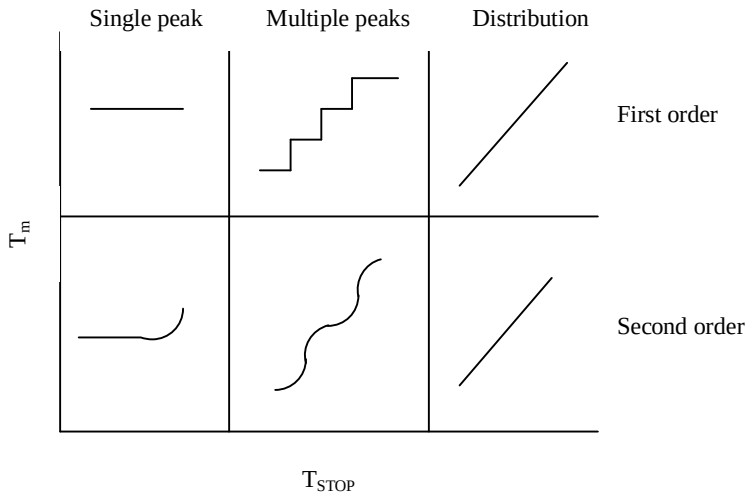

Fig. 3.3 Expected curves T_m - T_{STOP} shape method for first order and second order kinetic, in the case of a single, multiple peak or a distribution of traps. (Adapted from McKeever [85]).

Figure 3.2 shows how the peak evolves in function of trap filling in case of the second order equation (2.14). The position of the peak maximum changes slightly and it is necessary to take into account this small effect applying the technique.

T_m-T_{stop} method is simple and reliable. It gives useful information about composition of the peak, order of kinetic and eventual presence of a continuos distribution of traps.

According to McKeever[85] figure 3.3 shows the expected shape of the T_m versus T_{stop} graphs. Different possible cases are illustrated. The presence of several peaks, in a first order curve, is highlighted by a staircase shaped graph. The same graph has a smoother staircase shape in case of a second order kinetic equation. A straight line appears when a single peak of first order is present, while for a second order single peak an up-going line suddenly emerges. For both first and second order kinetic, we expect, in case of a continuous distribution of traps, a straight line with a pronounced slope.

The illustrated method, developed by McKeever, is time consuming but very easy to apply. However, it requires some experimental caution. It is particularly important to illuminate the sample exactly a the same temperature for each T_m - T_{stop} cycle in order to avoid spurious changes in the position of the peak maximum. In such case there is no control over the position of the temperature maximum of the peaks and the method is then inapplicable.

A different way, that can be followed in order to get information about the sensible parameters of a glow curve, is the peak shape method. This method involves only a few experimental points of the glow curves, but the most reliable ones; the peak maximum and the two points at increasing and at decreasing sides at half maximum[16], respectively.

The peak shape method is based on Lushchik's formula[86]. Figure 3.4 defines the quantities involved in the definition. Lushchik compares the area under the peak with the triangle that has the same width at

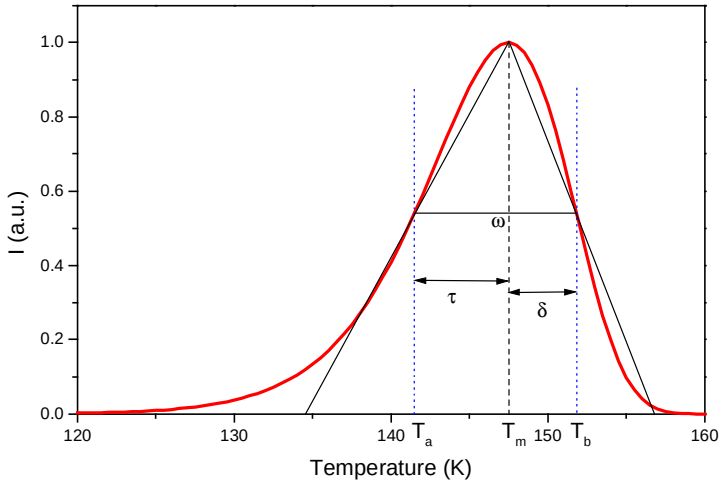

Fig. 3.4 TSL glow curve, ω indicate the total half intensity width T_b-T_a, $\delta = T_b$-T_m and $\tau = T_m$-T_a

half height and the same height (compare figure 3.4). This comparison can be mathematically expressed by means of the following equation (3.2).

$$\delta \cdot I_m = \beta \cdot n_m \tag{3.2}$$

Here I_m is the maximum thermoluminescence intensity, β is the heating rate and n_m the concentration of electrons at maximum intensity expressed by equation (3.3) and δ is the quantity defined in figure 3.4.

$$n_m = \int_{T_m}^{\infty} IdT \tag{3.3}$$

From equation (2.12) for the first order kinetic we can write the following equation (3.4),

$$\frac{I}{n} = s \cdot e^{-E/kT} \tag{3.4}$$

that at the maximum is:

$$\frac{I_m}{n_m} = s \cdot e^{-E/kT_m} \tag{3.5}$$

The maximum condition for the first order equation (2.14) is then the following equation (3.6).

$$\frac{\beta \cdot E}{k \cdot T_m^2} = s \cdot e^{-E/kT_m} \tag{3.6}$$

From equations (3.5) and (3.6) using the assumption (3.2) it is possible to write:

$$\frac{\beta \cdot E}{k \cdot T_m^2} = \frac{I_m}{n_m} = \frac{\beta}{\delta} \tag{3.7}$$

From the above equation follows Lushchik's formula for the first order kinetic, equation (3.8).

$$E = \frac{k \cdot T_m^2}{\delta} \tag{3.8}$$

Following the same route it is possible to extract an analogue formula for the second order kinetic, equation (3.9).

$$E = \frac{2k \cdot T_m^2}{\delta} \tag{3.9}$$

Both formulas are depending from the "triangle assumption" (3.2) that gives an error of about 2% for the first order and about 10% in the case of the second order kinetic.

In order to understand which formula of (3.8) and (3.9) should be applied, it is necessary to know previously the order of the kinetics. According to Halperin and Braner[87] we can determine the order using the symmetry factor μ defined by the following equation (3.10) in agreement with the quantities already defined in figure 3.4.

$$\mu = \frac{\delta}{\omega} \tag{3.10}$$

The so defined symmetry factor varies continuously as function of the re-trapping probability, from 0.42 in the case of pure first order, via negligible re-trapping, up to 0.52 for the pure second order, high re-trapping probability. The analysis of the possible intermediate numbers as well as the discussion of lower and higher symmetry factor values goes beyond this work and can be found in the valuable book of Chen[16].

The shape method has severe limits. First of all a lack of precision connected with the triangle assumption. Further, it is not possible to apply it to peaks not completely isolated. This peak analysis technique often gives controversial results with respect to the initial rise method, which gives always more reliable[88] values. However, the symmetry factor method can give a hint about the kinetic order[9,88] in order to perform further investigations and to use a more refined analysis.

3.2. Numerical simulations

In contrast to the initial rise and the peak shape method, the curve fitting procedure does not use only a few points or a simplified formula, but is based on all the available experimental points. The computing power for numerical simulations is not anymore a problem like in the recent past. In principle, thanks to the computing power of the modern personal computers it is possible to solve numerically the system of differential equations (2.2), (2.3) and (2.4). Unfortunately, the parameters involved in such set of differential equations are too many. Several different combinations[74] of the variables can fit the same peak shape, making impossible to decide what are their real values. Moreover, the presence of localised levels

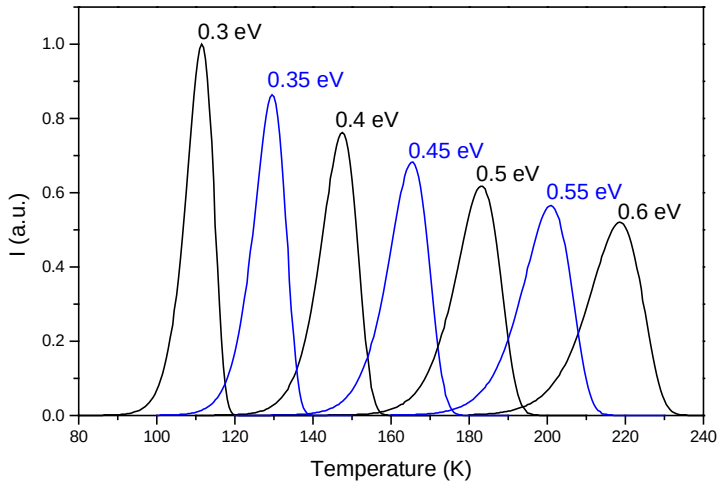

Fig. 3.5 TSL simulated first order glow curves in function of different values of energy *E*. Simulation parameters: $n_0 = 1x10^{16}$ cm^{-3}, $\beta = 0.1$ K/s and $s = 10^{12}$ s^{-1}.

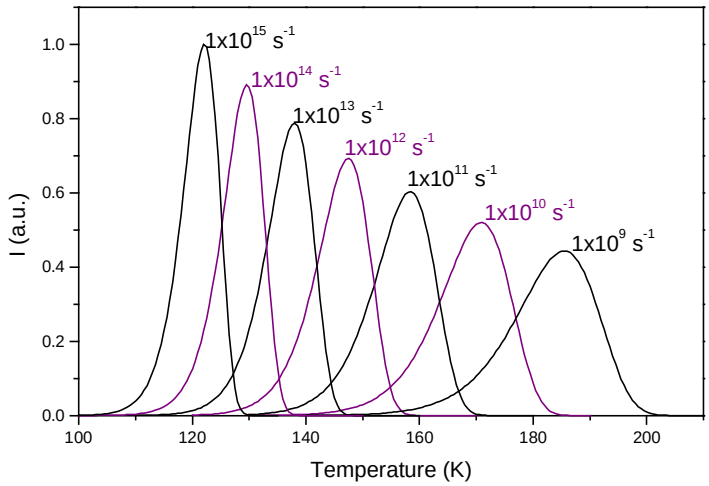

Fig. 3.6 TSL simulated first order glow curves in function of different values of frequency factor *s*. Simulation parameters: $n_0 = 1x10^{16}$ cm^{-3}, $\beta = 0.1$ K/s and $E = 0.4$ eV.

having a certain type of distribution further complicates the problem, increasing the number of parameters freely floating. For this reason it is fruitful to use a simplified approach that implies the analytical solutions of the differential rate equations (2.14) and (2.22).

Equations (2.14) and (2.22), for the first and the second order kinetic, respectively, are numerically solved by means of a personal computer and the computing program Wolfram Mathematica[89]. Both equations contain the integral of the energy that takes the trapping states density distribution into account.

The fitting procedure usually follows a scheme which consists in the sequential variation of the main parameters involved in the equations, energy depth, frequency factor and the variables of the density of states distribution, in order to obtain the best curve shape, matching an experimental peak.

The figures inside this section show how the different parameters involved in equations (2.13)-(2.21) interplay and which is the effect of different types of trap distributions on the curve shape. The main

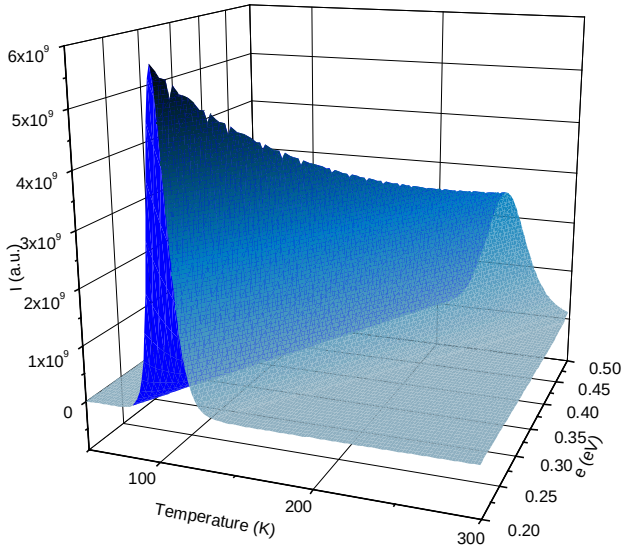

Fig. 3.7 TSL simulated second order glow curves in function of different energy values. Simulation parameters: n_0 = 1x10^{12} cm^{-3}, β = 0.1 K/s, N = 1x10^{14} cm^{-3}, s = 1x 10^{10} s^{-1} and A_r/A = 1.

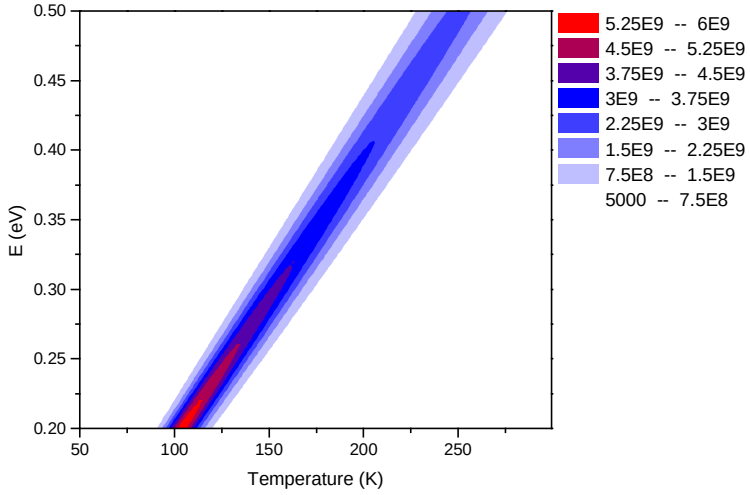

Fig. 3.8 TSL intensity map of the simulated second order glow curves in function of different frequency factor values. Simulation parameters: n_0 = 1x10^{12} cm^{-3}, β = 0.1 K/s, N = 1x10^{14} cm^{-3}, s = 1x 10^{10} s^{-1} and A_r/A = 1.

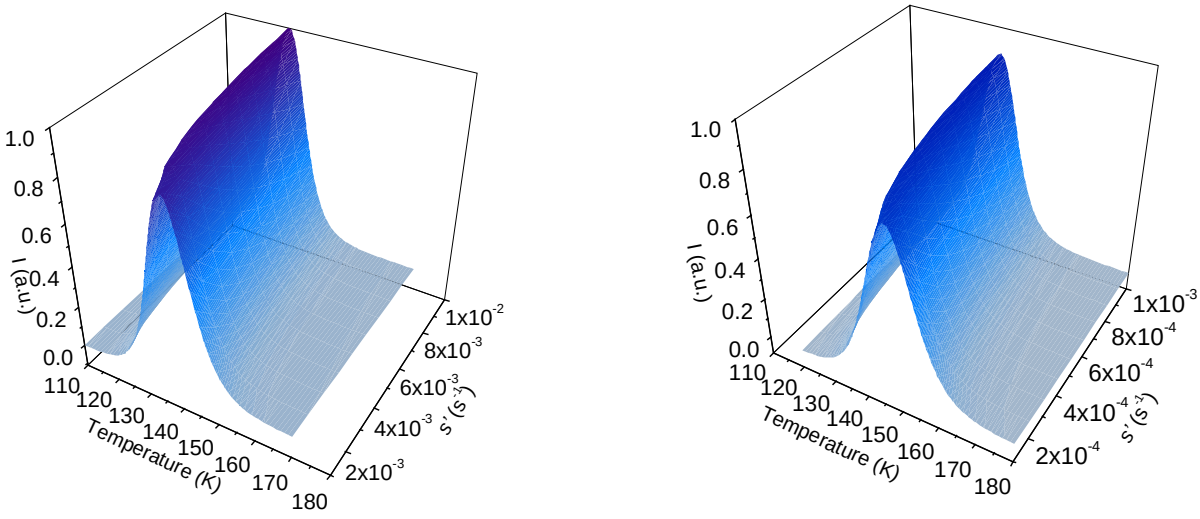

Fig. 3.9 TSL 3-D numerical simulation of second order glow curves. Simulation parameters: n_0 = 1x10^{16} cm^{-3}, β = 0.1 K/s and E = 0.4 eV.

goal is to be able to obtain, from first order kinetic and from second order kinetic rate equations, curve shapes suitable to fit the real TSL curves and then to study their behaviour under systematic parameter variation.

We start with the simple first order equation (2.13) illustrated by means of the numerical simulation of figure 3.5. Keeping the frequency factor at a fixed value, s = 1x10^{12} s^{-1}, the simulation shows how the peak evolves in function of different values of the energy, ranging from E = 0.2 eV to E = 0.5 eV. A small variation in energy changes significantly the curve. Analysing the peaks we can observe that while the curve at low energy is quite symmetrical, at higher energy the peak tends to be more asymmetric with a considerable reduction of maximum intensity. However, the area under the peaks is always the same, being the number of released electrons from the localised levels constant for each peak.

The variation of the frequency factor s allows to obtain a new set of curves looking exactly like the peaks of figure 3.5. The energy, in the simulations of figure 3.6, has a fixed value, E = 0.4 eV, only the frequency factor changes. The TSL peak evolves from a symmetric shape, at low temperature, to a completely asymmetric one at higher temperature, but, with respect to figure 3.5, it is less shifted on the temperature scale. The frequency factor has a smaller influence on the curve shape with respect to the energy depth of the localised levels E. It is necessary to vary s by several orders of magnitude, from 1x10^{-9} s^{-1} to 1x10^{-15} s^{-1}, in order to obtain a sensible variation of the glow curves, which is possible to observe in case of the present numerical simulations.

Hence, the dependence of the thermostimulated glow curves on s is significantly smaller than the dependence on E. This effect is disadvantageous performing the fitting procedure of real glow curves. Several values of the frequency factor can fit a real peak quite well making sometimes impossible to extract an exact value of it. Just to extract a reasonable order of magnitude for s is ,sometimes, already a very good result. Both simulations of figures 3.5 and 3.6 have the same concentration of trapped electrons at the starting time t_0 of n_0 = 1x10^{16} cm^{-3}.

The 3 dimensional (3-D) graph of figure 3.7 represents the numerical simulation of the second order equation (2.21) in function of temperature and activation energy. On the contrary of the first order kinetic, the peaks are more symmetric. Furthermore, increasing the energy the peaks shift from a maximum at T_m = 105 K to T_m = 245 K. At high temperature the shape of the peak is still symmetric, but the relative intensity,

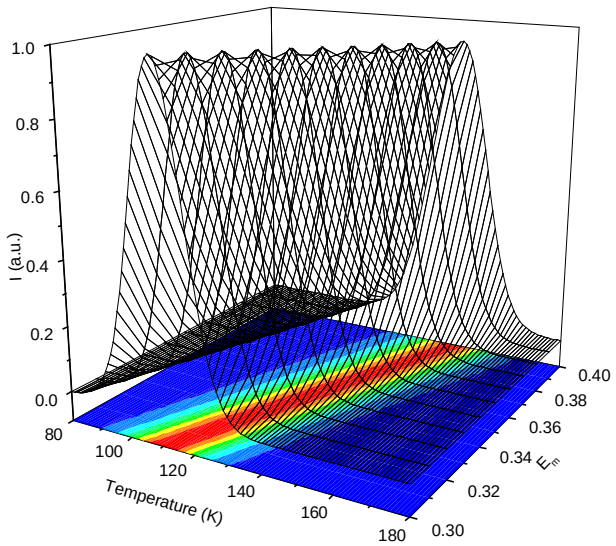

Fig. 3.10 TSL numerical simulation of Gaussian distributed first order glow curves. Simulation parameters: n_m = 1x10^{16} cm^{-3}, β = 0.1 K/s, s = 1x10^{12} s^{-1}, σ = 0.02 eV, E_1 = 0.4 eV and E_2 = 0.6 eV.

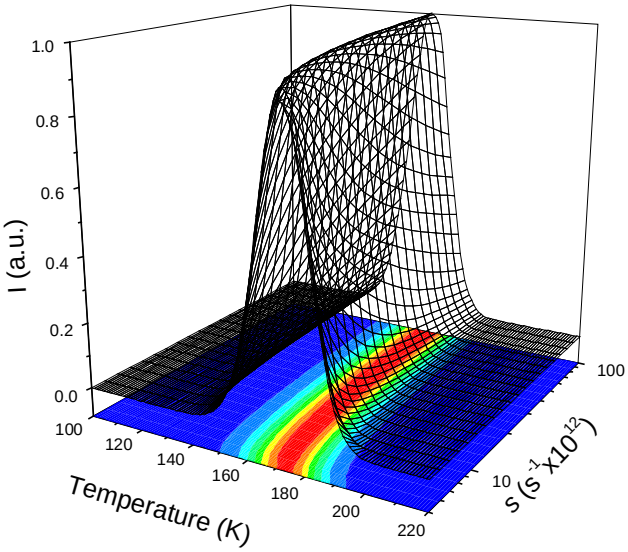

Fig. 3.11 TSL numerical simulation of Gaussian distributed first order glow curves. Simulation parameters: n_m = 1x10^{16} cm^{-3}, β = 0.1 K/s, E_m = 0.5 eV, σ = 0.02 eV, E_1 = 0.4 eV and E_2 = 0.6 eV.

according to figure 3.8 decreases from $5.5x10^9$ a. u. to $3.5x10^9$ a. u..

Figure 3.8 shows simply the intensity map of the peaks of figure 3.7. This kind of graphical presentation allows to appreciate the evolution of the position of the peak maximum and its broadening as a function of temperature.

The two graphs of figure 3.9 show the simulation of the second order kinetic equation 2.21 as a function of the variation of the pseudo-frequency factor *s'* from 10^{-2} s^{-1} to 10^{-4} s^{-1}. Considering the A_r/A ratio equal to 1 and keeping constant all other parameters, this corresponds to a variation of *s* of two orders of magnitude from 10^{12} s^{-1} up to 10^{14} s^{-1}. Again, like in case of first order kinetics it is possible to observe a shift of the peak maximum from low to high temperature in function of decreasing values of *s*. And again, similarly to the first order case, the impact of the pseudo-frequency factor on the peak position is much smaller than the influence of the energetic depth of the traps.

Like in the first-order case also in case of second order kinetic equations, the peak shape changes slowly with varying *s*. This fact makes it very difficult to fine-tune the pre-exponential factor values during the fitting procedure of an experimental glow curve.

The equations of first and second order kinetics for a single trap level are numerically easy to be solved. In fact both are depending only on the two parameters *E* and *s*, where the second one changes the peak only weakly with respect to the first one. The other parameters, like the density of traps, do not play any role on the position of the peak, in case of first order, or have a small impact on it in case of second order. Considering that, it is possible, in most cases, to get fundamental information about the energetic depth by means of the initial rise method and of the cleaning techniques. In such easy cases, substantially, the only parameter left is the frequency factor.

Assuming a level of density of trapping states higher than 10^{14} cm^{-3}, the application of the fitting procedure with the initial rise method gives very reliable results.

3.2.1. Gaussian distribution

With respect to the simple first and second order kinetic equation having only a single level of traps the introduction of a Gaussian distribution of localised states, equations (2.14) and (2.22) has a deep impact on the TSL peak shape. The Gaussian distribution was already described in chapter 2, by means of equation (2.15) and the related figure 2.3. The main parameter governing such distribution is the distribution width, σ (see equation (2.15)) that determines how broad is the distribution of localised states.

Introducing the Gaussian function inside equations (2.13) and (2.21) we must deal with a further difficulty connected with the limits of the energy integral. The two limits, E_1 and E_2, how we will see in the following discussion, play a major role in the determination of the shape of a TSL peak. In general we can regard them like a single parameter, in effect they are strictly related though, in principle, they can vary independently.

The 3-D graph of figure 3.10 shows the position of the peak maximum as function of various energy values in case of the first order kinetic with a Gaussian distribution of states, equation (2.14), while 3-D figure 3.11 shows the impact of the frequency factor variation on the same first order equation.

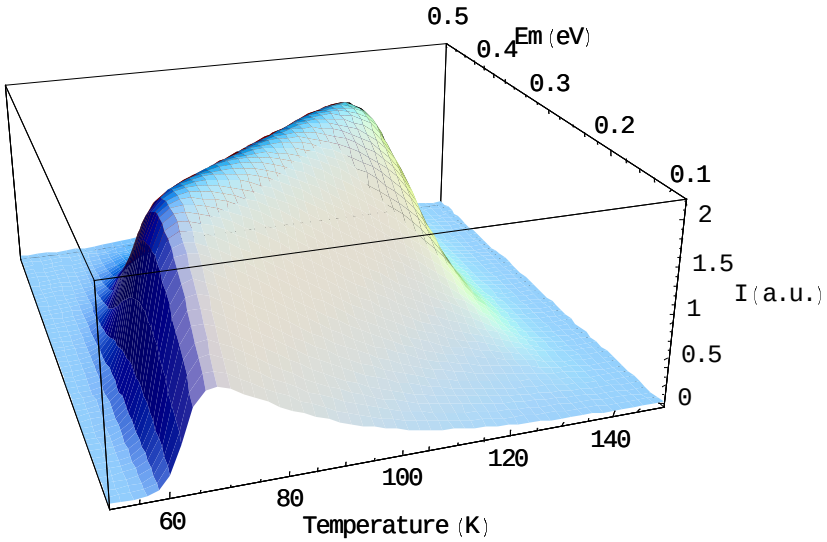

Fig. 3.12 TSL numerical simulation of Gaussian distributed second order peaks. Simulation parameters: n_m = 1x10^{16} cm^{-3}, β = 0.1 K/s, σ = 0.1 eV, E_1 = 0.2 eV, E_2 = 0.4 eV, N = 1x10^{16} cm^{-3}, s = 1x 10^{14} s^{-1} and A_r/A = 1.

Energy maximum E_m and frequency factor s have a weaker influence on the shape and also on the relative intensity of the curves with respect to the peaks calculated for the pure first and second order kinetics. The variation of the energy maximum peak from E_m = 0.3 eV to E_m = 0.4 eV imposes, how it is possible to observe in figure 3.10, a variation in the temperature maximum of the peak from T_m = 110 K up to T_m = 140 K. Furthermore, the density map graph, displayed under both figures, shows that the width of the curves is negligibly influenced and it is still almost unchanged in the full range under investigation.

Like in the pure first order, the frequency factor has a smaller impact than the maximum energy E_m on the general shape and on temperature maximum position of the peaks. In the 3-D simulation of figure 3.11 s varies by two orders of magnitude, from s = 1x10^{12} s^{-1} up to s = 1x10^{14} s^{-1}, while the temperature maximum position diminishes slowly from T_m = 170 K to T_m = 160 K. Moreover, the intensity and the symmetry of the peak remain almost unchanged.

The same effect can be observed in case of the second order equation with a Gaussian distribution of localised levels, equation (2.22). Like in the pure second order the curves are more symmetric with respect to the first order case, and also the temperature maximum of the peak changes slowly in function of the pseudo frequency factor s'.

Figure 3.12 shows the 3-D numerically calculated glow curve for the second order kinetic equation with a Gaussian distribution of states (2.22). In that 3-D graphical representation the varying parameter is the maximum energy E_m, while the other sensitive values, listed in the figure caption, are still the same. The integration limits for the energy are E_1 = 0.2 eV, E_2 = 0.4 eV, while the value of the maximum distribution E_m varies continuously in the interval from E_m = 0.1 eV to E_m = 0.5 eV. Shape and position of the maximum of the peak change dramatically depending on where the point of the maximum of the distribution lies, whether inside or outside of the integration interval. In this case the maximum peak temperature varies from T_m = 70 K to T_m = 125 K. At the low temperature side the peak rises steeply for

low activation energies, while it decreases with a long tail on the high-temperature side. On the high energy side of the plot the peak symmetry is different. It grows slower at the low-temperature side and then it decreases slightly faster on the high temperature side compared to the curves with low activation energy. This behaviour of the peak can be better figured out by means of the 3-D graph of figure 3.13. This numerical simulation has the same set of parameters as used for figure 3.12, but it shows the peaks from an opposite point of view.

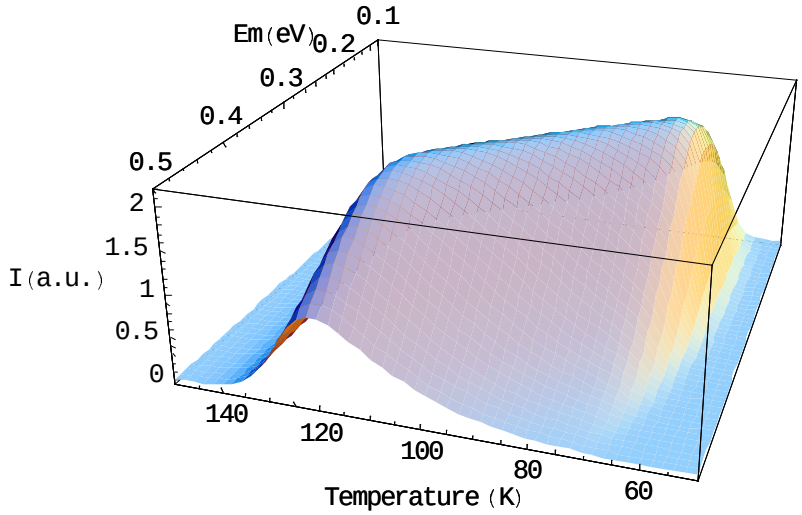

Fig. 3.13 TSL numerical simulation of Gaussian distributed second order glow curves. Simulation parameters: n_m = 1x10^{16} cm^{-3}, β = 0.1 K/s, σ = 0.1 eV, E_1 = 0.2 eV, E_2 = 0.4 eV, N = 1x10^{16} cm^{-3}, s = 1x 10^{14} s^{-1} and A_r/A = 1

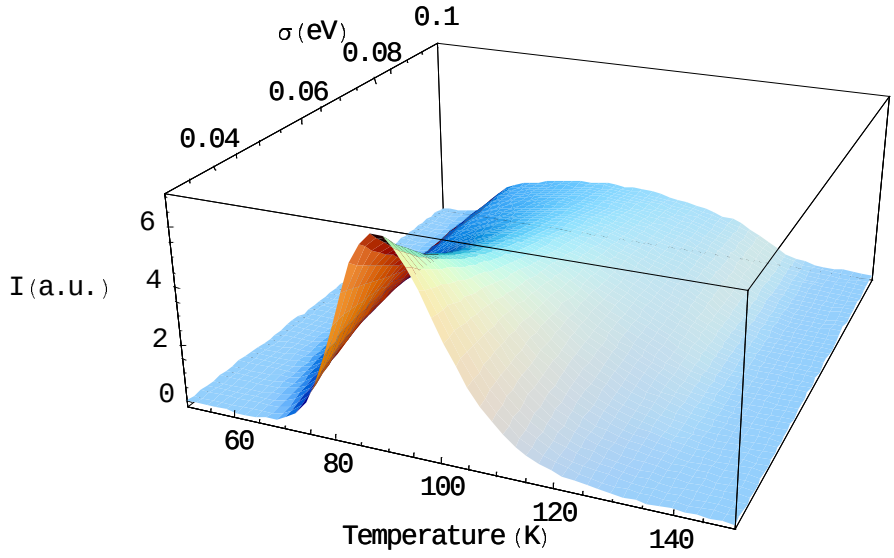

Fig. 3.14 TSL numerical simulation of Gaussian distributed second order glow peaks. Simulation parameters: n_m = 1x10^{16} cm^{-3}, β = 0.1 K/s, E_m = 0.3 eV, E_1 = 0.2 eV, E_2 = 0.4 eV, N = 1x10^{16} cm^{-3}, s = 1x 10^{14} s^{-1} and A_r/A = 1.

Before to discuss the physical meaning of the position of the maximum distribution energy peak E_m outside values of the integration limits, we further consider the incidence of the variation of the width of the distribution, σ, and the influence of the integration limits on the peak shape.

Figure 3.14 shows the 3-D numerical simulation of the second order glow curve varying σ by two orders of magnitude, from σ = 0.03 eV to σ = 0.3 eV. We can observe that the lower values of σ do not have any impact on the peak shape. The value σ = 0.03 eV is very small and the peak is almost not influenced by the presence of the trap distribution. It keeps the same shape and symmetry like a single trap level peak of the second order equation 2.13. Increasing the distribution width the peak shape changes completely, though the position of the temperature maximum remains untouched. For high values of σ, exceeding 0.05 eV, the peak looses its typical shape and starts to flatten. In this case the charges are broadly distributed in energy and such distribution can be considered as a quasi continuous one.

Changing the integration limits, E_1 and E_2, the position of the temperature maximum of a TSL peak does not change in both first and second order kinetic cases. Figure 3.15 shows, in particular, the position and the shape of a second order kinetic TSL peak in function of the variation of the upper limit E_2 of the integral. Increasing this value, exclusively the dimension and shape of the high temperature tail of the peak changes. At higher values of E_2 the tail assumes a broad shape and after a certain value, E_2 = 0.8 eV in the current example, the shape does not change significantly. For that reason it is an easy task to find the best integration interval during the fitting procedure. In the particular case of the simulation parameters used in order to obtain the peak of figure 3.15, there is no influence at all on the tail shape due to the occurrence of values of E_2 higher than 0.8 eV.

In general the integration limits of both equations (2.14) and (2.22) should be chosen in a way which takes into account the influence that they have on the curve tails. One should also consider the minimum integral interval necessary in order to optimise the computing time. The opportunity to change the shape of the low and high temperature tail of the curve without influencing the peak temperature maximum position, is a good feature of the model, that allows to fine-tune the fit of the peak tails of an experimental TSL glow curve.

The same features are observed for the lower integral limit E_1. In this case, a decreasing value of E_1 means to enlarge the integration range on the low energy side. The maximum peak position does not change, but the shape of the low temperature tail is broadened. Like in case of E_2 there exists a minimum value of E_1 below which a further lowering of this value does not influence the shape of the low temperature side of the calculated TSL peak.

The value of the maximum energy E_m is a further important parameter for curves having a Gaussian distribution of localised states. In principle the value of E_m should lies inside the integration interval E_1-E_2. Effectively, only in such case we are considering the full distribution of states with its characteristic Gaussian shape. Otherwise, the shape of the distribution is not Gaussian anymore, and the distribution assumes an exponential like form related to only one side of the whole former distribution.

Figure 3.16 shows the numerical simulation of the second order equation (2.22) with a Gaussian distribution of localised states. In this case we change the position of the energy maximum from E_m = 0.2 eV to E_m = 0.02 eV. The integration limits are E_1 = 0.2 eV and E_2 = 0.4 eV. In this way we are moving the

distribution maximum from the coincidence with the lower extreme of the integration limits to a value completely outside of them. This procedure is equivalent, in a real experiment, to apply the partial cleaning technique. Furthermore, it is also equivalent to a not completely filled up distribution of localised states. In both cases the resulting TSL peak only apparently has an exponential distribution of traps. Effectively, this is not true, the resulting exponential distribution, that often is invoked in order to explain the results, is just an artefact of the experimental conditions.

The above numerical simulations proof that it is not possible to apply the fitting procedure to thermal cleaned peaks or to levels of traps only partially filled in order to obtain the shape of the localised state distribution without to take into account the effect on the distribution shape related to particular experimental conditions.

When the value of E_m is lower than the value of E_1 like in the case of figures 3.16 and 3.18, the distribution of state is not anymore Gaussian. We are considering only a branch of the former Gaussian distribution. However, though the maximum of the distribution resides outside, it is still an important parameter, determining the shape of the exponential. This point is further illustrated by means of figure 3.17. The graph shows a Gaussian distribution of states between 0 eV, the edge of the conduction band in our model, and 1 eV inside the energy gap. If during the numerical simulation we integrate equations (2.14) and (2.22) considering the integral limits only between E_1 = 0.2 eV and E_2 = 0.4 eV the resulting general shape of the distribution is not Gaussian but it has the shape of a certain portion of the Gaussian side i.e. the shape is related to an exponential.

This situation is illustrated by means of the red line superimposed onto the lower Gaussian distribution branch in figure 3.17. The inclination and the position of this pseudo-exponential distribution are still fully determined by the parameters of the former Gaussian, but the resulting distribution of states,

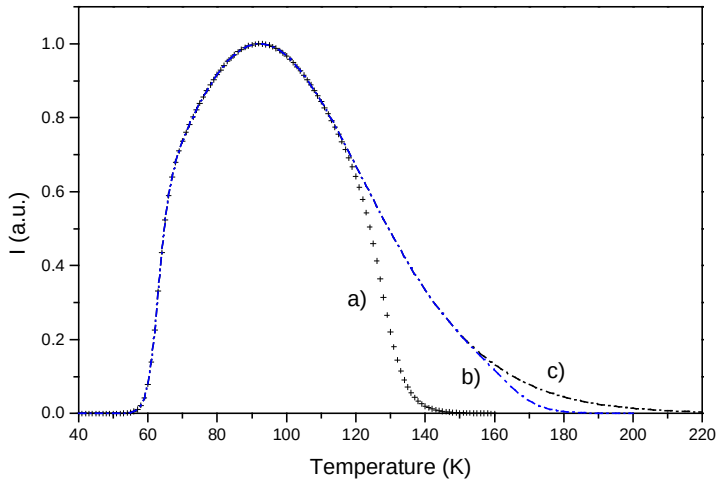

Fig. 3.15 TSL numerical simulation of the gaussian distributed second order glow curve for different values of one integration limits E_2. a) E_1=0.2 E_2=0.4, b) E_1=0.2 E_2=0.5, c) E_1=0.2 E_2=0.8. Simulation parameters: n_m=1x10^{16} cm^{-3}, β =0.1 K/s, E_m=*0.3* eV, N=1x10^{16} cm^{-3}, s=1x 10^{14} s^{-1} and A_r/A=1.

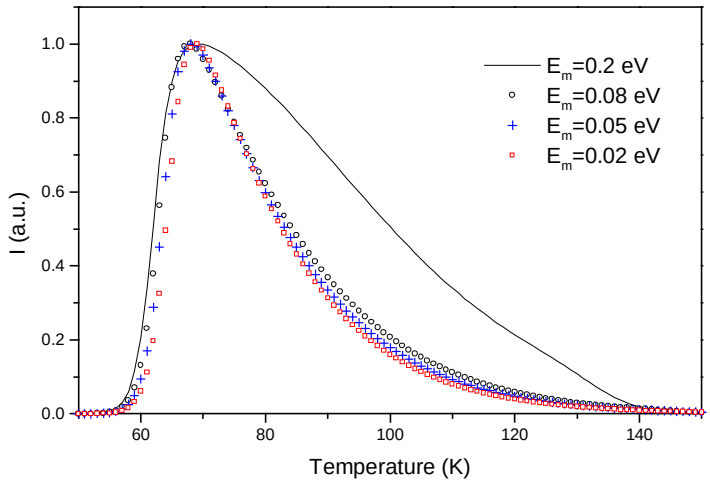

Fig. 3.16 TSL numerical simulation of Gaussian distributed second order peaks in case of different values of maximum energy E_m. Simulation parameters: n_m = 1x10^{16} cm^{-3}, β = 0.1 K/s, E_m = *0.3* eV, N = 1x10^{16} cm^{-3}, s = 1x 10^{14} s^{-1} and A_r/A = 1.

with an appropriate choice of the integral boundaries, is clearly exponential. This fact will be particularly important interpreting the results emerging during the fitting procedure of partially cleaned peaks. In such case, because of the thermal cycling, the distribution is just a branch of the Gaussian original one and gives an apparent exponential distribution, however the Gaussian parameters are still under the apparent exponential shape and in principle they can be easily extracted through the fitting procedure.

A further remark, concerning the figures 3.16 and 3.15 showing TSL peaks numerically calculated

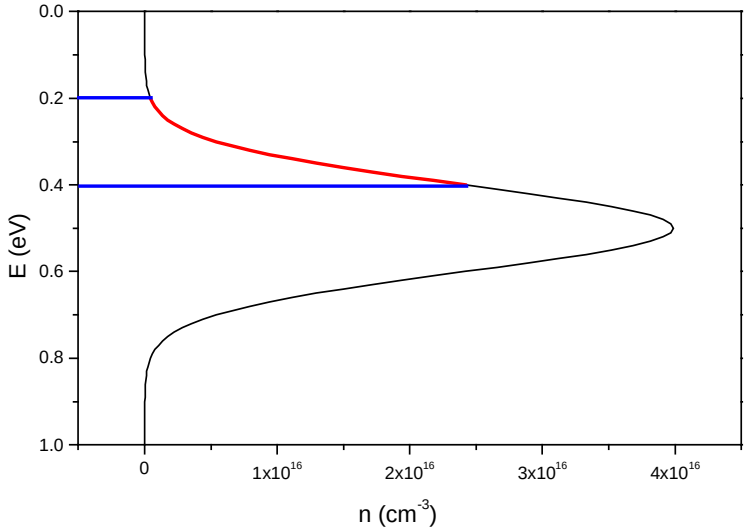

Fig. 3.17 Gaussian distribution of states. n_m = 1x10^{16} cm^{-3}, σ = 0.1 eV, E_m = 0.5 eV.

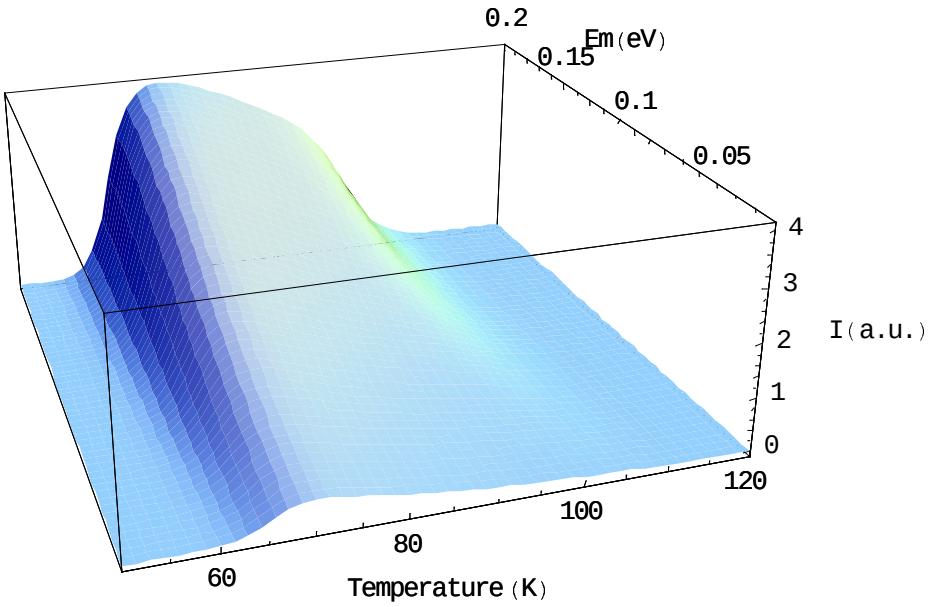

Fig. 3.18 TSL numerical simulation of Gaussian distributed second order peaks. Simulation parameters: n_m = 1x10^{16} cm^{-3}, β = 0.1 K/s, σ = 0.1 eV E_1 = 0.2 eV, E_2 = 0.4 eV, N = 1x10^{16} cm^{-3}, s = 1x 10^{14} s^{-1} and A_r/A = 1.

under assumption of a Gaussian distribution of energy. Here different integration limits have been used for the energy range. All peaks are normalised to 1. Figure 3.18 contains a 3-D graph showing TSL peaks for different values of the mean energy E_m, which lies outside of the integration limits as mentioned above. Here the peak area is normalised. This implies an obvious change of TSL peak intensity due to the pronounced changes of the peak shape. In such a way it is possible to visualise the influence of the position of E_m on the intensity of the peak. Like expected, the intensity of the peaks diminishes and the curve is flattened due to the smaller amount of electrons available to recombine. This effect appears clearly also in the experimental curves and can be taken as a further sign indicating the occurrence of a pseudo-exponential distribution of localised states arising from a incompletely filled distribution of traps.

3.2.2. Uniform and exponential distributions

Although from the statistical point of view one always expects a Gaussian distribution of traps, in literature especially on inorganic materials, the broad TSL peaks are often explained by means of an exponential distributions of localised levels. In the discussion above we have shown already that a Gaussian distribution can appear exponential like because of the thermal cycling. Nevertheless, we further consider some features of the exponential and uniform distributions though the physical basis of such kind of distributions is not well understood and on can assume that they are often just an experimental artefact.

The exponential and the quasi continuous distribution inserted in the first and second order TSL equations (2.14) and (2.22) are described by the following equations (3.9) and (3.10), respectively.

$$n(E) = n_e e^{-\frac{(E-E_b)}{kT_c}} \qquad (3.9)$$

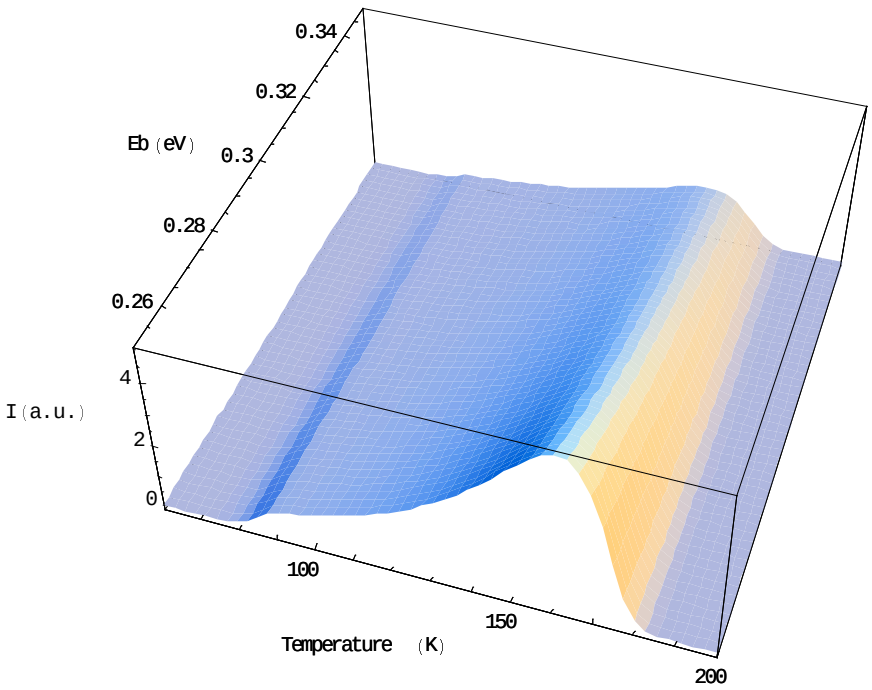

Fig. 3.19 TSL numerical simulation of exponential distributed first order peaks. Simulation parameters: n_e = 1x10^{15} cm^{-3}, β = 0.1 K/s, s = 1x10^{10} s^{-1}, T_c = 1000 K, E_1 = 0.2 eV and E_2 = 0.4 eV.

$$n(E) = n_c\left[\frac{E - E_a}{E_b - E_a}\right] \qquad (3.10)$$

Here n_e and n_c are the constant density of localised states of the exponential and continuous distribution respectively, while E_a and E_b indicate the edges of the energy distributions. In case of an exponential distribution we assume the starting point, E_a, equal to zero. T_c is the characteristic temperature of the exponential distribution and this parameter affects especially the curvature radius of the function. Using these distributions it is possible to solve equations (2.14) and (2.22) numerically.

The 3-D graph of figure 3.19 shows the numerical simulation of the exponential first order kinetic equation (2.14). The value of E_b ranges from E_b = 0.25 eV to E_b = 0.35 eV. The characteristic temperature chosen for this simulation is 1000 K. This value allows a distribution shape, in interplay with the other parameters, compatible with the numerical simulations of the Gaussian distribution shown in the previous part of this chapter. The integration limits used in the equation in order to obtain the graph are E_1 = 0.2 and E_2 = 0.4 eV, while the value of the constant is n_e = 1x10^{15} cm^{-3}, s = 1x10^{10} and the heating rate is fixed like usual to β = 0.1 K/s.

Examining figure 3.19 at low temperature, around 80 K, it is possible to observe the typical step occurring always with this kind of distribution. Then the curve increases smoothly and after the peak it decreases more steeply on the high temperature side. With respect to the analogous Gaussian type the curve

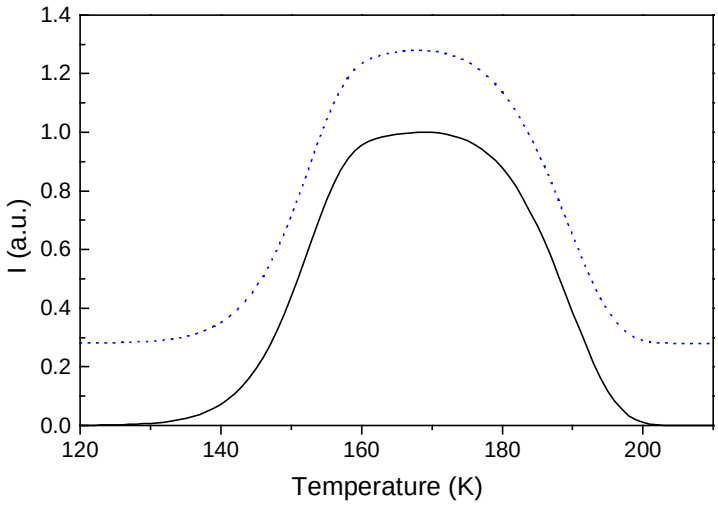

Fig. 3.20 Solid line: numerical simulation of the quasi continuous linear distributed first order peak. Dotted line Gaussian distributed first order glow curve. Simulation parameters: β = 0.1 K/s, s = 1x10^{10} s^{-1}, E_1 = 0.36 eV, E_2 = 0.44 eV, n_e = 1x10^{16} cm^{-3}, E_a = 0 eV, E_b = 2 eV, n_m = 1x10^{16} cm^{-3}, σ = 0.12 eV and E_m = 0.43 eV.

is more asymmetric. Nevertheless, it is possible to adjust the parameters in order to obtain two glow curve shapes perfectly matching to both distributions.

The next figure 3.20 shows a single first order glow curve having the quasi continuous trap distribution of equation 3.10 compared with a similar Gaussian first order equation. Both the Gaussian and the quasi linear distribution have the same integral boundaries, E_1 = 0.36 eV, E_2 = 0.44 eV, the pre-exponential factor is s = 1x10^{10} s^{-1} and heating rate is still fixed at β = 0.1 K/s. The densities of traps are n_c = 1x10^{16} cm^{-3} and n_m = 1x10^{16} cm^{-3}, respectively. While the characteristic parameters of the Gaussian are σ = 0.12 eV and E_m = 0.43 eV, the parameters for the quasi-continuous distribution are E_a = 0 eV and E_b = 2 eV. The two simulated glow curves are indistinguishable. A large flat region on the top of the curves indicates the broad trap distribution that in case of the quasi-continuous distribution cover an extension of 2 eV while in case of the Gaussian the width parameter is only σ = 1.2 eV. A Gaussian distribution with an appropriate choice of parameters can perfectly simulate the quasi continuous one, representing a sort of degeneration of the Gaussian case. There are several other examples like the one presented in figure 3.20 where the same curve can be described by completely different distribution functions.

This fact indicates that the Gaussian distribution can be considered to be a flexible universal distribution function. This suggests that the only real distribution of localised states occurring in a material is a Gaussian one. This kind of distribution can degenerate into different forms depending on the traps filling conditions or, like in the quasi continuous case on the total amount of traps. Using the correct parameters, a Gaussian type of distribution can give very sharp asymmetric peaks, like an exponential distribution as well as symmetric and very broad peaks.

Moreover the physical meaning of such kind of distribution can be understood as consequence of the statistical disorder typical for organic materials. However, the number of parameters involved during the fitting procedure of an experimental peak can rise always to a certain degree of uncertainty. Especially for very symmetric peaks, sometimes, different combination of parameters can describe the same shape of the peak. In general, the analysis of the experimental glow curves is not an easy task and the results have always to be cross checked with different techniques.

4. Experimental

Depolarisation processes and localised states in polymers and low molecular compounds are detected by means of thermally stimulated depolarisation current (TSDC), dielectric spectroscopy (DES) and thermally stimulated luminescence (TSL), respectively. The measurements are performed with a custom set-up and the data are automatically collected with a computer program specially designed and developed for this purpose.

The TSDC measurements are performed on two kinds of polyphenyl-quinoxalines: poly[2,2'-(1,4-phenylene)-6,6'-bis(3-phenyl quinoxaline)] shortly called PPQ IA, shown in figure 1.6 and poly[2,2'-(4,4-oxy biphenylene)-6,6'-oxybis(3-phenylquinoxaline)], PPQ IIB, of figure 1.7. TSDC curves of both polymers show several peaks and especially PPQ IA has a particularly rich thermogram.

The synergy between TSDC and DES allows to distinguish between depolarisation and de-trapping peaks. PPQ IA shows a so called α peak at 550 K, a transport peak at T_m = 420 K and several depolarisation peaks at lower temperature. Furthermore, a particularly complex structure, around T_m = 240 K, results from the overlapping of three single peaks having activation energies at E = 0.95 eV, E = 0.67 eV, and E = 0.60 eV respectively. Although PPQ IIB it has a molecular structure very similar to PPQ IA (see figures 1.6 and 1.7), it shows a less complex thermogram where it is possible to distinguish only a transport peak and an α-peak. A further low temperature peak is also detected. There is no evidence that this peak can be found by means of DES measurements.

The TSL thermograms of the two polymers demonstrate the presence of a broad distribution of localised levels having low activation energy, lying between E = 60 and E = 80 meV for both polymers. Such distribution is characterised by a second order kinetic, i.e. the electrons can be easily get re-trapped before recombination.

The TSL thermograms of the low molecular compounds 1,3,5-Tris[(3-phenyl-6-trifluoromethyl)-quinoxaline-2-yl]benzene (CF_3-TPQ) and amphiphilic substituted 2-(p-nitrophenyl)-5-(p-undecylamidophenyl)-1,3,4-oxadiazole (NADPO) drawn in figures 1.9 and 1.10 respectively, show unambiguously the presence of localised states. The peaks, analysed with the help of both first and second order kinetic equations introduced in chapter 2, give evidence of the presence of distributions of shallow traps in both materials having activation energies in the range of E = 0.07 and E = 0.004 eV respectively, and of the presence of further distributed localised states at higher energy.

Well ordered Langmuir Blodgett (LB) NADPO films show particularly rich glow curves with three well-recognizable peaks at T_m = 197.7 K, T_m = 221.5 K and T_m = 254.2 K, respectively. It is possible to analyse them successfully by means of first order kinetic equations characterised by a Gaussian distribution of localised states. The three peaks have activation energies of E = 0.55 eV, E = 0.63 eV and E = 0.66 eV, respectively. The three peaks have different origins; while the lowest energy one clearly originates from the induced disorder, the peak characterised by the highest energy level has, probably, its origin in the presence of chemical contaminants.

The importance and the origin of the shallow traps in such polymers and low molecular compounds are discussed in more detail in the following chapter.

4.1. Experimental set-up

The perfect control of the heating rate parameter β in equations (2.14), (2.22) and (2.31) is of fundamental importance performing TSL, TSC and TSDC experiments in order to minimise the errors studying the activation energies and the frequency factors of the experimental curves. Therefore, the thermally stimulated techniques require a cryostat having an excellent temperature control systems. All measurements of the present work are carried out with the custom set up illustrated in figure 4.1.

The cryostat has a temperature range varying from liquid nitrogen temperature up to 550 K with an excellent linearity of the rate parameter in the range $\beta = 10 \div 0.01$ K/s. Measurements are performed under high vacuum conditions with minimum base pressure of 5×10^{-6} Torr. The thermal contact between the cryostat cold finger and the sample is assured by a silver paint coating layer. Furthermore, the electrical insulation, in case of electro-optical measurements, is achieved by means of a thin ceramic high ohmic foil interposed between the cold finger and the sample.

Two calibrated thermocouples measure the temperature. The first one lies directly on the cold finger plate and is connected with the temperature controller. The second one lies near, or on the sample,

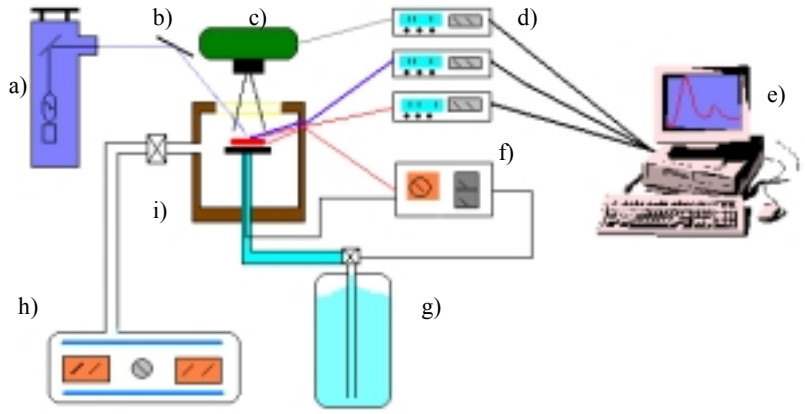

Fig. 4.1 Scheme of the experimental set-up. a) Xenon lamp, b) mirror, c) photomultiplier, d) voltammeter, picoammeter and multimeter, e) computer, f) temperature controller, g) dewar, h) pumping system, i) cryostat. Inside the cryostat: sample (red), cold finger (black), the two thermocouples red lines) and the electrical contacts on the sample (violet line).

depending on the particular measurement involved, and it registers directly the surface sample temperature. The cryostat is also equipped with a quartz window and two electrical feedthroughs.

The excitation source is a 1000 W Xenon lamp equipped with a mirror particularly designed to dissipate the infrared radiation and to fully reflect the visible and near ultraviolet range with enhanced reflectivity in the range 600÷200 nm.

In order to perform TSDC and TSC measurements, the current is measured with a pico-ammeter having resolution of 0.1 fA, directly connected to the sample terminal in the shortest possible way through a rigid connector. The thermoluminescence signal is detected with a sensitive photomultiplier tube Hamamatsu. All measured signals are recorded as a function of time and temperature with a personal computer. The exact knowledge of this two parameters allows especially to check carefully “on line” the

time-temperature dependence by means of a computer program especially written for this purpose with the graphical programming language HP VEE that is illustrated in appendix A.

The picture in figure 4.1 shows, in a schematic way, the full apparatus. The three fundamental instruments, the programmable electrometer Keithley 617 directly connected with the sample, the multimeter HP 34401A, connected with the thermocouple and the sensitive voltmeter, Keithley 195A coupled with the photomultiplier, are labelled with letter d). The temperature controller, a West instrument model 5010, labelled with f) is connected with a double power supply and an automatic valve. The first line of the power supply rules the cryostat heating, while the second power line, once the valve is closed, permits to cool the system, allowing the circulation of liquid nitrogen inside the cold finger. The 10 litres liquid nitrogen dewar, letter g) in the figure, allows more than 10 hours of measurements at low temperature. The pumping system, letter h) consisting of a pre-vacuum rotary pump and a diffusion pump, allows a rapid chamber evacuation. Very remarkable are the dimension of the cold finger, 2.5 cm diameters. Because of the built-in capillary system that permits the nitrogen circulation, the top of the cold finger has a very high temperature homogeneity. Furthermore, generous dimensions of the sample housing area are a major advantage in TSL measurement, allowing a well detectable signal coming from large samples.

The DES measurements are performed with a precision LCR meter Hewlett Packard model 4284A. The samples are shortly connected with the instrument and the measurements are made in the frequency range from 20 Hz up to 1 MHz keeping the temperature constant.

4.2. TSDC, DES and TSL measurements on polymers

A promising candidate for electron transport hole blocking layers in OLED devices is the class of polymeric phenylquinoxalines PPQ[90]. Quinoxalines are already discussed, from the chemical point of view, in the first chapter § 1.4. Figures 1.6 and 1.7 show the chemical structure of the two polymers under

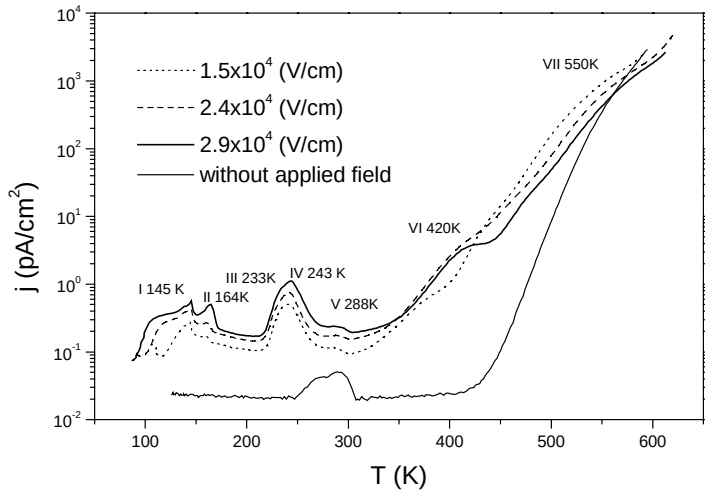

Fig. 4.2 TSDC spectra of a PPQ IA sample

investigation. We studied the electrical properties and the electronic structure of two polymers and of the related low molecular compounds shown in figure 1.8. Furthermore, we studied their electrical behaviour in single and multilayer devices[47].

4.2.1. TSDC on poly-phenylquinoxalines

In order to perform thermal measurements, samples of PPQ IA and PPQ IIB are cast from a chloroform solution onto an aluminium fresh coated copper plate of 1.5 mm thickness. A drying procedure is carried out after preparation, heating first the specimens to about 350 K in air for 8 hours and then, in order to remove any residual solvent, to T = 550 K for 1 hour under high vacuum conditions (base pressure ~1x10^{-6} Torr). The obtained films of about 30 μm thickness are then ready for TSL investigations. After the drying procedure some of the samples are coated on top with an aluminium electrode by vacuum deposition under high-vacuum conditions (pressure = 1x10^{-6} Torr) in order to perform TSDC, DES and further

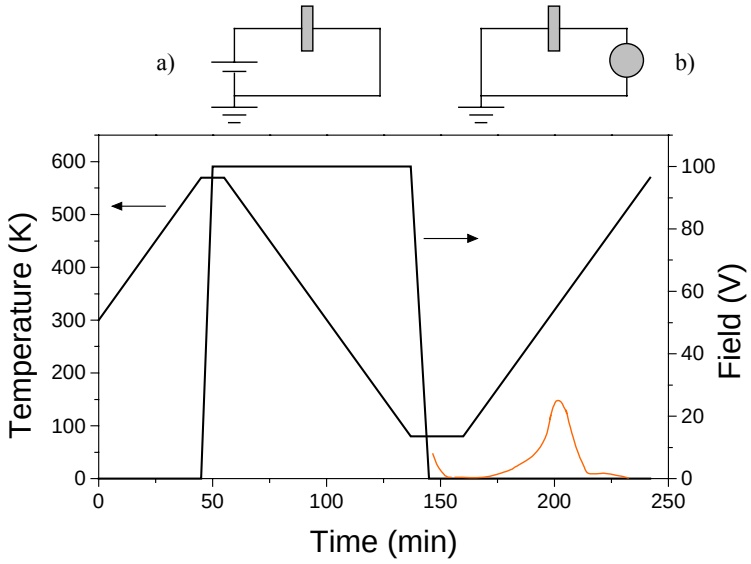

Fig. 4.3 TSDC method. Polarisation process: circuit a). Depolarisation process (TSDC signal): circuit b).

electrical investigations.

Figure 4.2 shows the measured TSDC spectra of a PPQ IA sample. During the TSDC measurements according to scheme of figure 4.3, the sample is polarised at high temperature, T = 600 K, cooled down with the applied field (see figure 4.3 circuit a), then shorted at low temperature (see figure 4.3 circuit b) and subsequently heated up keeping a constant heating rate, β = 0.1 K/s.

During the charging process either dipoles are oriented and charges are trapped in carrier traps of different energetic depth. The subsequent heating process depolarises polymer chains and side groups and both dipole reorientation and charge release from traps produces the TSDC peaks which are analysed in order to get detailed information on the microscopic processes taking place in the sample.

The dipole moment of PPQ IA was estimated[9,47] by theoretical simulations using the semi-empirical quantum chemical calculation methods AM1 and PM3. This organic compound shows a weak dipole

moment perpendicular to the main chain of 0.2 D per repeat unit. The phenylene sides groups, attached to the quinoxaline unit (see figure 1.6), are twisted with respect to the quinoxaline unit. The quinoxaline moieties are also bent and twisted in their relative positions along the main chain. That results in a complex conformation of the polymer that is bent and twisted at once. Hence, both charge transport and dipolar relaxation processes are expected to occur in the polymer.

The complex spectra of PPQ IA, shown in figure 4.2 together with the zero line graph, reveals a steady increase toward higher temperature and several peaks. The thermograms are measured for different applied polarisation fields ranging from 1.5×10^4 V/cm to 2.9×10^4 V/cm. The observed steady increase of the current can be ascribed to a thermo-electromotoric force caused by the unavoidable slight asymmetry in the electrochemical potential of the electrodes. The peaks at lower temperature, labelled with the roman

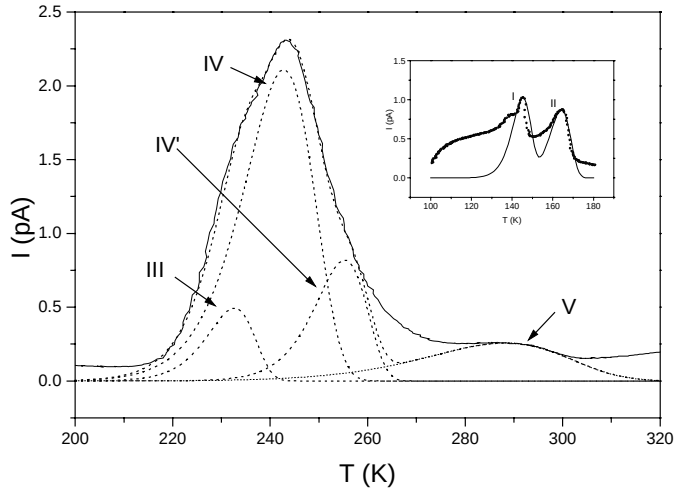

Fig. 4.4 Peak analysis of the low temperature relaxation process of the PPQ IA sample. In the inset: fit of peaks I and II

numbers from I to V, could have a dipolar origin, while the higher temperature peaks, above T = 300 K labelled with VI and VII, are connected with charge transport processes.

Actually, dipole peaks do not change their position at different poling field, while the charge transport peaks shift. This fact is clearly observed for peak VI and VII in figure 4.2. Moreover, peaks I to V have their area proportional to the polarisation field like one should expect for dipole peaks, while it is not the case for peaks VI and VII, showing certainly their charge transport origin. In particular, peak VII develops in a region near to the caloric glass transition for PPQ IA that reaches values between 590 K and 620 K depending on the molar mass. In that region there is a strong increase of the free volume resulting, from the electrical point of view, in a segmental relaxation, id est a motion of a large part of the polymer chain. The segmental relaxation in case of polar chains, like in our case, gives rise to a broad relaxation peak, the so called α-peak. For the above cited reasons it is straightforward to assume that peak VII is an α-peak.

Transport properties at high temperature are affected by the molecular motion of the polymer and by the energetic distribution of the hopping sites. The molecular motion influence very much, indeed, the mean hopping distance and the polarisation energy. Since there is evidence in DES spectra for peak VII but not for peak VI we assume the latter one to be connected to charge transport. Usually ionic transport occurs at temperatures above the α-process so that peak VI has a quite unusual peak temperature below the α-process. Since the transport of ions needs free volume only obtainable above glass transition we believe that peak VI is of electronic origin. A more detailed analysis is very difficult, because this peak is deeply hidden in the proximity of the α-region and only a modest part of it is visible.

The complex structure centred around T = 240 K shows clearly to be composed at least of two peaks. The first one at T_m = 233 K labelled with the roman number III and the main one at T_m = 243 K labelled with number IV. A satellite minor peak, that brings some interpretation troubles, appears at T = 288 K and is labelled with the number V. A detailed peak analysis of this rich structure is presented in figure 4.4.

A complex thermogram, in principle, can be analysed assuming a continuos distribution of relaxation times, or a superposition of a discrete number of single TSDC Debye peaks, each being characterised by a single relaxation time having a specific temperature dependence. The analysis of the complex structure of figure 4.4 can be carried out in a consistent manner if one assumes a number of discrete Debye peaks, including peak III at T_m = 233 K. The result of this analysis, as given in the graph of figure 4.4, is certainly very good.

The calculated curve, shown in figure 4.4 by means of a dotted line, follows very well the experimental one (full line). The other Debye peaks are labelled with roman numbers IV, IV' and V, respectively, where the latter has its maximum at higher temperature, T_m = 288 K.

According to equations (2.31) and (2.45) the quantities E and α_r determine the temperature position

Table 4.1

PPQ IA peak	Peak temperature	Peak energy	Natural frequency
I	145 K	0.39 eV	$1x10^{12}$ Hz
II	164K	0.45 eV	$1x10^{12}$ Hz
III	233K	0.95eV	$1x10^{14}$ Hz
IV	243K	0.67 eV	$1x10^{12}$ Hz
IV'	253K	0.6 eV	$1x10^{10}$ Hz
V	288 K	0.47 eV	$1x10^{6}$ Hz

of a Debye peak. For local relaxation processes we expect activation energies reaching values between 0.1 and 1 eV, while the natural frequency factor α_r should range typically between 10^6 up to 10^{14} Hz, depending on the involved processes.

Peak III centred at T_m = 233 K has an activation energy and natural frequency of E = 0.95 eV and α_r = 1x10^{14} Hz respectively, peak IV has its temperature maximum at T_m = 243 K, E = 0.67 eV and α_r = 1x10^{12} Hz. Peak IV', almost completely hidden under the two other peaks, is necessary in order to fit well the decreasing side of the resulting structure and is characterised by a maximum temperature of T_m = 253 K, a peak activation energy of E = 0.6 eV and a natural frequency, α_r = 1x10^{10} Hz.

The described three peaks have decreasing frequency factor and activation energy. Peak number IV is the most intense one, while peaks III and IV' have less than half of that the intensity, giving a smaller contribution to the whole structure.

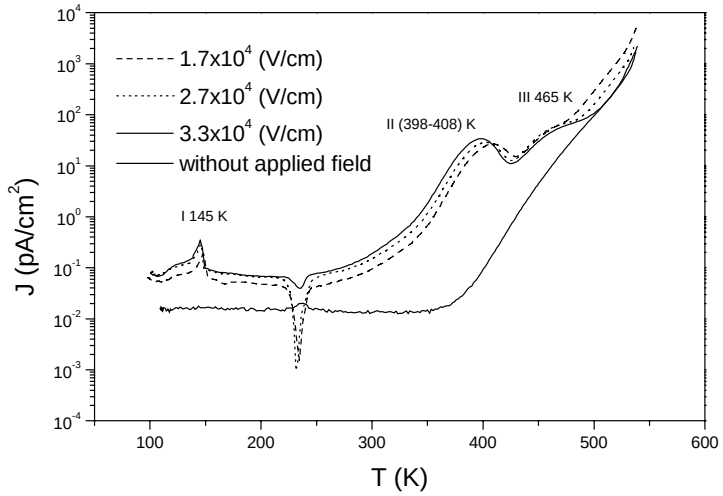

Fig. 4.5 TSDC spectra of a PPQ IIB sample.

Peak number V, though successfully fitted with a small pre-exponential factor, α_r = 1x10^6 Hz, still gives some interpretation problems. Besides the quite small natural frequency, a thermogram change in the zero line, obtained performing the measurement without a previous applied polarisation of the sample, is also observed how it results in figure 4.2, line labelled "without applied field". This peculiar feature could be connected with geometric changes or internal transitions of the sample, appearing in the same region of the peak and probably connected with it. For the above reasons the nature of this peak cannot be completely figured out.

The inset of figure 4.4 shows the results of numerical simulations of the peaks labelled with the roman numbers I and II. This two peaks are very near, the best fit has the same natural frequency value, α_r = 1x10^{12} Hz, for both and a similar activation energy of E = 0.39 eV and E = 0.45 eV is found, respectively. However, the numerical analysis, in this case, in spite of a relatively good agreement with the experimental curve, is questionable, because both peaks are very small and in a relatively noisy part of the thermogram.

Table 4.1 summarises the activation energy E, the natural frequency α_r, and the temperature maximum T_m used to fit the peaks of figure 4.2 and the structure shown in figure 4.4. The natural

frequencies have reasonable values and the calculated activation energies clearly indicate the occurrence of local relaxation processes.

Figure 4.5 shows the TSDC spectra of a PPQ IIB sample. The thermogram with respect to thermogram of polymer PPQ IA is less complex. It is possible to observe only three peaks. The first one, labelled with roman number I, at T_m = 145 K could have a dipolar origin and is very similar in shape and position to analogous peak I and II of PPQ IA. Peak number II around T = 400 K clearly changes its position in function of the applied field and should be, therefore, a charge transport peak as analogous peak

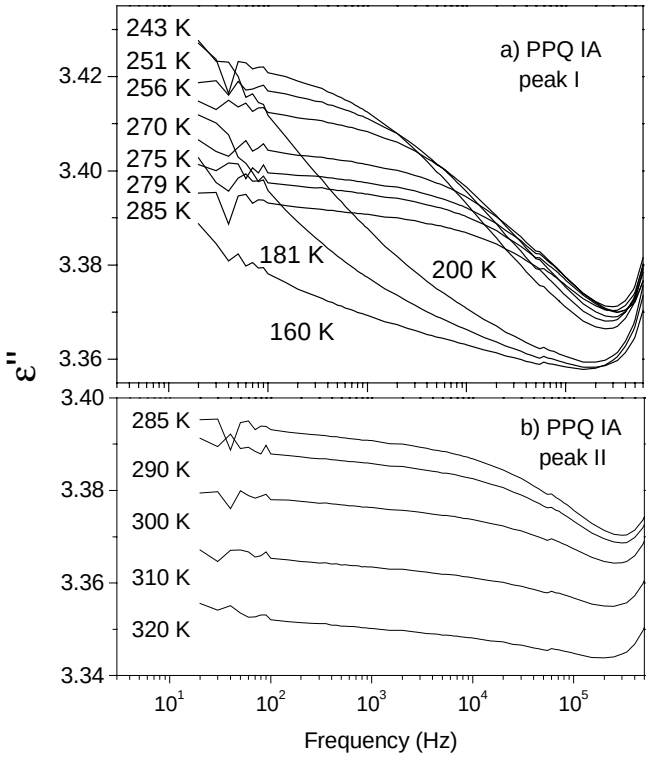

Fig. 4.6 DES spectra of a PPQ IA sample related to peak I (a) and peak II (b) of the TSDC thermogram.

number VI of PPQ IA. The last peak, peak number III, around T = 465 K, is correlated with the glass transition which occurs in PPQ IIB between T = 480 K and T = 530 K depending on the molar mass (see § 1.4.1.). Furthermore, at T = 230 K we observe a current reversal that could arises from the coexistence of homo-charges and hetero-charges[73] or internal transitions.

While the polarisation processes lead to hetero-charges frozen-in at low temperature, the homo-charges are connected with trapping phenomena. Deep traps can induce, especially in high resistivity materials, polarised states characterised by long lifetime. If the homo-charges decay by external conduction, the homo- and hetero-currents will have the same direction, but if the decay proceeds by internal conduction, like in the case of a TSDC experiment, the direction of the corresponding external

current will be opposite to the normal hetero-current, resulting in possible current reversals when the relaxation times of two types of charges differ widely. Afterwards the reverse peak at 230 K could be explained in terms of competitive homo, hetero-charges processes.

The pronounced difference in the dipole and transport peaks between PPQ IIB and PPQ IA can be found in the slightly different chemical structure of the two polymers. While PPQ IIB has an oxygen bridge in the main chain (see figure 1.7) acting as a flexibiliser and conjugation breaker, the structure of PPQ IA bears no oxygen at all (figure 1.6). This results in a lower glass transition temperature and in a lower conductivity of PPQ IIB. It should be also noticed that PPQ IIB is a better insulator than the formally conjugated polymer PPQ IA.

According to AM1 quantum chemical calculations PPQ IIB has the main chain bent by an angle of 114° and posses a dipole moment of 2.3 D per repeat unit perpendicular to it[47].

4.2.2. DES on poly-phenylquinoxalines

A way to proof the dipolar nature of the observed TSDC peaks is to carry out DES measurements. Assuming a single elementary relaxation process for each single peak and an Arrhenius law for the relaxation frequency it is possible to determine, through equation (2.45), the temperature range, around the maximum temperature value, to be analysed in order to verify whether the peaks in TSDC spectra have a

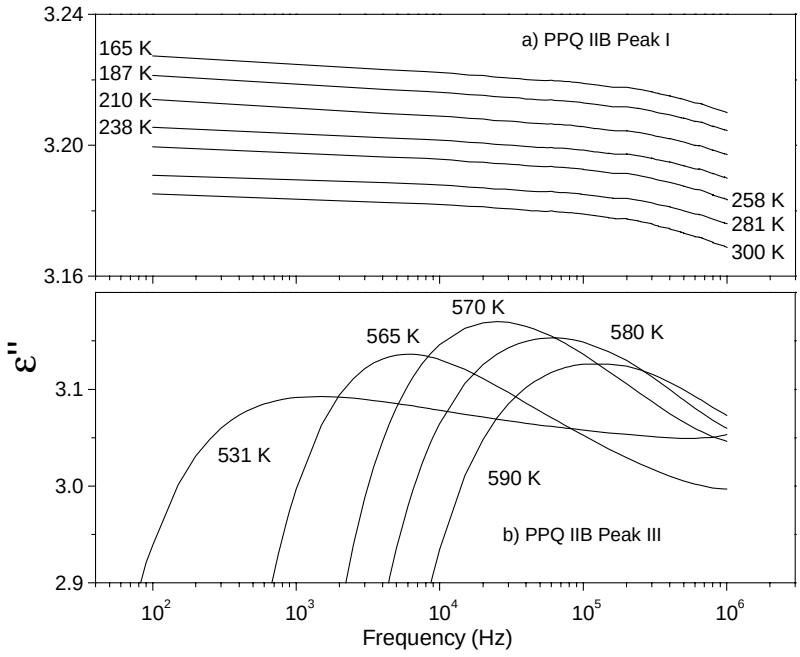

Fig. 4.7 DES spectra of a PPQ IIB sample related to peak I (b) and peak III (c). of the TSDC thermogram

dipolar origin.

The numerical analysis of a TSDC peak determines the values of its frequency factor α_r and activation energy E. Substituting this two experimentally found values in equation (2.45), we are able to get the expected temperature at which the dielectric relaxation maximum, equivalent at a certain TSDC peak, occurs enabling a cross check of the previous results. In effect, the two experimental methods are strictly correlated, but while DES can be carried out as an isothermal technique, i. e. the measurements are performed at different fixed temperatures, TSDC is by definition non-isothermal, i. e. the temperature changes at fixed rate during the measurement. Although the values of the TSDC numerical analysis are subject to a certain degree of uncertainty, according to the fit quality, it is possible to extract a temperature range inside which the DES peak maximum should appear.

Figure 4.6 a) shows the dielectric spectra related to peak I of PPQ IA TSDC thermogram shown in figure 4.2. According to numerical analysis data of table 4.1, and using equation (2.45), the dielectric relaxation process is calculated to occur in the temperature range between T = 245 K and T = 285 K. A dielectric peak, appearing at temperatures above 200 K in figure 4.6 a), reduces slowly in intensity when the temperature reaches higher values. Below T = 200 K no dielectric peaks are observed because the maxima are outside the frequency window. This confirms that peak number I of PPQ IA has a dipolar origin. The same kind of analysis, always based on the TSDC data summarised in table 4.1, is performed for peak number II of PPQ IA. The dielectric relaxation peak should appear in the temperature range between T = 283 K and T = 320 K. However, in that case, as can be seen in figure 4.6 b), no sign of dipolar relaxation is observed. Hence, the TSDC peak II could originate from a de-trapping process. However, it is not possible to exclude completely that such finding can be connected to a lack in accuracy of the fitting

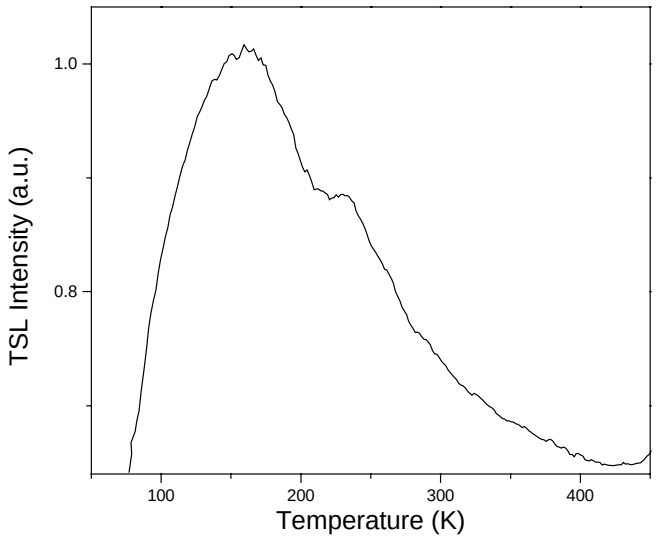

Fig. 4.8 Example of a TSL glow curve of PPQ IA.

procedure of the TSDC thermogram. This fact could lead to inaccurate parameters, and consequently preventing a correct estimation of the DES maximum temperature range. Furthermore, the absence of the peak could be also related to the inadequate resolution of the dielectric spectroscopy experiment, as discussed in chapter 3. In principle TSDC has a better resolution and much higher sensitivity in comparison to dielectric spectroscopy.

The same analysis on peak number I of PPQ IIB is shown in figure 4.7 a). This peak does not show any sign of dipolar relaxation. We can reasonably conclude that peak II of PPQ IA and peak I of PPQ IIB have the same origin in structural or chemical defects of the polymer, leading to a level of localised states and do not have a dipolar origin. Figure 4.7 b) shows a further example of a dielectric spectroscopy peak. In this case temperature range is calculated on the basis of TSDC parameters corresponding to peak number III of PPQ IIB.

The TSDC peak III, shown in figure 4.5, is almost completely hidden in the ionic current and only a wide range of parameters is possible to extract from its uncertain numerical fitting. The extracted values for the natural frequency and activation energy allows to predict a wide temperature range between T = 400 K and T = 600 K.

The DES peak appears, clearly, to have a maximum at T_m = 570 K at the expected frequency α = $2x10^4$ Hz. This finding proofs the dipolar origin of the related TSDC peak. Peak number II of PPQ IIB, although completely hidden under the ionic current, is extremely difficult to analyse by DES. In fact the typical peak temperature derived from the numerical analysis lies outside of the available temperature range. The group of peaks around T = 250 K for PPQ IA shows according to the numerical simulation data, also dielectric peaks in inaccessible temperature ranges.

4.2.3. TSL on poly-phenylquinoxalines

In order to clear-up the presence of trapping states in the thermograms a further analysis is necessary. TSL is probably the most powerful technique in order to unambiguously observe the presence of localised states in a material. For such reason samples of PPQ IA and PPQ IIB, without the upper aluminium contact, prepared in the same way as described for the TSDC and DES investigations, are analysed by TSL.

In order to perform TSL experiments, the samples of the two polymers PPQ IA and PPQ IIB are heated up at about T = 500 K and subsequently cooled down to liquid nitrogen temperature. Then the samples are illuminated with a 1000 W Xenon lamp for 15 minutes and after switching off the light they are heated up with a constant rate of β = 0.1 K/s. The TSL signal is collected during the heating process with the photomultiplier and the measured signal is recorded as function of time and temperature. The 15 minutes of illumination are long enough to fill-up completely the levels. Preliminary experiments show that for an excitation time above 12 minutes no changes in intensity of the glow curves can be detected. It is therefore possible to assume that all levels of traps are completely filled.

Figures 4.8 and 4.9 show examples of glow curves of PPQ IA and IIB respectively. The spectra are recorded several times and both materials do not show any sign of degradation. Both glow curves appear quite broad and complex. For that reason the thermograms are analysed by means of different methods. According to Halperin and Braner[87] the peak shape method, introduced in chapter 3, allows to estimate the symmetry factor μ appearing in equation (3.9). Such finding can reveal the kinetic order of the peaks. This is a necessary information to understand the type of microscopic recombination processes involved. In case of first-order kinetics the typical value for μ is 0.42. In first order kinetic the recombination process is characterised by a negligible re-trapping. On the other hand $\mu = 0.52$ is the typical value in case of pure second order kinetic, that means prevalent re-trapping. Values between these two describe an intermediate case where electrons have a certain increased probability to get re-trapped before to recombine at increasing values of μ. Values above $\mu = 0.52$ are often interpreted in terms of fast re-trapping processes[74]. The PPQ IA glow curve, shown in figure 4.8, is characterised by two peaks. The main one has the maximum temperature at $T_m = 159.1$ K and the second, of intensity roughly the half, at $T_m = 230.7$ K. Both are broad and the minor is almost completely hidden by the main peak. The peak at $T_m = 159.1$ K has a symmetry factor $\mu = 0.54$, very near to the typical value for the second order kinetic. This fact gives an hint that in PPQ IA an electron, before to recombine, has high probability to get re-trapped several times. Activation energy, E, of this first peak, calculated with the initial rise method based on equation (3.1), lies between $E =$ 60 meV and $E = 80$ meV. The initial rise method, despite the fact that it involves only a few experimental points, that are in a critical temperature range (see chapter 3), is very suitable to get the value of the activation energy without previous knowledge of the other sensitive parameters. However, the shape and especially the large width of the glow curve, confirms that the traps are widely distributed in energy.

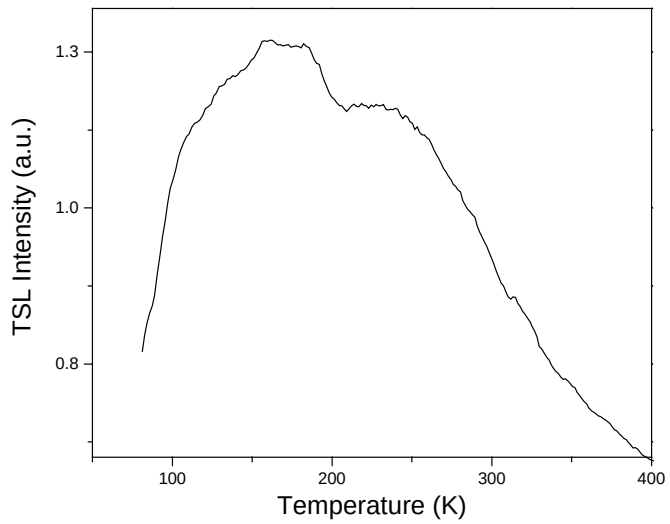

Fig. 4.9 Example of TSL glow curve of PPQ IIB

Because of its hidden position the analysis of the minor peak of PPQ IA appearing at T_m = 230.7 K is very difficult. From investigations performed by means of the partial cleaning technique, a value of the activation energy around E = 0.18 eV and a symmetry factor quite high, μ = 0.6, are found. The partial cleaning technique gives reliable results only in case of the inversion point, i. e. the starting temperature of a hidden peak, is clearly determinable. Only in such case it is possible to completely reveal the hidden peak by a partial thermal cycle that "cleans" the major one emptying its localised levels. Unfortunately, in the present case, to isolate the inversion point is not unambiguous. The calculated values give only an order of magnitude of the quantities under investigation.

Figure 4.10 shows the numerical fitting of the main TSL peak of PPQ IA. The fit is performed by means of the second order equation (2.22) characterised by a Gaussian distribution of traps. While the high temperature side perfectly fits the glow curve, the low temperature side do not follow the curve shape. For that reason the numerical simulation is not completely satisfactory. The distribution has a width σ = 0.12 eV and the distribution maximum is at E_m = 0.37 eV. The energy maximum E_m lies exactly in the middle of the integration limits E_1 = 0.25 eV and E_2 = 0.49 eV, having the distribution in such case a perfect Gaussian shape. The natural frequency s of this peak can be estimated to be in the order of $s = 1\text{x}10^{10}$ s^{-1}, considering, like usual, the recombination coefficient / trapping coefficient ratio equal to 1 and a density of traps of 10^{14} cm^{-3}.

The value of E_m, derived by the numerical analysis, is far from the expected energy depth of trap calculated with the initial rise method. However, this mismatching can be explained considering the

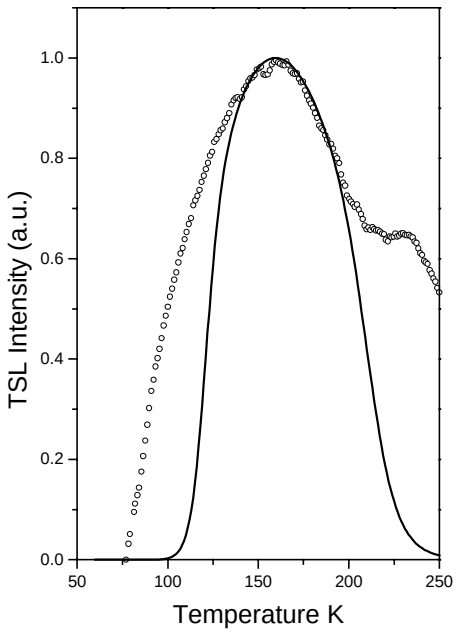

Fig. 4.10 TSL glow curve of a PPQ IA sample (dot line) compared with the second order numerical simulation of the first peak

particular complexity of the peak that could result from the sum of at least two distributed peaks. In effect the initial rise procedure reveals the activation energy of a hidden peak at low temperature. This is a relevant point to be clarified because of importance of presence of shallow traps in materials suitable for plastic electronic applications. Shallow traps are, at room temperature, empty and they play a crucial role in the electron transport property of organic materials.

While the TSDC thermograms of PPQ IA and PPQ IIB are completely dissimilar, being the prior much more complex, the TSL glow curves are very similar. The glow curve of PPQ IIB shown in figure 4.9 is characterised by large structures like the thermogram of PPQ IA. The first complex structure lying between $T = 100$ K and $T = 200$ K reach the maximum at $T_m = 160.4$ K and the second structure, less bright and almost completely hidden by the major ones, has its peak maximum at $T_m = 226.1$ K. Both structures of the PPQ IIB glow curves nevertheless look complex, having an unusual irregular shape and being characterised by several satellite peaks. In such case the analysis is extremely difficult to perform. Data, in principle, can be extracted through several cycles of peak cleaning and exciting the sample at several different temperatures in order to reveal the localised states with a tedious and time consuming procedure. The activation energy of the lowest temperature peak, calculated with the initial rise method, is in the range between $E = 10$ meV and $E = 80$ meV, while the activation energy and the symmetry factor, estimated with the peak shape method, by means of equations (3.8) and (3.9), are $E \sim 30$ meV and μ lies between 0.52 and 0.56. The highest temperature peak has an estimated activation energy around $E = 0.11$ eV while the symmetry factor is not possible to estimate. Also in this case it is possible to argue that the first peak of PPQ IIB, like for PPQ IA, is characterised by predominant electron re-trapping processes before recombination takes place.

The combination of the three techniques TSDC, DES and TSL demonstrates the presence, in both polymers PPQ IA and PPQ IIB, of both depolarisation phenomena and broad distributions of localised levels. While it is possible to analyse and examine the single Debye depolarisation peaks, the traps, shown by means of TSL technique, are characterised by very broad distributions having almost the shape expected for an amorphous glass.

However, it is possible to observe, in both polymers, two main structures very similar that could be due to breaks in polymer conjugation and presence of contaminants like oxygen. A direct correspondence between the observed TSDC and the TSL peaks is not possible and also the analysis of the indubitable presence of shallow level of traps should be subject to further analysis. Exciting the samples at liquid helium temperature and analysing furthermore the spectra of the emitted light it is possible to extract more reliable data on the shallow traps and to study the recombination centres. Only in this way it is possible to understand the nature of the traps and recombination centres as well as to uncover distributions of localised states fully.

4.3. TSL on low molecular compound

The special needs for electron transport materials for organic LEDs and for plastic electronic applications stimulated the synthesis of many new polymers and low molecular compounds. This new materials of the last generation are characterised by improved thermal stability, high ionisation potential, better film

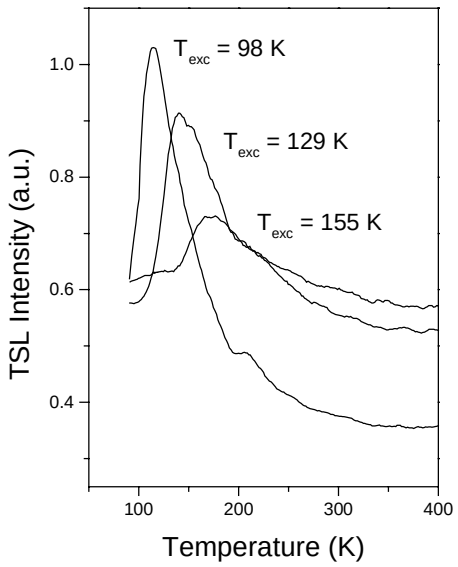

Fig. 4.11 TSL glow curve of cast TPQ samples at different excitation temperatures.

forming properties, good solubility in common solvents, making them very promising materials for future electronic applications. In particular we analysed the TSL spectra of the star starburst 1,3,5-Tris[(3-phenyl-6-trifluoromethyl)-quinoxaline-2-yl]benzene (CF_3-TPQ or simply TPQ in the following) shown in figure 1.9 and of the well ordered and stable Langmuir–Blodgett (LB) multilayers films with very smooth and uniform surface structure of the amphiphilic substituted 2-(p-nitrophenyl)-5-(p-undecylamidophenyl)-1,3,4-oxadiazole (NADPO) shown in figure 1.10.

4.3.1. TSL on trisphenylquinoxaline

A very interesting material matching the needs for electron transport layer in OLEDs is the star shaped trisphenylquinoxaline shown in figure 1.9. TPQ has a high glass transition temperature and its electrons overall mobility is quite high approaching 10^{-4} cm^2/V at large field ($U \approx 10^6$ V/cm)[49]. We studied TPQ samples by means of the thermal techniques in order to highlight the presence of localised states that plays a major role in the transport properties of the compound.

We prepared films of TPQ both by vacuum deposition and by solution casting. The vapour phase deposition is done in a high vacuum chamber onto a flat silicon wafer covered with a freshly evaporated aluminium surface. The preparation chamber is equipped with graphite crucibles and the evaporation temperature control of the material is assured by a thermocouple inserted in a housing carved directly into the crucible. This particular arrangement gives the actual temperature of the system organic-crucible. The thickness is detected in situ by means of a quartz micro balance and ex situ with ellipsometric

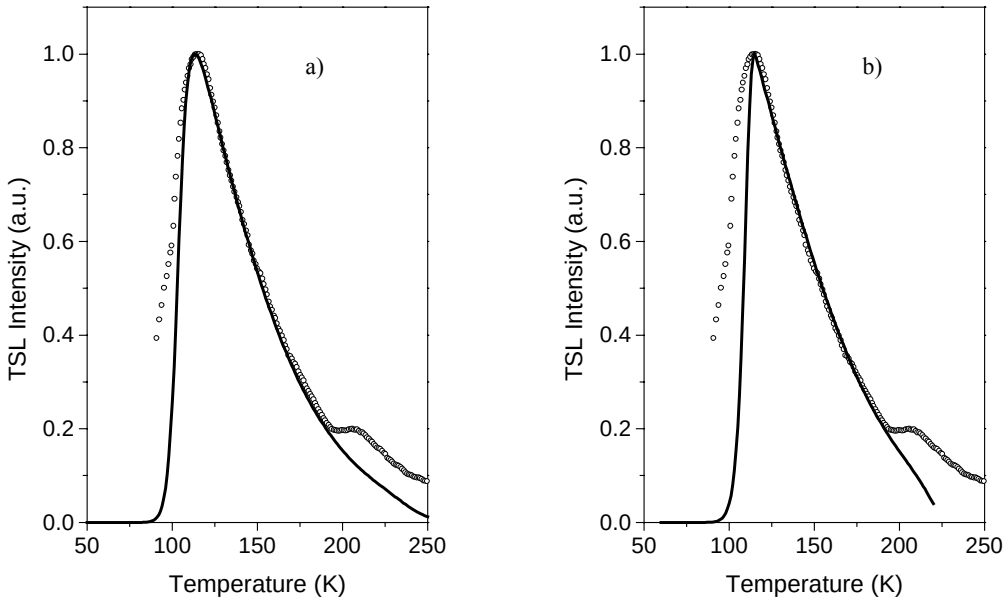

Fig. 4.12 TSL glow curve of a TPQ cast sample (dot line) compared with a) second order numerical simulation, b) first order numerical simulation.

measurements. The substrate is kept at room temperature. The evaporated samples have typically a thickness of about 100 nm.

Cast samples, typically about 10 μm thick, are prepared from a chloroform solution on a silicon wafer covered with a freshly evaporated aluminium surface. The preparation of samples by casting requires several days. In order to obtain smooth and uniform surfaces the quinoxaline is deposited by means of several subsequent steps with different decreasing solution concentrations. The deposition is done in a glove box in a nitrogen inert atmosphere. After preparation the cast films are heated up under high vacuum conditions (P = 1x10^{-6} Torr) up to T = 350 K for 8 hours and furthermore for 1 hour at T = 420 K (TPQ glass temperature) in order to remove, with the thermal treatment, any residual solvent that could interfere with the TSL measurements.

A TSL measurement requires, how already underlined, a perfect sample temperature control in a wide temperature range. The silicon substrate, used in both cast or evaporated samples, glued on top of the cryostat cold finger with the help of a layer of silver paste, assures the compulsory excellent thermal contact between the cold finger and the overlying sample film.

Figure 4.11 shows some of the glow curves recorded in case of cast TPQ. For different excitation temperatures a shift of the peak maximum and a broadening of the main peak, probably related to sample degradation, are observed. The glow curves show clearly two peaks; the first one for an excitation temperature of T_{exc} = 98 K at T_m = 114.6 K is highly asymmetric and bright.

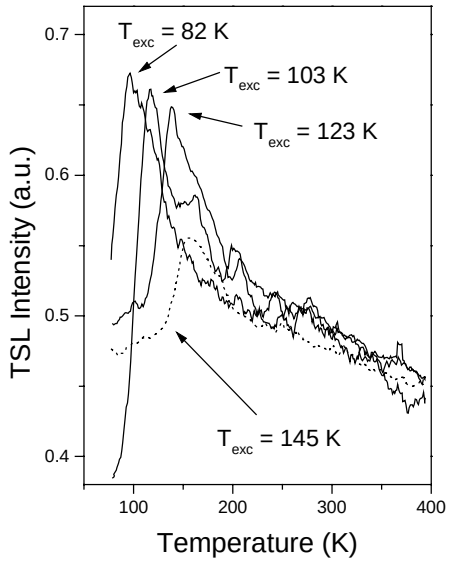

Fig. 4.13 TSL glow curve of evaporated TPQ samples at different excitation temperatures.

A second peak at the same excitation temperature appears at T_m = 206.4 K. This second peak is small and partially hidden in the long tail of the main peak. Besides, it tends to disappear, absorbed into the main peak, with increasing number of thermal cycles.

The main parameters of TPQ glow curves are calculated using different methods: initial rise, peak shape and curve fitting by numerical simulations. The activation energy of the main peak, calculated using the Lushchik's formula (3.8), gives values between E = 0.1 eV and E = 60 meV while the initial rise method gives, for the same parameter, different values, between E = 10 meV and E = 20 meV. The resulting symmetry factor μ = 0.70 is very high and gives puzzling information about the electron kinetic.

Nevertheless, numerical simulations, shown in figure 4.12 for the first and second order kinetics, give an insight into the main features of the curves. The simulations are performed playing around the activation energy values, given by Lushchik's formula and the initial rise method. Both first and second order kinetic equations (2.14) and (2.22) including a Gaussian distribution of localised states are used. Because of the organic nature of the material and further considering the high purity of the starting TPQ, we assume, for statistical reasons, that the distribution of localised states should be Gaussian. However, how already discussed in chapter 3 the manipulation of the Gaussian parameters allows easily to get different distribution shapes.

Figures 4.12 a) and b) show the experimental glow curve of a cast TPQ sample compared with the simulations made using equations (2.14) and (2.22) for the first and second order kinetic respectively. The results are quite satisfactory and clearly the experimental curve is better simulated assuming a second order kinetic that means re-trapping probability for a released electron not negligible. The best fit is obtained keeping the energy maximum of the Gaussian distribution at E_m = 0.12 eV in agreement with Lushchik's formula. The integration limits E_1 and E_2 of equation (2.22) are respectively E_1 = 0.29 eV and E_2 = 0.61 eV.

Assuming a maximum density of traps $N = 1x10^{16}$ cm^{-3} and, like usual, the ratio $A_r/A = 1$ it is possible to estimate the frequency factor $s = 1.5x10^{12}$ s^{-1}. The width of the distribution $\sigma = 0.19$ eV is quite broad and considering also the above parameters the distribution maximum results outside of the integration limits.

According to figure 3.17 and taking into account the theoretical consideration mentioned in the same chapter, we can argue that the effective distribution used in the present case is not a pure Gaussian but we are only considering the upper energy side between the integration limits. Moreover, the low energy tail of the distribution of states penetrate into the conduction band. This particular feature of the simulation is reasonable and consistent with the model. According to such description, defects, leading to the trap levels, are distributed energetically also inside the conduction band.

The fact that only the distribution's higher energetic tail contributes to the TSL peak can be explained by the fact that at liquid nitrogen temperature the traps distribution side, nearest to the conduction band, gives a very small contribution to the overall collected light. The proposed model can be proofed, however, by exciting the sample at very low temperature. Only in this case the very shallow traps are filled for a time long enough to give a complete TSL glow curve and then a complete picture of the shallow traps involved in the recombination processes.

The parameters used for the first-order numerical simulation of figure 4.12 b) are very similar to the set of parameters used for the second-order fit: energy recombination maximum $E_m = 0.12$ eV, integration limits $E_1 = 0.3$ eV and $E_2 = 0.6$ eV, maximum density of states $n_m = 1x10^{16}$ cm^{-3}, $\sigma = 0.2$ eV, and $s = 1.5x10^{12}$ s^{-1}. It is important to note here, that the attempt of a numerical fit with a simple exponential distribution of traps, does not give enough satisfactory results. Only the Gaussian distribution so modified gives a satisfactory fit. This finding further confirms that the observed distribution of traps is just a tail of a more extended Gaussian distribution of localised states that is possible to be extracted by means of a numerical simulation starting from a single branch of it.

It is difficult to explain why the initial rise method and Lushchik's formula both give such a low activation energy with respect to the numerical fit. The very shallow traps filled at $T = 98$ K get empty very fast at the beginning of the heating-up cycle of the sample. However, the symmetry factor indicates that the electrons before definitely leaving the trapped states get re-trapped several times. The effect of repetitive trapping and de-trapping could, in principle, explain the low activation energy registered. Furthermore, it should be noted that the indication of the activation energy between the initial rise and the curve shape method is quite contradictory. The initial rise method uses in order to calculate the activation energy only the initial points of the glow curves, which are the more disturbed by the heating start fluctuations and the electron traffic between traps and the conduction band.

The TSL spectra of TPQ samples prepared by vapour phase deposition show more complex features with respect to samples prepared by solution casting. Figure 4.13 illustrates four different glow curves obtained exciting the sample at different temperatures. The glow curves are more noisy probably because of the reduced thickness (about 100 nm) with respect to the cast samples. However, the main peak preserves its features, while the small one, clearly recognisable for the previous samples, appears to be hidden between several other small peaks that characterise these spectra. The peak shape analysis confirms an activation energy for the main peak between $E = 0.07$ eV and $E = 0.1$ eV like for the cast one, and the

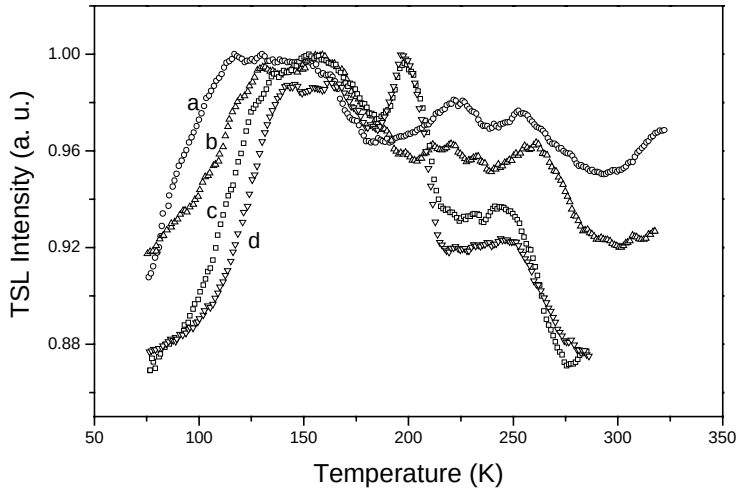

Fig. 4.14 TSL glow curves after irradiation at 77.5 K. Curve (a) as irradiated sample. Curves (b) to (d) at T_{stop} : (b) 108.6 K, (c) 112.8 K and (d) 123.7 K.

initial rise gives, in agreement with the values registered for the cast samples, values of E between $E = 0.04$ eV and $E = 0.01$ eV depending on the excitation temperature. The symmetry factor can be estimated to be about $\mu = 0.70$, in exact agreement with the cast sample.

From the above analysis results that the main peak of samples prepared with two completely different preparation techniques, casting and vapour deposition, has exactly the same origin. It is only possible to speculate about such origin, having a limited amount of data. Considering the high purity of starting material and considering the equivalence of the results between the two preparation techniques we can argue that the traps referred to the main peak of TPQ are physical shallow traps that can be connected with reticular distortion, broken ends, morphological conformations and even molecular polarons. Such kind of trap rules the transport properties of the material and are unavoidable in sample preparation.

4.3.2. TSL on diphenyloxadiazole

The amphiphilic derivative of 2,5-diphenyl-1,3,4-oxadiazole (NADPO) shown in figure 1.10 has the property to form very smooth and well ordered films when prepared under the appropriate conditions by vapour deposition as well as by Langmuir Blodgett (LB) technique. We investigate LB films by means of ultraviolet photoelectron spectroscopy (UPS) and TSL in order to get information about the ionisation potential, the electron affinity, to localise the energetic position of valence and conduction band[35] and to highlight the intra band gap features.

The LB film deposition is performed on a KSV 5000 trough (KSV Instruments, Helsinki, Finland) equipped with a Wilhelmy plate surface pressure sensor. The spreading solutions is obtained by dissolving 0.4 mg/ml of substance in chloroform. The monolayer is formed by spreading 320 µl of the solution on the

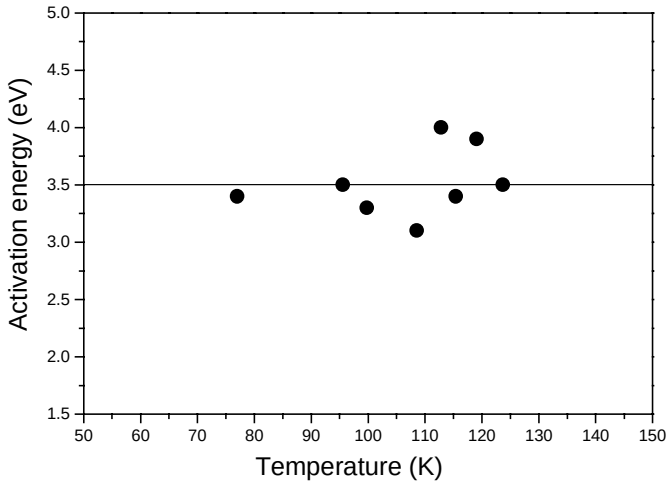

Fig. 4.15 Activation energy versus partial cleaning temperature evaluated by using the initial rise method. The first point is evaluated taken into account the glow curve without applying the partial cleaning method, in this case the abscissa is the starting temperature.

water subphase provided by a Milli-Q system (Millipore). The subphase temperature is held constant at 20°C and the water pH was 5.6. The constant barrier speed compressing the film is 15 cm^2/min. The films composed of 10 monolayers are deposited on a cleaned silicon wafer previously hydrophobized by treatment with hexamethyldisilazane (HMDS). The target pressure and the dipper speed up and down applied are 30mN/m and 3 mm/min up, 10 mm/min (Y-type transfer) down, respectively.

TSL measurements are performed under high vacuum conditions with the pressure in the range of $P = 1x10^{-6}$ Torr. Preliminary results show that to illuminate the samples for 10 minutes at liquid nitrogen temperature with the 1000 W Xenon lamp ensures a complete trap filling. After the excitation at T_{exc} = 77.5 K the samples are heated up with a linear rate of β = 0.1 K/s. The TSL emission is detected with the Hamamatsu photomultiplier tube.

The rich TSL glow curves are characterised by a complex structure in the temperature range between T = 120 K and T = 160 K and two further peaks, one at T_m = 224 K and the last one a T_m = 253 K. The glow curves are unexpectedly complex and difficult to analyse. The different peaks clearly indicate the presence of trap distributions localised in the band gap region. The localised state distributions can be due to extrinsic as well as intrinsic defects. Structural defects, lattice distortions and chemical contaminations due to the preparation procedure of the organic compound are likely the reason of such complex features. In order to discriminate the several peaks and then to analyse the different traps levels, we apply the maximum temperature recording technique, as described in chapter 3, and the usual numerical analysis of the peaks.

In the maximum temperature recording technique, shortly called T_m-T_{Stop} technique, we illuminate the sample at minimum temperature, T_{exc} = 77.5 K in the present case, and afterwards the whole glow curve is recorded for a first thermal cycle heating up the sample in a controlled way, i.e. β = 0.1 K/s. During a second cycle we illuminate the sample exactly at the same temperature of the previous one, in order to

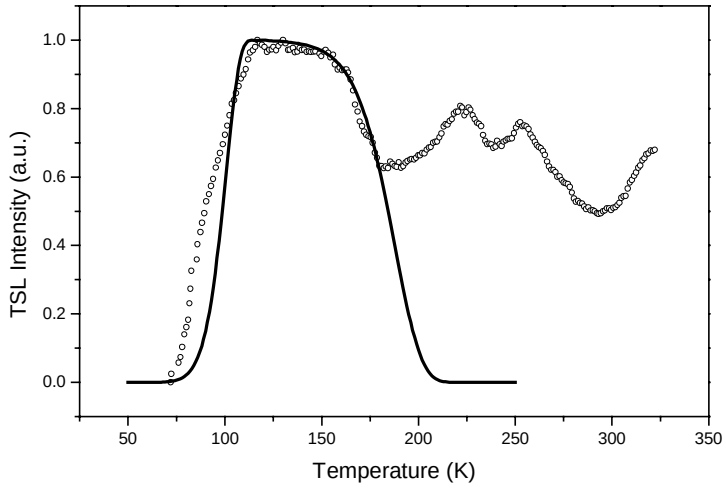

Fig. 4.16 TSL glow curve (dot line) compared with the numerical simulation (full line).

avoid spurious position modifications of the peak maximum. Afterwards, the samples are heated up to an intermediate temperature T_{Stop}. Then, the sample is cooled down again, reheated in the same controlled way and the glow curve registered. A certain number of excitation, heating, cooling cycles, each with a different incremental T_{Stop}, are necessary in order to "clean" the complex glow curve and then to reveal the hidden internal structure.

A selected number of the T_m-T_{Stop} curves are shown in figure 4.14. The small sample's size, 12x10 mm, limits the overall amount of collected light. The curves appear to be noisy, but the peaks are enough clear to be analysed without particular problems. An unexpected peak suddenly rises after several thermal cycle at T_m = 202 K, as can be seen in the curves labelled with letters c and d in figure 4.14. Such peak can be easily connected to a level of traps probably arising from the ageing effect that lowers the degree of order of the otherwise highly ordered LB film.

The initial rise method enables one to determine the activation energy independently from other parameters, and applied to the low temperature complex structure, gives the value $E = 3.5 \pm 0.3$ meV. This value is the average determined from the values calculated for the different cleaned peaks shown in figure 4.15.

The numerical simulation shown in figure 4.16 gives a deeper description of the trap distribution. In order to get the flat shape of the main structure the numerical analysis is performed keeping nearly fixed the activation energy calculated by means of the initial rise method and consequently varying, around this slowly changing value, the other parameters. The successful numerical fit, shown in the figure, emerges using a value for E_m = 4 meV and using the integration limits E_1 = 0.12 eV and E_2 = 0.22 eV in the first order equation (2.14) having a Gaussian distribution of localised states. The maximum of the distribution lies outside the integration limits, this means again that the distribution we are considering is only the

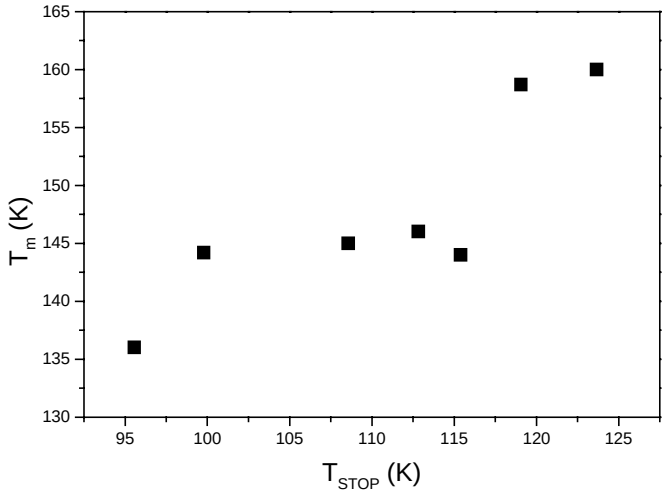

Fig. 4.17 $T_m - T_{stop}$ curve.

lowest lying energetic tail of a full Gaussian. The energetic distribution of localised states penetrate deeply into the conduction band, i.e. the defects are distributed in a wide energetic range also inside the conduction band. This finding suggests that we are dealing with a large distribution of shallow traps having physical origin or with molecular polarons.

In order to get the particular shape of the complex structure under examination it is necessary to consider a distribution of defects energetically widely distributed with σ = 0.7 eV. In agreement with the particular shape of the peak and considering the integration limits, the distribution could be considered quasi-continuous, flat and wide.

A further sensitive parameter is the frequency factor *s*. For this particular peak it is quite low, *s* = $1x10^4$ s^{-1}. However, it should be noted here that such low *s* values are not very rare in organic materials. Effectively a very low frequency factor of about 10^3 s^{-1} was recently found for the peak at 67 K of a 8-hydroxyquinoline aluminum (Alq_3) sample[91]. A slow recombination mechanism could be invoked in order to explain this values for the frequency factor. Such recombination mechanism, that should involve a slow vibrational mode for a side molecular group combined with an electron jump from one molecule to a second one in the same vibrational mode, could in principle, approximately, account for the low value of *s*. Numerical simulations, performed imposing higher values of *s*, do not fit the curve so tightly like the one shown in the figure. However, the low signal level and the noisy nature of the TSL signal, for this particular samples, do not exclude that this especially low frequency factor can be just an artefact of the specific experimental conditions. More investigations in the direction of such singular low *s* values should be done comparing curves recorded after excitation at liquid helium temperature.

The comparison between the experimental data and the numerical simulation provides the result that the complex structure is not only due to the main peak discussed above, but there is also a minor peak contributing at lower temperature. The agreement between experimental and theoretical curve, is, in effect,

very satisfactory in the higher glow curve temperature side. However, the low temperature side does not fit in the same satisfactory way and one possibility to explain this discrepancy can be the assumption of the presence of a minor distinct peak completely hidden under the main peak, and it only accidentally emerged because of the specific excitation temperature used during the experiment. In order to disclose the eventual presence of such hypothetical secondary peak, the maximum peak temperature T_m is plotted versus the partial cleaning temperature. The result is shown in figure 4.17. According to figure 3.3 and the theory introduced in chapter 3 a step like shape indicates the presence of a second peak in case of the first order kinetic. The figure shows clearly the predicted shape and confirms, according to McKeever[85] and the consideration in chapter 3, the assumption that the analysed complex structure belongs to an overlapping of two first order peaks, very close in energy. From figure 4.15, showing the activation energy calculated with the initial rise method versus the cleaning temperature, it is not possible to discriminate more than one value and an average energy is given. Therefore, TSL measurements have clearly indicated the occurrence of one or more broad distributions of shallow traps localised in the band gap. Because of their low activation energy, these distributions play an active role in the transport properties of the material, being also important in OLED operation.

Besides the broad structured peak at low temperature originating from shallow traps, two more peaks are observable in all glow curves of figure 4.14. The two peaks at T_m = 221.5 K and T_m = 254.2 K, respectively, are clearly visible in the first TSL run of figure 4.14, labelled with letter a, and then they tend to lower and to disappear with the increase of the number of thermal runs. The origin of such behaviour is not completely clear, it is probably connected with the appearance of the third peak at T_m = 197.7 K. The nature of this peak seems to be connected, how we will discuss later, with the increase of the film disorder.

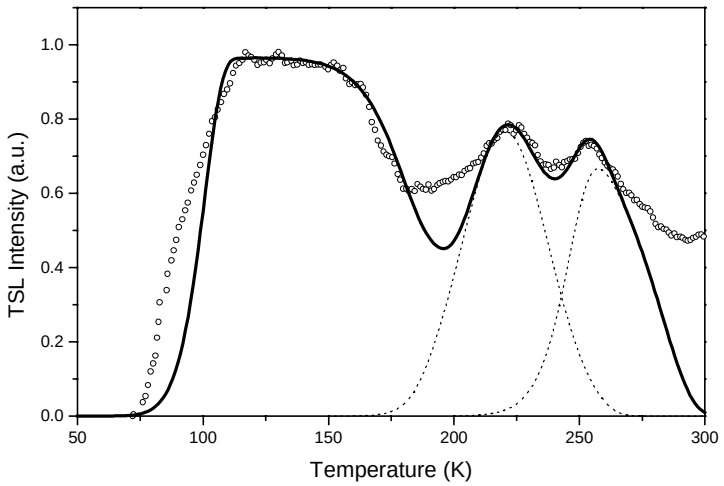

Fig. 4.18 TSL glow curve (open circles) compared with the numerical simulations sum (full line) and the two minor peaks (dot line).

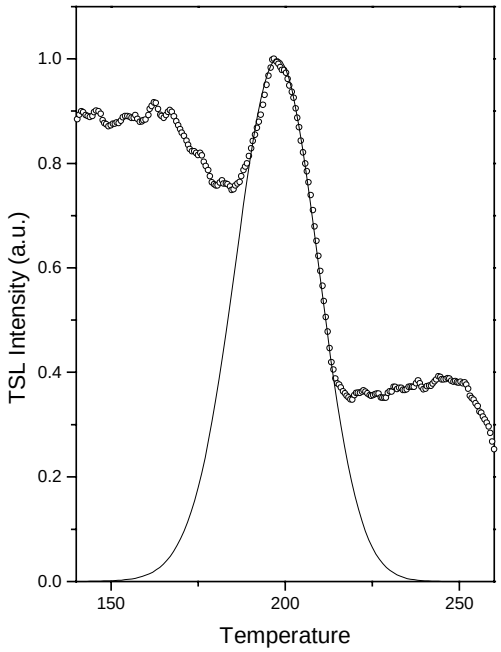

Fig. 4.19 TSL glow curve (open circles) compared with the numerical simulation (full line) of the single peak arising with the number of thermal cycles.

Figure 4.18 shows the numerical simulation of the main peak and the two peaks at higher temperature. Because of the reciprocal influence, the actual experimental temperature position of the maximum of this last two peaks is not coincident with of the calculated one. The experimental peak at T_m = 221.5 K has the numerical maximum at T_m = 220.5 K while the experimental T_m = 254.2 K has the numerical simulation maximum at a slightly higher temperature, T_m = 257.7 K. The numerical simulation fits in an excellent way the experimental curve and unmistakable reveals the presence of a third peak around T_m = 197 K also in this first TSL run. Both peaks are fitted with a first order equation with a Gaussian distribution of localised states described by equation (2.14). The peak at T_m = 220.5 K has the distribution maximum at E_m= 0.63 eV. The integration boundaries are E_1 = 0.53 eV and E_2 = 0.73 eV, respectively. The distribution width, σ = 0.045 eV, is small, while the frequency factor s = 2.4x10^{12} s^{-1} has a reasonable order of magnitude. The assumed density of traps for both numerical simulations is n_m = 1x 10^{16} cm^{-3} and the heating rate is like usual β = 0.1 K/s.

The peak at T_m = 257.7 K has a more asymmetrical shape. The energy distribution maximum E_m = 0.66 eV is very near to the previous one, but in order to get a reasonable fit, it is necessary to set the integration limits E_1 = 0.65 eV and E_2 = 0.75 eV in an asymmetric way. This means that the distribution is not fully Gaussian, but drops suddenly at 0.65 eV, slightly after the maximum. This indicates that the actual trap distribution for this second peak is an exponential one. While statistical fluctuations of the potential in the trap levels due to intrinsic disorder of the organic materials are described using Gaussian distributions, exponential distributions, quite frequently invoked in inorganic compounds, arise generally from atomic

substitutions in the crystalline boundaries. In organic crystals, an exponential distribution could arise from unintentional chemical doping. The different chemical nature of this second peak in principle could explain why the peak is almost unaffected by increasing the internal disorder of the film with the number of the thermal cycles, while the previous one get completely absorbed with the rise of the peak at T_m = 197.7 K. The peak at T_m = 254.2 K looses the shape and starts to get broader with the increase of the introduced morphological disorder in the film, but does not disappear like the peak at T_m = 221.5 K. The frequency factor emerging from the simulation, s = 1.85x10^{11} s^{-1}, is one order of magnitude lower than s of its neighbour peak and confirms the different origin of this peak. The width of the distribution, σ = 0.088 eV determines the shape of the distribution that is not particularly wide.

Figure 4.19 shows the numerical simulation of the peak that starts to appear clearly after some TSL cycles at T_m = 197.7 K. How above underlined, this peak is already present in the first TSL run, but only at very last cycles has its maximum extent. Figure 4.19 shows only the peak related to the curve labelled with d) in figure 4.14 with its best fit. The numerical analysis, also in these case, is performed with the first order equation (2.14) containing a Gaussian distribution of traps. Like the other simulations, the density of traps is set at n_m = 1x 10^{16} cm $^{-3}$ and the heating rate at β = 0.1 K/s. The activation energy of the trap level is centred at the maximum of the dispersion at E_m = 0.55 eV while the integration limits are E_1 = 0.45 eV and E_2 = 0.65 eV representing the lowest and the highest respectively. The distribution is perfectly symmetric with a quite small width σ = 0.028 eV. The frequency factor in such simulation is s = 1.15 x 10^{12} s^{-1} which has the same order of magnitude for its neighbouring peak at T_m = 221.5 K. This result confirms the same origin of the two peaks. The simulation is very satisfactory; the calculated curve follows exactly the experimental one.

4.4. Shallow traps

All the calculated values of the sensitive parameters of TSL curves for the polymer and for the low molecular compound peaks are summarised in table 4.2. The occurrence of shallow traps is observed in all studied materials in a range of energy from a few meV up to 80 meV. To study the presence of shallow traps is of capital importance in order to understand how their presence can influence the transport properties of an organic film.

At room temperature their occupation is in thermal equilibrium with transport states. Hence, this kind of shallow distributed defects plays a major role determining the transport characteristic of an organic material acting as hopping sites for electrons. Although the presence of shallow traps is incontrovertible, having an experimental evidence, the origin of shallow traps is not clear; they can originate from both structural defect or chemical impurities. Furthermore, this type of defects is present in both classes of materials under examination: polymers and low molecular compounds. This finding could suggest that this particular kind of traps originates from chemical contamination. On the other hand the significant presence of shallow traps also in the highly purified TPQ sample, evaporated under high-vacuum conditions, tends to exclude this possibility, then the detected shallow traps have, probably, a physical origin.

The distribution of the detected shallow traps is Gaussian. Although we used a priori this kind of distribution to perform the numerical analysis it should be noticed that other kinds of distributions do not give the same excellent fit. By means of our experimental set-up it is possible to observe only the tail of the Gaussian distribution, this means that the observed distributions are pseudo-exponential. Furthermore we observe that using such description, having a Gaussian distribution of localised states, defects are supposed to penetrate deeply into the conduction band.

The experimental conditions, in particular the excitation carried out in our case at liquid nitrogen temperature, play a relevant role in determining the shape of the distribution. We are revealing only one part of the real distribution because of the relatively high temperature and this deforms the obtained TSL glow curves. Studies performed on glasses, where the expected distribution for statistical reasons must be perfectly Gaussian, show that the TSL glow curve shape is strongly affected by the previous temperature excitation and by the peak partial cleaning procedure[92] followed. In such cases the calculated distributions, originating from so distorted peaks, have an exponential shape.

The use of the thermally stimulated techniques together with the numerical analysis gives evidence on the trapped states of the studied thin films and highlights the importance of shallow traps in the transport properties. The described results are well confirmed in literature. Measurements on several materials suitable for OLEDs show the presence of shallow traps. An energy depth of about E = 0.06 eV determined by means of TSL measurements[91], and E = 0.07 eV by means of TSC[93] has been stated for 8-hydroxyquinoline, the well known Alq_3. A naphtyl-substituted benzidine derivative (NPB) measured by TSL[91] shows shallow traps having a depth of around E = 0.05 eV and E = 0.08 eV. For poly(p-phenylenevinylene) (PPV) shallow traps depth values[79] of E = 0.03÷0.06 eV have been determined by means of TSC measurements. A similar value, E = 0.06 eV, was found for an amorphous soluble methyl-substituted ladder-type poly (para-phenylene) (m-LPPP) again by TSC[69]. All this values are coherent and

Table 4.2: Summary of the thermally stimulated luminescence parameters

Substance		T peak (K)	E_m (eV)	s (s^{-1})	σ (eV)	order
PPQ IA		159.1	0.06÷0.08	/	/	2nd
		230.7	0.18	/	/	
PPQ IIB		160.4	0.01÷0.08	/	/	
		226.1	0.11	/	/	
TPQ	cast	114.6	0.12	1.5×10^{12}	0.19	2nd
	evap.	103	0.07÷0.1	/	/	
NADPO		120÷160	0.004	1×10^{4}	0.7	1st
		197.7	0.55	1.15×10^{12}	0.028	
		224	0.63	2.4×10^{12}	0.045	
		253	0.66	1.85×10^{11}	0.08	

indicate the constant presence of shallow traps in both low molecular compounds and polymers used for light emitting devices. Unfortunately up to now, no systematic studies were undertaken to determine the shape of the shallow trap distribution. In this contest more systematic investigation on a wide range of materials suitable for organic electronics are necessary in order to establish a well founded correspondence between the presence of shallow traps, the shape of their distribution on one side and the transport and emitting properties on the other side.

Almost all numerical simulations in this sections are carried out using a density of traps of about 10^{16} cm^{-3}. How underlined in chapter 2 a lower density of localised states can be detrimental in that respect. To use the quasi-adiabatic approximation, equation (2.7), is not justified for lower trap concentrations. However, the maximum trap density employed for the numerical simulations is consistent with the literature reports, giving for such kind of organic materials values from 10^{16} cm^{-3} to 10^{17} cm^{-3} also for very purified substances. This fact makes us confident about the consistency of our numerical simulations.

4.5. Deep traps

The presence of deeper traps is also very important in OLED technology and organic electronic, in order to understand the electron transport properties, recombination and electroluminescence quenching mechanisms. All studied materials, both polymers and oligomers, show the presence of at least of one deep trapping level in the energy range between $E = 0.18$ eV and $E = 0.66$ eV.

The Gaussian or, in one case, true exponential trap distributions are influenced by the pre-history of the sample and can vary slightly in position from sample to sample. Deep traps are strongly influenced by the preparation conditions to which the sample was exposed and by the subsequent thermal cycles necessary in order to perform the measurements. A quantitative analysis of these peaks, with the important exception of the peaks appearing in the NADPO sample, is difficult to perform and is not very accurate because of the superposition of several peaks and dynamical changes during the experiment.

The comparison between amorphous samples and well ordered samples show unexpectedly more structured TSL structures for this second type. This can be explained by means of the higher level of order. A well ordered structure does not show the wide TSL signal glowing from the broad distribution of defects. This signal in general hides the fine structures arising from chemical defects. For that reasons samples being more ordered or grown under high vacuum conditions show with respect to similar samples, grown completely amorphous or in air, a more rich structure. A complete and systematic analysis of well-ordered samples and pure materials grown under well controlled conditions, like measurements performed after sample expositions to oxygen or moisture, are highly desirable.

5. Conclusions

New polymers and low molecular compounds, suitable for organic light-emitting devices and organic electronic applications, have been synthesised in these years in order to obtain electron transport characteristics compatible with requirements for applications in real plastic devices. However, despite of the technological importance and of the relevant progress in device manufacture, fundamental physical properties of such class of materials are still not studied sufficiently. In particular the presence of distributions of localised states has a strong impact on their electronic properties. The presence of shallow traps as well as the influence of the sample preparation conditions on deep and shallow localised states have not been systematically explored until now.

Thermal techniques are a powerful tool in order to study localised levels in inorganic and organic materials. Thermally stimulated luminescence, thermally stimulated currents and thermally stimulated depolarisation currents allow, when applied in synergy, to investigate in details shallow traps and deeper levels. They also permit to study, in synergy with dielectric spectroscopy, polarisation and depolarisation effects.

The analysis of the thermograms, emerging from the thermal techniques, can be performed starting from the differential rate equations of the de-trapping phenomena. Such approach, allowed by the computing power of the modern calculators, is not the most fruitful, while the number of free variables involved in the numerical resolution of the rate differential equations is too high. Sometimes completely different sets of parameters can fit the same thermally stimulated peak and ambiguous results are often achieved.

For the above reasons in order to analyse the glow curves we decided to explore the possibilities offered by a different approach. It is well known that the rate differential equations describing the thermally stimulated processes can be solved, in the frame work of band theory, analytically using the adiabatic approximation. The integration results in two equations valid in case of negligible re-trapping, first order kinetic, i.e. a released electron recombines directly with a hole, or valid in the opposite case, the so called second order kinetic equation, an electron has an high probability to get re-trapped and is then released and trapped several times before recombination.

First and second order kinetic equations are generally applied in case of a single level of localised states. However, the intrinsic disorder, intimately connected to the structure of polymeric compounds and in general to organic crystals, must be taken into account and then added to both kinetic equations. We obtain, in such way, a first and a second order equation that includes a distribution of localised states. The resulting equations can be numerically solved. We studied the Gaussian, the exponential and the quasi-continuous distributions. The shape of the theoretical peaks of a thermal experiment are investigated by systematic variation of the two main parameters of the equations i. e. the energy trap depth E and the frequency factor s and of the parameters regulating the distribution, in particular, for a Gaussian distribution, the distribution width σ and the integration limits.

The effect of the presence of a distribution of localised states is reflected by the peak shape. In comparison with a single level of traps, a glow curve containing a distribution is characterised by an enhanced symmetry and enlarged dimensions. We demonstrate that the first and second order kinetic equations containing a Gaussian distribution of localised states can be considered to be universal. Manipulating the Gaussian parameters it is possible to obtain peak shapes analogous to the shapes of peaks rising from the other two kinds of distributions. In particular tuning the energetic limits and the energy depth maximum E_m of the Gaussian distribution inside the first and second order equations, it is possible to account for experimental glow curves resulting from partial cleaning procedure or from not completely filled levels of traps, that are usually fitted with unphysical exponential distributions.

The theoretical findings have been applied to two classes of materials suitable for electron transport hole blocking layer in OLEDs: the two polymers Poly[2,2'-(1,4-phenylene)-6,6'-bis(3-phenyl quinoxaline)], shortly called PPQ IA, and poly[2,2'-(4,4-oxy biphenylene)-6,6'-oxybis(3-phenylquinoxaline)] PPQ IIB, a low molecular quinoxaline, the star starburst 1,3,5-Tris[(3-phenyl-6-trifluoromethyl)-quinoxaline-2-yl]benzene, TPQ, and the well ordered and stable Langmuir–Blodgett (LB) multilayers films of the amphiphilic substituted 2-(p-nitrophenyl)-5-(p-undecylamidophenyl)-1,3,4-oxadiazole (NADPO).

All studied samples show rich thermograms revealing several levels of localised states.

The polymers have been studied by means of TSL, TSDC and DES in order to discriminate between depolarisation peaks and de-trapping features. Despite the fact that PPQ IA and PPQ IIB have almost the same chemical structure, the TSDC thermograms look completely different. PPQ IA has a rich thermogram characterised by the presence of two peaks at low temperature, having a dipolar origin with T_m = 145 K and a second one that could arise from de-trapping processes at T_m = 164 K. Furthermore, a complex structure around T = 240 K has been successfully analysed by means of overlapping of a minimum number of single Debye relaxation processes. A transport peak around T = 420 K was also extracted as well as an α-peak around the glass transition temperature at T = 550 K.

The PPQ IIB TSDC thermogram is characterised by the presence of an α-peak around T = 465 K and a transport peak around T = 398÷408 K. A low temperature peak, T_m = 145 K, has a probable de-trapping origin like the second peak of PPQ IA.

The differences between the experimental findings on the two similar polymers can be found in the presence in PPQ IIB of an oxygen bridge in the main chain that acts as flexibilizer and conjugation breaker, while the structure of PPQ IA bears no oxygen at all. This results in a lower glass transition temperature and in a lower conductivity of PPQ IIB.

The TSL glow curves of both polymers are characterised by the presence of two broad peaks. Both peaks are connected with broad distributions of localised states, a characteristic feature of glasses and disordered materials. Furthermore, in both polymers the peaks are characterised by second order kinetics and a low activation energy.

A further material under investigation is TPQ, a very promising organic compound for electronic applications because of its high electron mobility. The thermograms reveal the presence of a wide distribution of shallow traps that can act as hopping levels and which are consequently influencing the

transport properties. There are no substantial differences between cast and evaporated samples. The Gaussian distributed levels of shallow traps characterised by second order kinetics, have an energy depth of E = 0.12 eV and an estimated frequency factor of about $s = 1\text{x}10^{12}$ s^{-1}, can be attributed to physical traps.

The well ordered NADPO LB film was extensively studied by means of ultraviolet photoelectron spectroscopy in order to determine experimentally its electronic band structure. Surprisingly, such materials are characterised by a rich thermogram. A wide region of shallow traps localised at E_m = 4 meV has been successfully fitted by means of a Gaussian distribution with a first order kinetic equation.

Two further peaks, having a different origin, characterise the thermograms. The peaks at T_m = 221.5 K and T_m = 254.2 K have activation energies of E_m = 0.63 eV and E_m = 0.66 eV, frequency factors of $s = 2.4\text{x}10^{12}$ s^{-1} and $s = 1.85\text{x}10^{11}$ s^{-1}, and distribution widths of σ = 0.045 eV and σ = 0.088 eV, respectively.

After an increasing number of thermal cycle, there suddenly appears a peak at T_m = 197.7 K probably connected with structural defect. The numerical analysis of such a peak is performed by means of a first order equation containing a Gaussian distribution of traps. The activation energy of the trap level is centred at E_m = 0.55 eV. The distribution is perfectly symmetric with a quite small width of σ = 0.028 eV. The frequency factor in such simulation is $s = 1.15 \text{ x } 10^{12}$ s^{-1} resulting in the same order of magnitude as its neighbour peak at T_m = 221.5 K, having both probably the same origin.

This work demonstrates that the shape of the glow curves is strongly influenced by the excitation temperature and by the thermal cycles. In such a way a Gaussian distribution of localised states can be transformed into an almost exponential distribution. The previous thermal history of the samples including the peak cleaning can lead to certain trap occupation which resembles an exponential distribution.

The constant presence of shallow traps in all studied materials confirms their importance in transport properties. The numerical simulations of the experimental curves are a reliable tool in order to analyse the experimental glow curves and to get information about localised levels. However, further systematic studies are necessary in order to find reliable connections between the presence of shallow traps and the transport properties in organic materials.

The thermal techniques are powerful investigation tools when synergistically applied. However, very low excitation temperatures are necessary in order to study the presence of shallow traps and to determine completely the shape of the trap distribution. Furthermore, comparison of samples prepared under different conditions and with trap levels introduced on purpose must be studied systematically in order to find a correspondence between the thermogram peaks and the introduced levels and then surely attribute each peak to a certain kind of introduced defect.

Appendix

Graphical programming

A commercial graphical programming language is the chosen tool in order to achieve the instrument operations control and the data collection during the experiments. We use Hewlett-Packard visual engineering environment (HP-VEE) graphical programming language for this purpose. HP-VEE is optimised for instrument control, it is easy to learn and to use, furthermore it allows to prepare user friendly graphical interfaces in a easy way and in a short time.

Figure A shows the flow chart of the program performing simultaneous TSL and TSC measurements. Analogous programs are developed for TSDC, current-voltage as well as electroluminescence measurements. The shown graph consists of tools, the so called objects, logically connected by lines defining the program progress. With respect to a program written in a textual language basically there are no logical differences, although in such case the programmer should follow the strict rules and syntax terms of programming language that generally are not intuitive and that require considerable learning and training time. In case of a graphical program the function of each object (that is equivalent to a string of commands or to a subroutine) is intuitive and the basic rules are easy to understand and to be followed.

The result is a sort of flow diagram where each simple step, the object, connected with lines, performs a specific function. Such graphical pattern is the analogous of the source program in a textual programming language. The data inputs are on the left side of the objects and the data outputs are on the right. The chronological progression, or in other terms, the sequence flow, can be determined when necessary by the lines connecting the objects from top to bottom.

In graph A we can distinguish four important blocks. The instrument commands include the instrument initialisations (see also figures B and C) at the beginning of the program, the reading and averaging loop (read & mean box in the figure) that performs the operations of reading on the instruments and makes, on request of the operator, a data averaging operation.

The output is constituted of two different blocks, the three graphs, thermoluminescence versus temperature, current versus temperature and temperature versus time, show “on line” the measurement progress and a block, including the file name selection at the program beginning and the “to-file” object, that collects the data and stores them in a file during the program execution.

A last loop, enveloping the whole program, measures the time elapsed between the measurement execution and the writing of the data on the file. It takes into account the real elapsed time. The collected data are also registered about the elapsed time in the resulting file. A beep announces the end of each measurement cycle.

The simple user interface (not shown) contains the three graphs, current vs. temperature, thermoluminescence vs. temperature and temperature vs. time, the number of data that the program should average before to be written into the data file, the total execution time, the voltage to be applied to the sample, and a starting and a stop button.

Figures B, C and D show details of the instrumental subroutines containing commands for initialisation of the instruments and data reading. Such command strings are specific for each instrument.

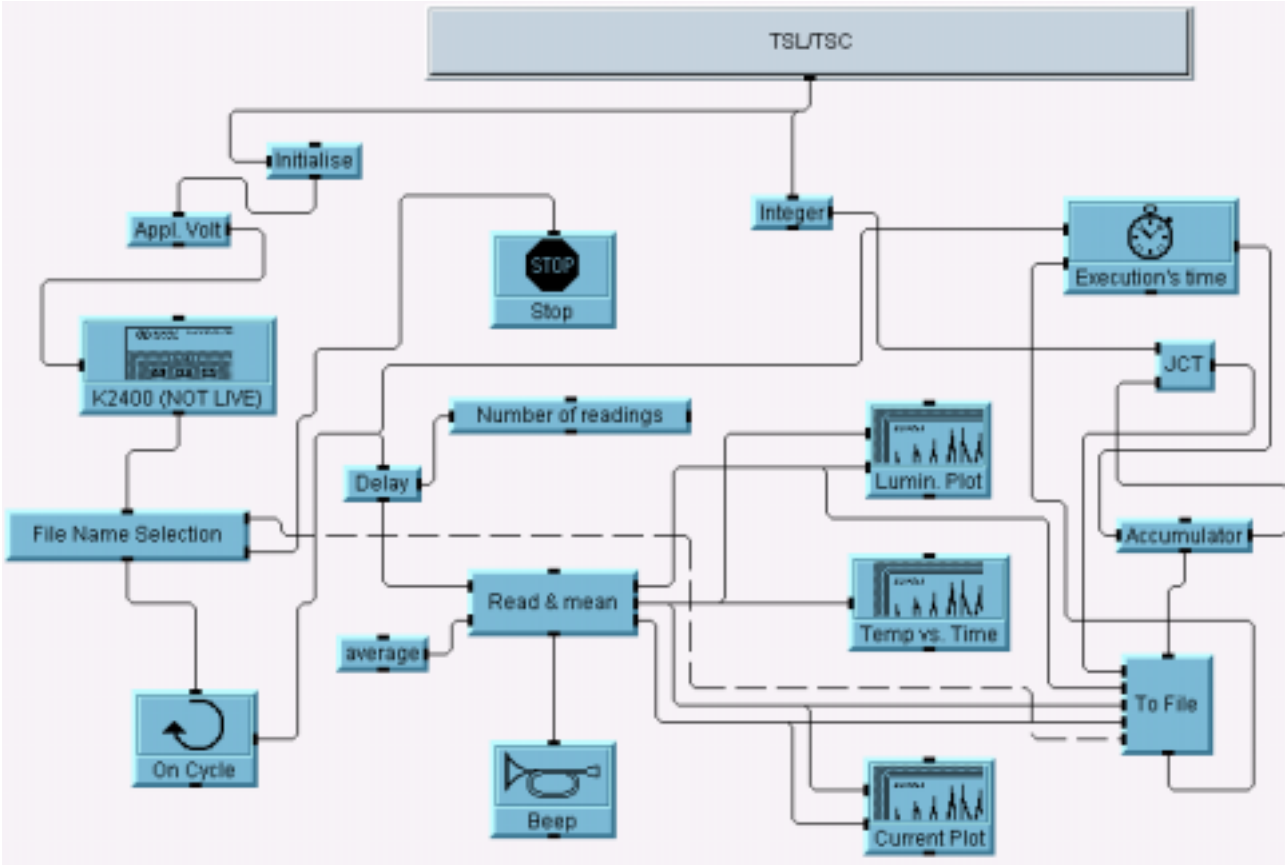

Figure A Data flow diagram of the program performing TSL/ TSC simultaneous measurements.

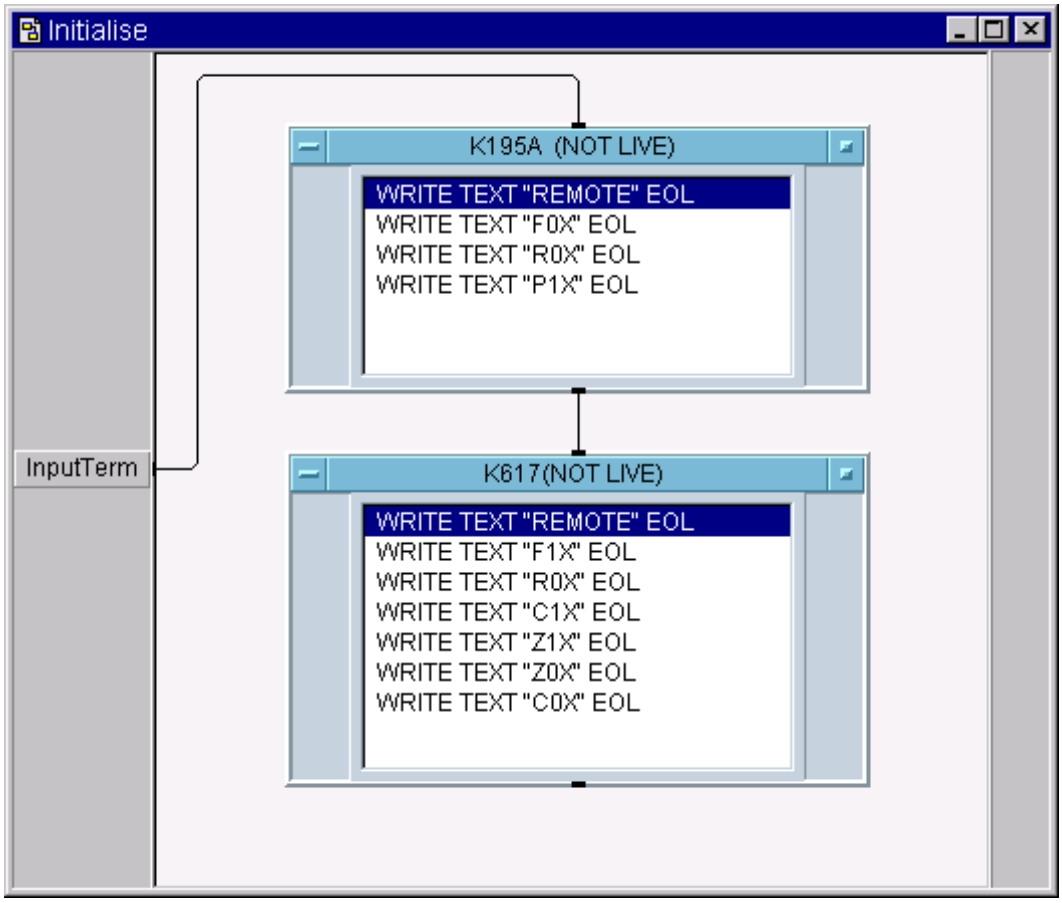

Figure B picoammeter and voltmeter initialisation sub routine.

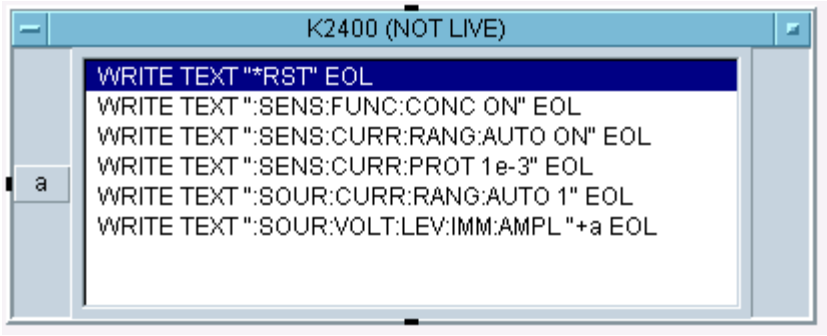

Figure C Keithley source meter initialisation commands list.

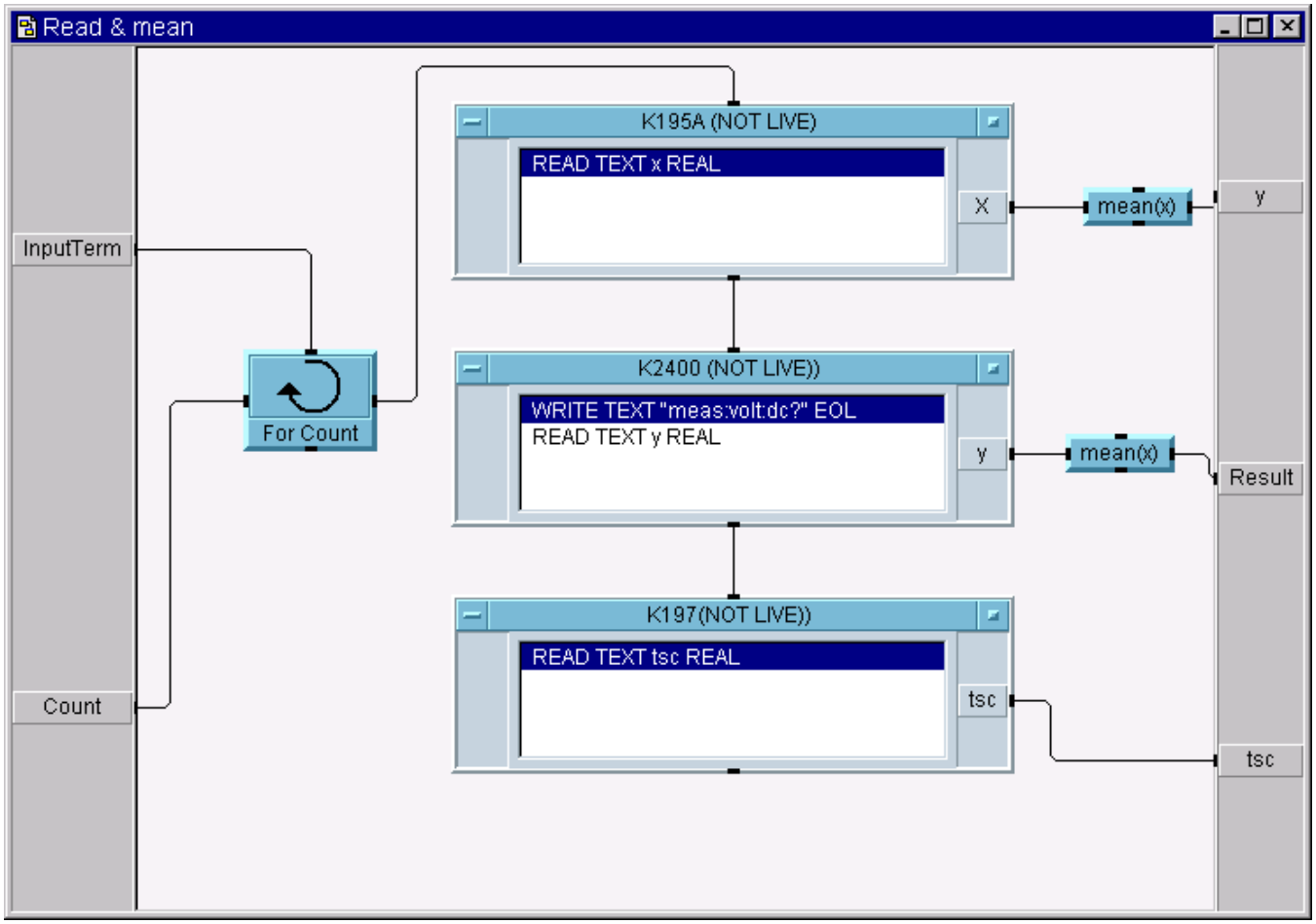

Figure D Measurements commands and averaging sub routine.

References

1. Sze, S. M. *Physics of Semiconductor Devices* (John Wiley & Sons, 1981).

2. Pope, M. & Swenberg, C. E. *Electronic Process in Organic Crystals and Polymers* (Oxford University Press, New York, 1999).

3. Gomes, H. L. et al. Analysis of Deep Levels in a Phenylenevinylene Polymer by Transient Capacitance Methods. *Appl. Phys. Lett.* **74**, 1144 (1999).

4. Campbell, A. J., Bradley, D. D. C. & Lidzey, D. G. Space-charge Limited Conduction with Traps in Poly(phenylene vinylene) Light Emitting Diodes. *J. Appl. Phys.* **82**, 6326 (1997).

5. Adam, D. et al. Transient Photoconductivity in a Discotic Liquid Crystal. *Phys. Rev. Lett.* **70**, 457 (1993).

6. Ettedugi, E., Razafitrimo, H., Park, K. T., Gao, Y. & Hsieh, B. R. *Surface and Interface Analysis* **23**, 89 (1995).

7. Karg, S., Meier, M. & Riess, W. Light-Emitting Diodes Based on Poly-p-phenylene-vinylene: I. Charge-Carrier Injection and Transport. *J. Appl. Phys.* **82**, 1951 (1997).

8. Stallinga, P. et al. Minority-Carrier Effects in Poly-phenylenevinylene as Studied by Electrical Characterization. *J. Appl. Phys.* **89**, 1713 (2001).

9. Imperia, P. et al. Thermally Stimulated Processes in Heterocyclic Materials Suitable for Heterolayer Organic Light Emitting Diodes. *Synth. Met.* **124/1**, 83 (2001).

10. Imperia, P., Schrader, S., Casu, M. B., Jandke, M. & Strohriegl, P. Quinoxaline Films for Hetero-Layer Light Emitting Devices. *Nonlinear Optics* **25**, 455 (2000).

11. Blom, P. W. M., de Jong, M. J. M. & Vleggaar, J. J. M. Electron and Hole Transport in Poly(p-phenylene) vinylene Devices. *Appl. Phys. Lett.* **68**, 3308 (1996).

12. Ioannidis, A., Forsythe, E., Gao, Y., Wu, M. W. & Conwell, E. M. Current-Voltage Characteristic of Organic Light Emitting Diodes. *Appl. Phys. Lett.* **72**, 3038 (1998).

13. Schön, J. H., Kloc, C. & Batlogg, B. Hole Transport in Pentacene Single Crystals. *Phys. Rev. B* **63**, 245201 (2001).

14. Ashcroft, N. W. & Mermin, N. D. *Solid State Physics* (Holt, Rinehart & Winston, New York, 1976).

15. Campbell, A. J., Bradley, D. D. C., Werner, E. & Brütting, W. Transient Capacitance Measurements of the Transport and Trap States Distributions in a Conjugated Polymer. *Organic Electronics* **1**, 21 (2000).

16. Chen, R. & Kirsh, Y. *Analysis of Thermally Stimulated Processes* (Pergamon Press, 1981).

17. Pope, M., Kallmann, H. P. & Magnante, P. Electroluminescence in Organic Crystals. *J. Chem. Phys.* **38**, 2042 (1963).

18. Tang, C. W., VanSlyke, S. A. & Chen, C. H. Electroluminescence of Doped Organic Thin Films. *J. Appl. Phys.* **65**, 3610 (1989).

19. Tang, C. W. & VanSlyke, S. A. Organic Electroluminescent Diodes. *Appl. Phys. Lett.* **51**, 913 (1987).

20. Burroughes, J. H. et al. Light-Emitting Diodes Based on Conjugated Polymers. *Nature* **347**, 539 (1990).

21. Wu, C. C., Wu, C. I., Sturm, J. C. & Kahn, A. Surface Modification of Indium Tin Oxide by Plasma Treatment: An Effective Method to Improve the Efficiency, Brightness, and Reliability of Organic Light Emitting Devices. *Appl. Phys. Lett.* **70**, 1348 (1997).

22. Furukawa, K., Terasaka, Y., Ueda, H. & Matsumura, M. Effect of a Plasma Treatment of ITO on the Performance of Organic Electroluminescent Devices. *Synth. Met.* **91**, 99 (1997).

23. Nüesch, F., Rothberg, L. J., Forsythe, E. W., Le, Q. T. & Gao, Y. A Photoelectron Spectroscopy Study on the Indium Tin Oxide Treatment by Acids and Bases. *Appl. Phys. Lett.* **74**, 880 (1999).

24. Andersson, A. et al. Fluorine Tin Oxide as an Alternative to Indium Tin Oxide in Polymer LEDs. *Adv. Mater.* **10**, 859 (1998).

25. Schlatmann, A. R., Wilms Floet, D., Hilberer, A., Garten, F. & Smulders, P. J. M. Indium Contamination from the Indium-Tin-Oxide Electrode in Polymer Light-Emitting Diodes. *Appl. Phys. Lett.* **69**, 1764 (1996).

26. Kugler, T., Lögdlund, M. & Salaneck, W. R. Polymer Surfaces and Interfaces in Light-Emitting Devices. *IEEE Journal of Selected Topics in Quantum Electronics* **4**, 14 (1998).

27. Hosokawa, C., Higashi, H., Nakamura, H. & Kusumoto, T. Highly Efficient Blue Electroluminescence from a Distyrylarylene Emitting Layer with a New Dopant. *Appl. Phys. Lett.* **67**, 3853 (1995).

28. Van Slyke, S. A., Chen, C. H. & Tang, C. W. Organic Electroluminescent Devices with Improved Stability. *Appl. Phys. Lett.* **69**, 2160 (1996).

29. Koch, N. et al. The Interaction of Aluminium and p-Sexiphenyl. *Synth. Met.* **101**, 438 (1999).

30. Grüner, J., Remmers, M. & Neher, D. Direct Determination of the Emission Zone in a Polymer Light-Emitting Diode. *Adv. Mater.* **9**, 964 (1997).

31. Salaneck, W. R., Stafstrom, S. & Bredas, J.-L. *Conjugated Polymer Surfaces and Interfaces: Electronic and Chemical Structure of Interfaces for Polymer Light Emitting Devices* (Cambridge University Press, Cambridge, 1996).

32. Ishii, H., Sugiyama, K., Ito, E. & Seki, K. Energy Level Alignment and Interfacial Electronic Structures at Organic/Metal and Organic/Organic Interfaces. *Adv. Mater.* **11**, 605 (1999).

33. Gasiorowicz, S. *Quantum Physics* (John Wiley & Sons, New York, 1974).

34. Silinsh, E. A. *Organic Molecular Crystals, Their Electronic States* (eds. Cardona, M., Fulde, P. & Queisser, H.-J.) (Springer Verlag, Berlin, 1980).

35. Casu, M. B. et al. in *Novel Methods to Study Interfacial Layers* (eds. Möbius, D. & Miller, R.) 121 (Elsevier, Amsterdam, 2001).

36. Jandke, M., Strohriegl, P., Berleb, S., Werner, E. & Brütting, W. Phenylquinoxaline Polymers and Low Molar Mass Glasses as Electron-Transport Materials in Organic Light-Emitting Diodes. *Macromolecules* **31**, 6434 (1998).

37. Casu, M. B. et al. Ultraviolet Photoelectron Spectroscopy on New Heterocyclic Materials for Multilayer Organic Light Emitting Diodes. *Synth. Met.* **124/1**, 79 (2001).

38. Fukuda, Y., Watanabe, T., Wakimoto, T., Miyaguchi, S. & Tsuchida, M. An Organic LED Display Exhibiting Pure RGB Colours. *Synth. Met.* **111-112**, 1 (2000).

39. Schön, J. H., Berg, S., Kloc, C. & Batlogg, B. Ambipolar Pentacene Field-Effect Transistors and Inverters. *Science* **287**, 1022 (2000).

40. Joachim, C., Gimzewski, J. K. & Aviram, A. Electronics Using Hybrid-Molecular and Mono-Molecular Devices. *Nature* **408**, 541 (2000).

41. Wohlgenannt, M., Tandon, K., Mazumdar, S., Ramasesha, S. & Vardeny, Z. V. Formation Cross-Sections of Singlet and Triplet Excitons in π-Conjugated Polymers. *Nature* **409**, 494 (2001).

42. Kraft, A. Organic Field-Effect Transistors. The Breakthrough at Last. *Chem. Phys. Chem.* **2**, 163 (2001).

43. Weaver, M. S. et al. Recent Progress in Polymers for Electroluminescence: Microcavity Devices and Electron Transport Polymers. *Thin Solid Films* **273**, 39 (1996).

44. Hergenrother, P. M. & Levine, H. H. *Journal of Polymer Science A-1* **5**, 1453 (1967).

45. Augl, J. M. & Booth, H. J. Thermomechanical Behaviour of a Polyphenylquinoxaline. *J. Pol. Science: Polymer Chemistry Edition* **11**, 2179 (1973).

46. Wrasidlo, W. & Augl, J. M. Phenylated Polyquinoxalines from Bis(phenylglyoxaloyl) Benzene. *Journal of Polymer Science A-1* **7**, 3393 (1969).

47. Schrader, S., Imperia, P., Koch, N., Leising, G. & Falk, B. in *Organic Light-Emitting Materials and Devices*, (ed. Kafafi, Z. H.) 209 (SPIE, San Diego, California, 1999).

48. Schürmann, H. et al. Ultraviolet Photoelectron Spectroscopic Study of Heterocyclic Model Compounds for Electroluminescent Devices. *Synth. Met.* **102**, 1069 (1999).

49. Redecker, M., Bradley, D. D. C., Jandke, M. & Strohriegl, P. Electron Transport in Starburst Phenylquinoxaline. *Appl. Phys. Lett.* **75**, 109 (1999).

50. Casu, M. B. et al. Valence Electronic Structure of Oxadiazoles and Quinoxalines Model Compounds. *Synth. Met.* **121**, 1397 (2001).

51. Jandke, M. in *Fakultät Biologie, Chemie und Geowissenschaften* (Universität Bayreuth, Bayreuth, 2000).

52. Schulz, B., Bruma, M. & Brehemer, L. Aromatic Poly(1,3,4-oxadiazole)s as Advanced Materials. *Adv. Mater.* **9**, 601 (1997).

53. Reiche, J. et al. Supramolecular Structures Formed from Heterocyclic Aromatic Molecules. *Thin Solid Films* **295**, 241 (1997).

54. Reiche, J. et al. Vacuum Deposition Films of Oxadiazole Compounds: Formation and Structure Investigation. *Materials Science and Engineering C* **8-9**, 237 (1999).

55. Kaminorz, Y., Schulz, B. & Brehmer, L. Optical and Electrical Properties of Substituted 2,5-diphenyl-1,3,4-oxadiazoles. *Synth. Met.* **111-112**, 75 (2000).

56. Hamada, Y., Adachi, C., Tsutsui, T. & Saito, S. Blue-Light-Emitting Organic Electroluminescent Devices with Oxadiazoles Dimer Dyes as an Emitter. *Jpn. J. Appl. Phys.* **31**, 1812 (1992).

57. Casu, M. B., Imperia, P., Schulz, B. & Schrader, S. Electronic Structure of Aromatic 1,3,4-Oxadiazoles Studied by Ultraviolet Photoelectron Spectroscopy. *Synth. Met.* **127**, 185 (2002).

58. Lampert, M. A. & Mark, P. *Current Injection in Solids* (eds. Booker, H. G. & DeClaris, N.) (Academic Press, New York, 1970).

59. Campos, M. Space Charge Limited Current in Naphthalene Single Crystals. *Molecular Crystals and Liquid Crystals* **18**, 105 (1972).

60. Karl, N. in *Organic Nanostructures: Science and applications. Proceedings of the CIL course of the International School of Physics "Enrico Fermi"* (eds. La Rocca, G. C. & Agranovich, V. M.) (2001).

61. Nešpurek, S. & Silinsh, E. A. Space-Charge-Limited Current Theory for Molecular Crystals with Gaussian Distribution of Local Trapping States. *phys. stat. sol. (a)* **34**, 747 (1976).

62. Nešpurek, S. & Smejtek, P. Space-Charge Limited Currents in Insulators with the Gaussian Distribution of Traps. *Czech. J. Phys. B* **22**, 160 (1972).

63. Meyer, H., Haarer, D., Naarmann, H. & Hörhold, H. H. Trap distribution for charge Carriers in Poly(paraphenylene Vinylene) (PPV) and its Substituted Derivative DPOP-PPV. *Phys. Rev. B* **52**, 2587 (1995).

64. Karl, N. in *Defect Control in Semiconductors* (ed. Sumino, K.) (Elsevier, Amsterdam, 1990).

65. Bucci, C., Fieschi, R. & Guidi, G. Ionic Thermocurrents in Dielectrics. *Phys. Rev.* **148**, 816 (1966).

66. Bucci, C. & Fieschi, R. Ionic Thermoconductivity, Method for Investigation of Polarization in Insulators. *Phys. Rev. Lett.* **12**, 16 (1964).

67. Jablonski, A. Über de Mechanismus der Photolumineszenz von Farbstoffphosphoren. *Z. Phys.* **94**, 38 (1935).

68. Randall, J. T. & Wilkins, M. H. F. The Phosphorescence of Various Solids. *Proc. Roy. Soc. A* **184**, 347 (1945).

69. List, E. J. W. et al. Charged Defects in Highly Emissive Organic Wide-Band-Gap Semiconductors. *Appl. Phys. Lett.* **76**, 2083 (2000).

70. Kadashchuk, A. et al. Thermally Stimulated Photoluminescence in Disordered Organic Materials. *Phys. Rev. B* **63**, 115205 (2001).

71. Bässler, H. Charge Transport in Disordered Organic Photoconductors, a Monte Carlo Simulation Study. *phys. stat. sol. (b)* **175**, 15 (1993).

72. Adirovitch, E. I. La Formule de Becquerel et la Loi Elémentaire du Décline de la Luminescence des Phosphores Cristallins. *J. Phys. Rad.* **17**, 705 (1956).

73. Vanderschueren, J. & Gasiot, J. in *Thermally Stimulated Relaxation in Solids* (ed. Bräunlich, P.) 135 (Springer-Verlag, Berlin, 1979).

74. Martini, M. & Meinardi, F. Thermally Stimulated Luminescence: New Perspectives in the Study of Defects in Solids. *Rivista del Nuovo Cimento* **20**, 1 (1997).

75. Imperia, P., Casu, M. B., Schulz, B. & Schrader, S. Analysis of Detrapping Processes of Aromatic 1,3,4-Oxadiazoles with Thermally Stimulated Luminescence. *Synth. Met.* **127**, 181 (2002).

76. Schrader, S., Casu, M. B., Imperia, P., Jandke, M. & Strohriegl, P. Electronic Structure and Localised States in Starburst Trisphenylquinoxaline. *Proceeding of SPIE* **at press** (2002).

77. Kelly, P., Laubitz, M. J. & Bräunlich, P. Exact Solutions of the Kinetic Equations Governing Thermally Stimulated Luminescence and Conductivity. *Phys. Rev. B* **4**, 1960 (1971).

78. Lewandowski, A. C., Markey, B. G. & McKeever, S. W. S. Analytical Description of Thermally Stimulated Luminescence and Conductivity without the Quasiequilibrium Approximation. *Phys. Rev. B* **49**, 8029 (1994).

79. Meier, M., Karg, S., Zuleeg, K., Brütting, W. & Schwoerer, M. Determination of Trapping Parameters in Poly(p-phenylenevinylene) Light-Emitting Devices Using Thermally Stimulated Currents. *J. Appl. Phys.* **84**, 87 (1998).

80. van Turnhout, J. in *Electrets* (ed. Sessler, G. M.) 81 (Springer Verlag, Berlin, 1980).

81. Schrader, S. & Schönhals, A. TSD-α-peak and Non-Equilibrium Processes. *Progr. Colloid Polym. Sci.* **80**, 93 (1989).

82. van Turnhout, J. *Thermally Stimulated Discharge of Polymer Electrets* (Krips Repro B.V., Meppel, 1972).

83. Schrader, S. (unpublished results, 2001).

84. Garlick, G. F. J. & Gibson, A. F. The Electron Trap Mechanism of Luminescence in Sulphide and Silicate Phosphors. *Proc. Phys. Soc.* **60**, 574 (1948).

85. McKeever, S. W. S. *Thermoluminescence of Solids* (eds. Cahn, R. W., Davis, E. A. & Ward, I. M.) (Cambridge University Press, Cambridge, 1985).

86. Lushchik, C. B. The Investigation of Trapping Centres in Crystals by the Method of Thermal Bleaching. *Soviet Physics JETP* **3**, 390 (1956).

87. Halperin, A. & Braner, A. A. Evaluation of Thermal Activation Energies from Glow Curves. *Phys. Rev.* **117**, 408 (1960).

88. Imperia, P. et al. Electronic Transport Properties of Heterocyclic Materials for Heterolayer Organic Light Emitting Devices. *Synth. Met.* **121**, 1673 (2001).

89. Wolfram, S. (Wolfram Media, Inc., Cambridge, 1996).

90. Weaver, M. S., O'Brien, D., Bleyer, A., Lidzey, D. G. & Bradley, D. D. C. in *Inorganic and Organic Electroluminescence* (eds. Mauch, R. H. & Gumlich, H.-E.) 207 (Wissenschaft und Technik Verlag, Berlin, 1996).

91. Forsythe, E. W., Morton, D. C., Tang, C. W. & Gao, Y. Trap States of Tris-8-(hydroxyquinoline) Aluminum and Naphthyl-Substituted Benzidine Derivative Using Thermally Stimulated Luminescence. *Appl. Phys. Lett.* **73**, 1457 (1998).

92. Sakurai, T., Shoji, K., Itoh, K. & Gartia, R. K. Origin of the Exponential Distribution of Traps in Glass. *J. Appl. Phys.* **89**, 2208 (2001).

93. Karg, S., Steiger, J. & von Seggern, H. Determination of Trap Energies in Alq_3 and TPD. *Synth. Met.* **111-112**, 277 (2000).

Publications

International reviews

1. H. Schürmann, N. Koch, P. Imperia, S. Schrader, M. Jandke, P. Strohriegl, B. Schulz, G. Leising and L. Brehmer, "Ultraviolet Photoelectron Spectroscopic Study of Heterocyclic Model Compounds for Electroluminescent Devices", Synth. Met., 102 (1999) 1069.
2. S. Schrader, P. Imperia, N. Koch, G. Leising and B. Falk, "Organic Light-Emitting Devices Based on New Heterocyclic Compounds", SPIE, 3797 (1999) 209.
3. P. Imperia, S. Schrader, M.B. Casu, M. Jandke and P. Strohriegl, "Quinoxaline Films for Hetero-Layer Light Emitting Devices", Nonlinear Optics, 25 (2000) 455.
4. C. Flueraru, M. Gardner, O. Buiu, R. Radoi, I. Cernica, P. Imperia, S. Schrader, "Spectroellipsometric Investigation of Optical Properties of SiO_2 Grown by Wet Thermal Oxidation", Surf. Sci., 482-5 (2001) 448.
5. M. B. Casu, P. Imperia, S. Schrader, B. Falk, "Ultraviolet Photoelectron Spectroscopy of Thin Films of New Materials for Multilayer Organic Light Emitting Diodes", Surf. Sci., 482-5 (2001) 1205.
6. M.B. Casu, P. Imperia, S. Schrader, B. Schulz, M. Jandke and P. Strohriegl, "Valence Electronic Structure of Oxadiazoles and Quinoxalines Model Compounds", Synth. Met., 121 (2001) 1397.
7. P. Imperia, M.B. Casu, S. Schrader, B. Falk, M. Jandke, P. Strohriegl, "Electronic Transport Properties of Heterocyclic Materials for Heterolayer Organic Light Emitting Devices", Synth. Met., 121 (2001) 1673.
8. P. Imperia, M.B. Casu, S. Schrader, B. Falk, M. Jandke and P. Strohriegl, "Thermally Stimulated Processes in Heterocyclic Materials Suitable for Heterolayer Organic Light Emitting Diodes", Synth. Met., 124/1 (2001) 83.
9. M.B. Casu, P. Imperia, S. Schrader, B. Falk, M. Jandke and P. Strohriegl "Ultraviolet Photoelectron Spectroscopy on New Heterocyclic Materials for Multilayer Organic Light Emitting Diodes", Synth. Met., 124/1 (2001) 79.
10. M.B. Casu, P. Imperia, S. Schrader, B. Schulz, F. Fangmeyer and H. Schürmann, "Electronic Structures of Ordered Langmuir-Blodgett Films of an Amphiphilic Derivative of 2,5-Diphenyl- 1,3,4-Oxadiazole", Colloids and Surface A, (2002) submitted.
11. P. Imperia, M.B. Casu, B. Schulz and S. Schrader "Analysis of Detrapping Processes of Aromatic 1,3,4-oxadiazoles with Thermally Stimulated Luminescence", Synth. Met., 127 (2002) 181.

12. M.B. Casu, P. Imperia, B. Schulz and S. Schrader “Electronic Structure of Aromatic 1,3,4-oxadiazoles Studied by Ultraviolet Photoelectron Spectroscopy”, Synth. Met., 127 (2002) 185.

13. M.B. Casu, P. Imperia, B. Schulz and S. Schrader “Electronic Structure at the Interface Between Metals and New Materials for Organic Light Emitting Diodes”, Surf. Sci., (2002) accepted for publication.

14. S. Schrader, M.B. Casu, P. Imperia, M. Jandke and P. Strohriegl “Electronic Structure and Localised States in Starburst Trisphenylquinoxaline”, SPIE, (2002) at press.

Monographs

1. M.B. Casu, P. Imperia, S. Schrader, B. Schulz, F. Fangmeyer and H. Schürmann, “Electronic Structure of Ordered Langmuir-Blodgett Films of an Amphiphilic Derivative of 2,5-Diphenyl- 1,3,4-Oxadiazole”, in “Novel Methods to Study Interfacial Layers”, D. Möbius and R. Miller editors, in the series “Studies in Interface Science”, Elsevier, 121 (2001).

Papers in Proceedings of International Conferences and Reports

1. N. Koch, S. Schrader, H. Schürmann, P. Imperia, B. Falk, P. Strohriegl, I. Pérez de Albéniz, G. Leising, L. Brehmer, “Ultraviolet Photoelectron Spectroscopic Study of Quinoxaline Model Compounds”, Bessy Jahresbericht 1998, 248 (1999).

2. S. Schrader, M.B. Casu, P. Imperia, B. Schulz, H. Schürmann, F. Fangmeyer and G. Leising, “Ultraviolet Photoelectron Spectroscopy of Oligophenyloxadiazoles”, Bessy Jahresbericht 1999, 414 (2000).

3. M.B. Casu, P. Imperia and S. Schrader, “Interface Properties of Aromatic Oxadiazoles”, Hasylab Annual Report 2001, 269 (2001)

4. M.B. Casu, P. Imperia, B. Schulz and S. Schrader “Electronic Structure of Aromatic 1,3,4-oxadiazoles”, in “Organic Nanostructures: Science and Applications”, Proceedings of the CIL course of the International School of Physics “Enrico Fermi”, G. C. La Rocca and V.M. Agranovich editors (2001) at press

5. P. Imperia, M.B. Casu, B. Schulz and S. Schrader “Detrapping Processes in Aromatic 1,3,4-oxadiazoles”, in “Organic Nanostructures: Science and Applications”, Proceedings of the CIL course of the International School of Physics “Enrico Fermi”, G. C. La Rocca and V.M. Agranovich editors (2001) at press

Proceedings of International Conferences

1. S. Schrader, M.B. Casu, P. Imperia, H. Schürmann, F. Fangmeyer and B. Schulz “Ultraviolet Photoelectron Spectroscopy of Oxadiazole Thin Films” BESSY Users Meeting, Berlin, Germany, December 9–10 1999.
2. S. Schrader, M. B. Casu, P. Imperia, B. Schulz, F. Fangmeyer and H. Schürmann “Band structure of ordered multilayers of a 2,5-diphenyl-1,3,4-oxadiazole”, Wilhelm und Else Heraeus Seminar, Physikzentrum Bad Honnef, Germany, 6-8 November 2000
3. M.B. Casu, P. Imperia, B. Falk and S. Schrader “Ultraviolet Photoelectron Spectroscopy on Heterocyclic Materials/Gold interfaces” BESSY Users Meeting, Berlin, Germany, December 7–8 2000.
4. M.B. Casu, P. Imperia, B. Falk, M. Jandke P. Strohriegl and S. Schrader “Ultraviolet Photoelectron Spectroscopy on Heterocyclic Materials for Organic Light Emitting Diodes” BESSY Users Meeting, Berlin, Germany, December 7–8 2000.
5. M.B. Casu, P. Imperia, F. Fangmeyer, H. Schürmann and S. Schrader “Electronic Structure of Ordered Oxadiazole layers” BESSY Users Meeting, Berlin, Germany, December 7–8 2000.
6. M.B. Casu, P. Imperia, M. Jandke, P. Strohriegl and S. Schrader “Valence Band Structure and Localised States in Starburst Trisphenylquinoxaline” ECAMP VII, Berlin, Germany, 2-6 April 2001, Europhysics Conference Abstracts, Vol. 25 B, Physik-Verlag GmbH, Weinheim (Germany) 2001.
7. P. Imperia, M.B. Casu, and S. Schrader “Analysis of Detrapping Processes in OLED Materials with Thermally Stimulated Luminescence”, European Conference on Organic Electronics and Related Phenomena ECOER ’01, Potsdam, Germany, 18-21 November 2001.
8. M.B. Casu, P. Imperia and S. Schrader “Interface Properties and Frontier Orbitals of Organic Materials for Photonics”, European Conference on Organic Electronics and Related Phenomena ECOER ’01, Potsdam, Germany, 18-21 November 2001.

Proceedings of National Conferences

1. S. Schrader, M.B. Casu, P. Imperia, M. Jandke, B. Falk and P. Strohriegl, “Valence Band Structure of Quinoxalines and other Heterocyclic Materials”, Deutschen Physikalischen Gesellschaft, Potsdam, Germany, 13-16 March 2000.
2. P. Imperia, S. Schrader, M.B. Casu and B. Falk, “Quinoxalines: Stable Materials for Organic Light Emitting Devices”, Deutschen Physikalischen Gesellschaft, Potsdam, Germany, 13-16 March 2000.
3. M.B. Casu, P. Imperia, S. Schrader, M. Jandke, P.Strohriegl and B. Falk, “Ultraviolet Photoelectron Spectroscopy on Heterocyclic Materials for Organic Light Emitting Devices”, Berliner Polymerentage 2000, Berlin, Germany, 9-11 October 2000.

4. P. Imperia, M.B. Casu, S. Schrader, M. Jandke, P.Strohriegl and B. Falk, “Thermally Stimulated Currents and Dielectric Relaxation Spectroscopy in Quinoxalines for Heterolayer Organic Light Emitting Diodes”, Berliner Polymerentage 2000, Berlin, Germany, 9-11 October 2000.

Posters

1. P. Imperia and S. Schrader, "Electronic Processes in Polyphenylquinoxaline Films" ICEL 2, 13-15 May 1999 Sheffield, United Kingdom.
2. P. Imperia, S. Schrader, B. Falk, N. Koch, G. Leising and L. Brehmer. “Quinoxalines: Stable Materials for Organic Light-Emitting Devices” Graduiertenkolleg Optoelektronik Mesoskopischer Halbleiter, Philipps-Universität Marburg, September 29, October 1, 1999, Marburg, Germany.
3. M.B. Casu, P. Imperia, M. Jandke, S. Schrader and P.Strohriegl, “Valence Electronic Structure of Quinoxalines and other Heterocyclic Materials”, TMR EUROLED MEETING, 8-10 November 1999, Strasbourg, France.
4. P. Imperia, S. Schrader, M.B. Casu, M. Jandke and P.Strohriegl, “Quinoxaline Films for Hetero-Layer Light Emitting Devices”, ICONO 5, 12-16 March, 2000, Davos, Switzerland.
5. P.Imperia, S.Schrader, M.B.Casu and B.Falk, “Quinoxalines: Stable Materials for Organic Light Emitting Devices”, Deutschen Physikalischen Gesellschaft, Potsdam, Germany, 13-16 March 2000.
6. P. Imperia, M.B. Casu, S. Schrader, B. Falk, M. Jandke and P. Strohriegl, “Thermally Stimulated Processes in Heterocyclic Materials Suitable for Heterolayer Organic Light Emitting Diodes”, E-MRS 2000 Spring Meeting, May 30, June 2, 2000, Strasbourg, France.
7. M.B. Casu, P. Imperia, S. Schrader, B. Schulz, M. Jandke and P. Strohriegl, “Valence Electronic Structure of Oxadiazoles and Quinoxalines Model Compounds”, E-MRS 2000 Spring Meeting, May 30, June 2, 2000, Strasbourg, France.
8. M.B. Casu, P. Imperia, S. Schrader, B. Falk, M. Jandke and P. Strohriegl “Ultraviolet Photoelectron Spectroscopy on New Heterocyclic Materials for Multilayer Organic Light Emitting Diodes”, ICSM 2000, 15-21 July 2000, Gastein, Austria.
9. P. Imperia, M.B. Casu, S. Schrader, B. Falk, M. Jandke and P. Strohriegl, “Electronic Transport Properties of Heterocyclic Materials for Heterolayer Organic Light Emitting Devices”, ICSM 2000, 15-21 July 2000, Gastein, Austria.
15. M.B. Casu, P. Imperia, S. Schrader and B. Falk, “Ultraviolet Photoelectron Spectroscopy of Thin Films of New Materials for Multilayer Organic Light Emitting Diodes”, ECOSS-19, 5-8 September 2000, Madrid, Spain.
16. S. Schrader, M.B. Casu, P. Imperia, B. Schulz, F. Fangmeyer and H. Schürmann “Band Structure of Ordered Multilayers of a 2,5-diphenyl-1,3,4-oxadiazole”, Wilhelm und Else Heraeus Seminar, Physikzentrum Bad Honnef, Germany, 6-8 November 2000.

17. M.B. Casu, P. Imperia, B. Falk and S. Schrader “Ultraviolet Photoelectron Spectroscopy on Heterocyclic Materials/Gold interfaces” BESSY Users Meeting, Berlin, Germany, December 7–8 2000.
18. M.B. Casu, P. Imperia, B. Falk, M. Jandke P. Strohriegl and S. Schrader “Ultraviolet Photoelectron Spectroscopy on Heterocyclic Materials for Organic Light Emitting Diodes” BESSY Users Meeting, Berlin, Germany, December 7–8 2000.
19. M.B. Casu, P. Imperia, F. Fangmeyer, H. Schürmann and S. Schrader “Electronic Structure of Ordered Oxadiazole Layers” BESSY Users Meeting, Berlin, Germany, December 7–8 2000.
20. M.B. Casu, P. Imperia, M. Jandke, P. Strohriegl and S. Schrader “Valence Band Structure and Localised States in Starburst Trisphenylquinoxaline” ECAMP VII, 2-6 April 2001, Berlin, Germany.
21. P. Imperia, M.B. Casu, B. Schulz and S. Schrader “Analysis of Detrapping Processes of Aromatic 1,3,4-oxadiazoles with Thermally Stimulated Luminescence”, E-MRS 2001 Spring Meeting, 5-8 June 2001, Strasbourg, France.
22. M.B. Casu, P. Imperia, B. Schulz and S. Schrader “Electronic Structure of Aromatic 1,3,4-oxadiazoles Studied by Ultraviolet Photoelectron Spectroscopy”, E-MRS 2001 Spring Meeting, 5-8 June 2001, Strasbourg, France.
23. M.B. Casu, P. Imperia, B. Schulz and S. Schrader “Electronic Structure at the Interface Between Metals and New Materials for Organic Light Emitting Diodes”, ECOSS-20, 4-7 September 2001, Krakow, Poland.
24. P. Imperia, M.B. Casu, and S. Schrader “Analysis of Detrapping Processes in OLED Materials with Thermally Stimulated Luminescence”, European Conference on Organic Electronics and Related Phenomena ECOER ’01, Potsdam, Germany, 18-21 November 2001.

Talks

1. P. Imperia and S. Schrader, “Thermally Stimulated Discharge Current Techniques” TMR EUROLED MEETING, Alghero, Italy 18-20 October 1998.
2. P. Imperia and S. Schrader, “Electronic Processes in Polyphenylquinoxaline Films” TMR EUROLED MEETING, Sheffield, United Kingdom, 16-18 May 1999.
3. P. Imperia, M.B. Casu and S. Schrader,“Thermally Activated Processes in Quinoxaline Films”, TMR EUROLED MEETING, Strasbourg, France, 8-10 November 1999.
4. P. Imperia, M.B. Casu, S. Schrader, B. Falk, M. Jandke and P.Strohriegl “Thermally Stimulated Processes in Heterocyclic OLED Materials”, TMR EUROLED MEETING, Gargnano, Italy, 22-23 June 2000.
5. P. Imperia, M.B. Casu and S. Schrader, “Localized States in OLED Materials”, TMR EUROLED MEETING, Bayreuth, Germany, 29-31 October 2000.

6. P. Imperia, M.B. Casu and S. Schrader, “Analysis of Localized States by Simulation of Thermally Stimulated Processes”, TMR EUROLED MEETING, Zurich, Switzerland, 4-6 April 2001.

7. P. Imperia, M.B. Casu and S. Schrader, “Analysis of Detrapping Processes in Aromatic 1,3,4-oxadiazoles”, TMR EUROLED MEETING, Potsdam Germany 11-13 October 2001

Acknowledgements

This research work has been carried out in the frame of the EUROLED network. The financial support of European Commission under contract number FMRX-CT97-0106 is gratefully acknowledged.

I would like to thank Prof. Ludwig Brehmer for his support and encouragement.

I am deeply indebted to Dr. Sigurd Schrader for his tireless help, deep scientific discussions and continuous encouragement.

I would like to thank all my colleagues of University of Potsdam, particularly my former colleague Ulf for his warm friendship, Costel and Vismants for their very useful advice, John and Sabine for their help; I learnt so much from all of them.

A very special thanks and love to Betty, for her invaluable help in many aspect of my scientific and "normal" life. Without her help and enthusiasm, without her continuous pointing to the goal probably this work would never have seen a happy end.

Micha, I thank you so much for such a beautiful thing that you keep deep in your heart.

Erklärung

Hiermit erkläre ich, daß die Dissertation mit dem Thema

Localised States in Organic Semiconductors and their Detection

an keiner anderen Hochschule eingereicht sowie selbständig und nur mit den angegebenen Mitteln angefertigt wurde.

Potsdam, 7 Februar 2002

Paolo Imperia